Universität Bremen

ALFRED-WEGENER-INSTITUT
HELMHOLTZ-ZENTRUM FÜR POLAR- UND MEERESFORSCHUNG

Seismic investigation of sediment structures to reconstruct ocean bottom currents east of New Zealand

Masterarbeit im Studiengang Geowissenschaften

Fachbereich Geowissenschaften

Universität Bremen

von

Lara Steinbrink

Bremen, 2017

1. Gutachter: Dr. Karsten Gohl

2. Gutachter: Dr. Tilmann Schwenk

Name, Vorname: Steinbrink, Lara Bremen, den 14.12.2017

Erklärung gem. § 10 Abs. 11 Allg. Teil d. Master-PO vom 27.10.2010

Ich versichere hiermit, dass ich meine Masterarbeit selbstständig verfasst und keine anderen als die angegebenen Quellen und Hilfsmittel benutzt habe. Wörtliche oder dem Sinn nach aus anderen Werken entnommene Stellen sind unter der Angabe der Quellen kenntlich gemacht.

Die Arbeit wurde nicht in einem anderen Prüfungsverfahren eingereicht.

Weiterhin erkläre ich, dass die Masterarbeit in unveränderter Fassung der Öffentlichkeit zur Verfügung gestellt werden kann.

Ort/Datum:

Unterschrift:

Table of contents

Abstract

Marine sedimentation is strongly influenced by oceanographic processes featuring bottom currents. Oceanographic impacts such as changes in the deep-water formation or the opening of ocean gateways can therefore be represented in sediment accumulations, generated by these currents. East of New Zealand a suite of sediment drifts and contourites, formed by along-slope current branches of the Deep Western Boundary Current (DWBC), which feeds the Pacific Ocean with cold deep-water, has been described by Carter et al. (1994). By the analysis of these sediment structures it is possible to reconstruct ocean bottom current regimes for different time periods. Seismic reflection data provides information about the subsurface, which can be analyzed and interpreted in reference to its oceanographic development.

The investigation of seismic multi-channel reflection data from the RV Sonne expedition SO246, which took place in 2016, enables to reconstruct bottom current conditions at the south-eastern Chatham Rise slope in the past 80 My. Therefore, three seismic profiles from the southern Chatham Rise were processed and interpreted. A supplementation of New Zealand seismic profiles together with Parasound and bathymetric data, which deliver complementary information on details of the uppermost layers and the lateral extension of sedimentary structures as well as bathymetric features of the environment, allowed a time-dependent mapping of sediment depositions and reconstruction of current regimes in the work area.

A classification of different sedimentary units compared with a lithostratigraphic model from Horn & Uenzelmann-Neben (2015) enabled to create an age model for these units. From the Cretaceous until the early Oligocene, smooth accumulation conditions were recognized. However, the occurrence of bottom current activity suggests the existence of a Proto-DWBC, which passed the work area in north-eastern direction. Subsequent to the opening of the Tasmanian Gateway in the early Oligocene the bottom current activity intensified and caused widespread erosion and the formation of a strong unconformity. During the Miocene current conditions often changed and led to common reworking of sediments. After the development of three main sediment conduits in the Plio-Pleistocene, a terrigenous sedimentation dominated. Current conditions were smoother than before. The occurrence of contourite depositions suggests an along-slope floating of bottom currents in many parts of the work area, especially at the eastern flank of the Chatham Rise, where a migration of sediment bodies points to a westward shifting of currents.

1. Introduction

One of the controlling factors of the Earth's climate is the circulation of cold, deep Antarctic Bottom Water. The 1000 km wide DWBC, which flows northeastwards along the continental margin east of New Zealand feeds 40 % of this water into the world ocean (Carter et al., 1996). Today, a suite of sediment drifts and contourites, deposited along the slope of the Chatham Rise, delivers information about the development of bottom currents since the early Oligocene. Oceanographic impacts such as changes in the deep-water formation or the opening of ocean gateways can be represented in these sediment accumulations. Various publications from the 1990's have investigated the sedimentation characteristics of accumulations east of New Zealand with seismic and 3.5-kHz sub-bottom profiles (Carter et al., 1994). Thereby, Carter et al. (1996) developed a scenario to describe the oceanographic and sedimentary processes in this area, called the 'ENZOSS (Eastern New Zealand Oceanographic Sedimentary System) model'. Sediment drifts located in this area were formed in response to the inception of the Antarctic Circumpolar Current (ACC), the global thermohaline circulation (THC) and the development of the New Zealand plate boundary (Carter et al., 2004). Contouritic sediment depositions, as found along the path of the DWBC east of New Zealand, provide information about the history of ocean circulation and climate, as well as small-scale ocean circulation patterns, current velocities and basin interconnectivity (Rebesco et al., 2014).

The aim of this master thesis is to reconstruct ocean bottom currents along the south-eastern margin of the Chatham Rise at least since the evolution of the ENZOSS by seismic investigations of sedimentary depositions, which were influenced by oceanographic processes. At first, an introduction into the conceptual background of deep sea sedimentary processes as well as previous knowledge about sedimentary processes in the work area give an overview of the subject of this work. Afterwards, the data sets are presented and the processing of three multi-channel seismic reflection profiles, obtained at expedition cruise SO246 is documented. In comparison with additional seismic data, the results are used to analyze the position and structure of sediment bodies. Geophysical parameters and sedimentological features of different units were determined and investigated to interpret them in relation to their development. In addition to the seismic reflection data, Parasound data, which were also taken on the ship cruise SO246, are used to illustrate details of the uppermost layers. Furthermore, bathymetric data from SO246 as well as the NIWA database (Mitchell et al., 2012) deliver information about the lateral extension of sedimentary structures and bathymetric features, which may have had an influence on their deposition. A main component of this work is the mapping and interpretation of sediment structures in relation to previous research results as well as a time-dependent reconstruction of current conditions in the past. Furthermore, the verification of the 'ENZOSS model' developed by Carter et al. (1996), as well as the refinement and extension of this scenario are discussed.

2. Conceptual background: Development of sediment drifts

2.1 - Deep sea sedimentary processes

Sedimentary deposition at oceanic margins is often influenced by a combination of gravitational and bottom currents related processes (Faugères et al., 1999). These currents are able to build extensive sediment accumulations, effected by associated oceanographic processes, involving dense bottom currents, tides, eddies, deep-sea storms, internal waves as well as tsunamis (Rebesco et al., 2014). Due to the occurrence of bathymetric features like seamounts, ridges etc. the flow can be forced to accelerate, if narrowed, or decelerate, if spread. A high current velocity leads to the erosion of sediment, while the decrease of current velocity causes deposition (Rebesco et al., 2014). An example for principal bottom current features is shown in Fig. 2.1.

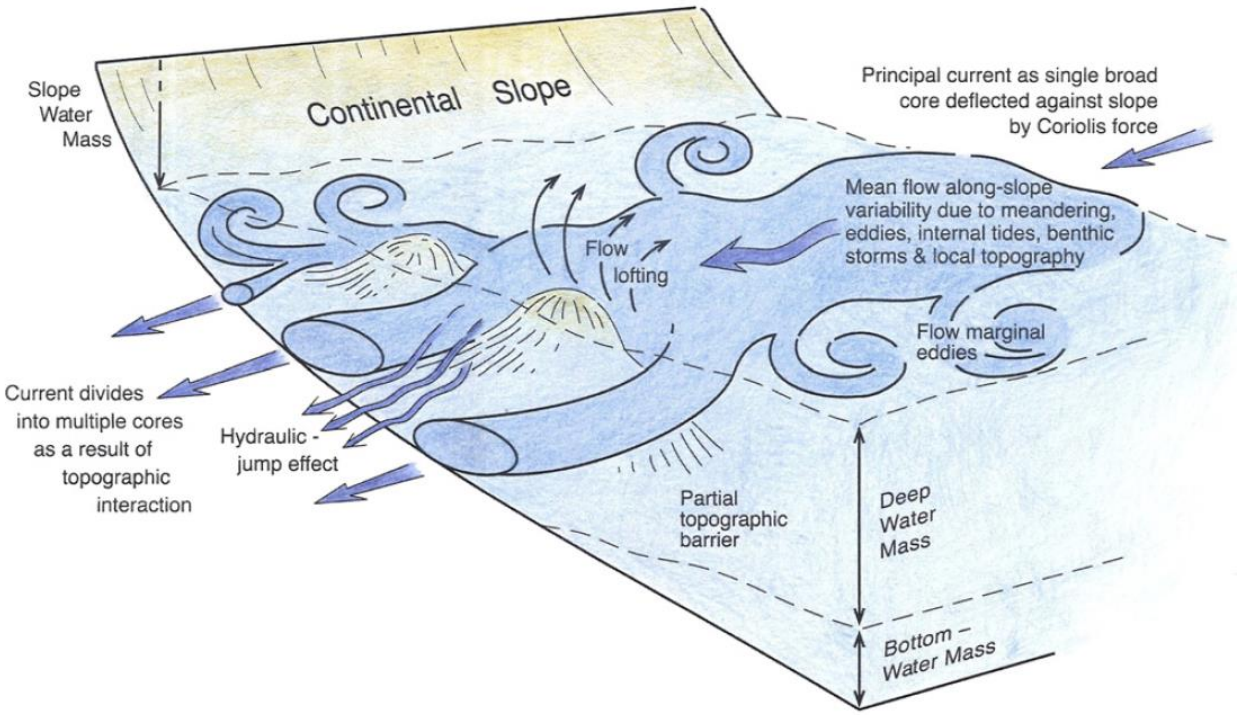

Fig. 2.1: Principal bottom current features along continental slopes. (from Rebesco et al., 2014)

The distinction of different types of deposits is one of the major difficulties in interpreting seismic profiles crossing oceanic margins (Faugères et al., 1999). Fig. 2.2 illustrates the three main types of sedimentary processes operating in the deep sea. The deposition by vertical settling of pelagic particles through the water column, which occurs only in very remote, abyssal areas, creates ‘pelagites’. Whereas ‘turbidites’ are deposited by downslope density currents, predominantly composed of terrigenous sediments. These high-energy density flows occur in episodic events and are often interacting with relatively permanent bottom current flows. ‘Contourites’ are originating in the along-slope flow of bottom currents consisting of

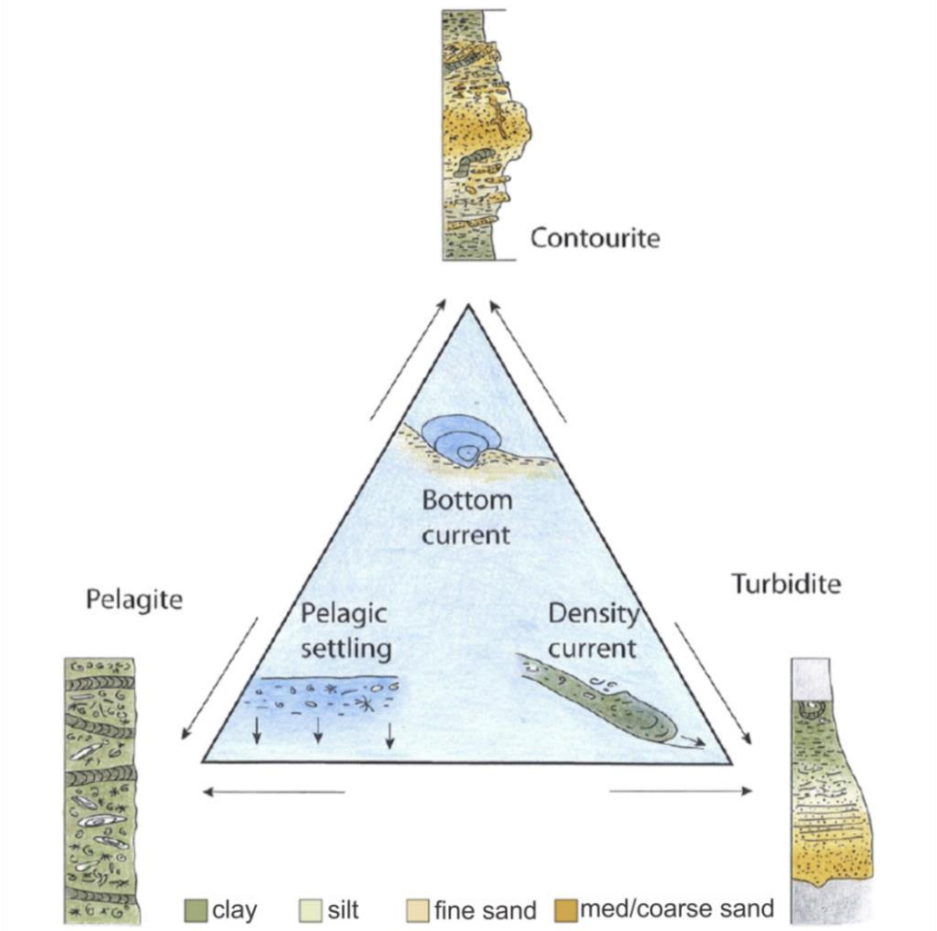

Fig. 2.2: Conceptional diagram of the main types of deep sea sedimentary processes and their facies models. (from Rebesco et al., 2014)

relatively clean bottom-water masses and are mostly elongated parallel or oblique to the margin (Rebesco et al., 2014). Contourite currents represent important transport paths and control lots of deep sea sedimentation. Therefore, a deeper understanding of these processes is one of the main subjects of this work.

2.2 - Contourites

Contourites, which were first described in the Northern and Southern Atlantic Ocean, but later discovered in every major ocean, play an increasing role in paleoclimatology and paleoceanography, slope-stability and geological hazard assessment, as well as hydrocarbon exploration (Rebesco et al., 2014). Contourites are sediment accumulations originating in the along-slope flow of bottom currents. They possess a mounded geometry, which is mostly elongated parallel or oblique to the margin, as illustrated in Fig. 2.3. Dimensions can range from small patch drifts to giant elongated drifts extending over several hundreds of kilometers with a width of more than 100 km, a thickness of up to 2 km and a relief of up to 1.5 km (Rebesco et al., 2014). Faugères et al. (1999) described three main features of contourites as follows. Major discontinuities are linked to erosion, a change of material composition or grain

size and are originating from a modification of the current strength. Moreover, contourite units can occur in a lenticular shape and upwardly convex geometry, which has been formed due to erosional events. Furthermore, the uppermost unit of a contourite can show aggradation and/or progradation, originating from the migration of the sediment body, due to a shifting of the operating water masses, causing an upward and oblique stacking of units (Faugères et al., 1999).

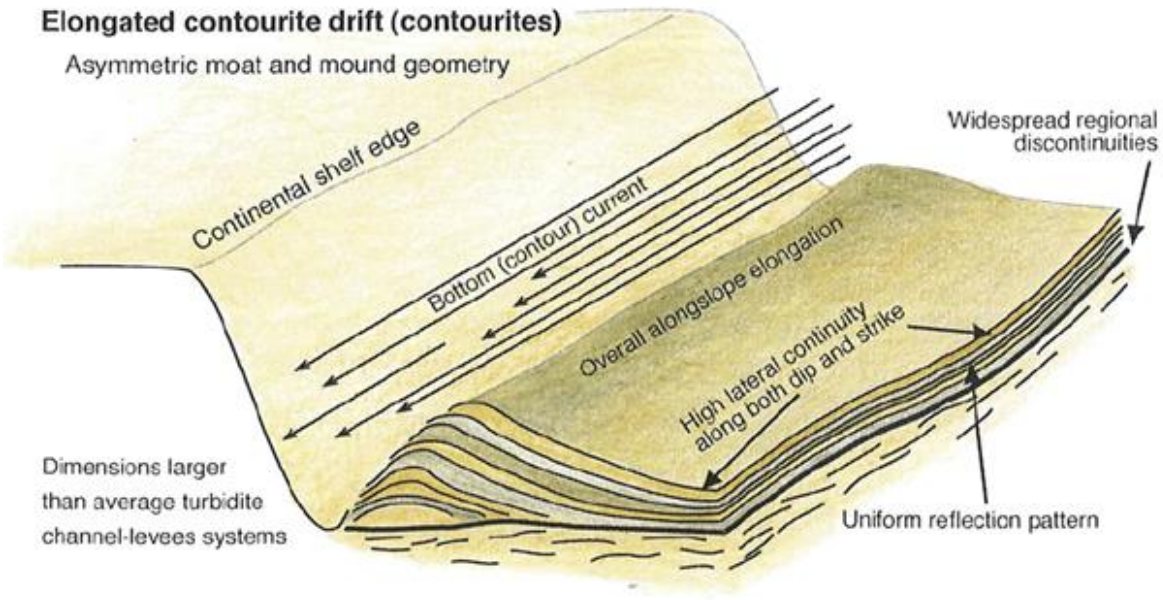

Fig. 2.3: Illustration of a contourite paradigm. (from Rebesco et al., 2014)

The deposition of contourites is controlled by bottom currents and their associated oceanographic processes. Although the contourite paradigm was conceived a few decades ago, there is still the need to establish a sound connection between contourite deposits, basin evolution and oceanographic processes. (Rebesco et al., 2014)

3. Regional setting

3.1 - Tectonic evolution of the work area

The supercontinent Pangea started to break-up at 200 Ma, when North-America moved apart from Europe. Afterwards, at 150 Ma, Laurasia began to divert from Gondwana and this initiated the break-up of Gondwana into single continents (Press et al., 2011). This final fragmentation caused divergent plate motions and led to the separation of Australia from Antarctica (Press et al., 2011; Stilwell and Consoli, 2012). Thus, the Zealandia block, including the Chatham Rise, was pulled away from the West Antarctic margin at ca. 85 - 80 Ma (see Fig. 3.1) with simultaneous rifting phases that created large horsts and grabens (Stilwell and Consoli, 2012; Wobbe et al., 2012). As a result of seafloor spreading, the Hikurangi Plateau is interpreted to have rifted and then entered the Gondwana subduction margin along the North Chatham Rise in the Late Cretaceous, where it led to deformation along the margin and the cessation of Mesozoic subduction at this section of the margin (Davy et al., 2008). Thereby, the Chatham Rise, which was initially part of the continental margin of Gondwana in the Paleozoic rifted and was uplifted (Stilwell and Consoli, 2012). Afterwards it was subsided during the Mesozoic (Stilwell and Consoli, 2012). The Campbell Plateau and Chatham Rise rotated against each other and the Bounty Trough was opened (Wobbe et al., 2012). In the Cenozoic the Chatham Rise evolved into a relatively stable, submerged marine plateau (Stilwell and Consoli, 2012).

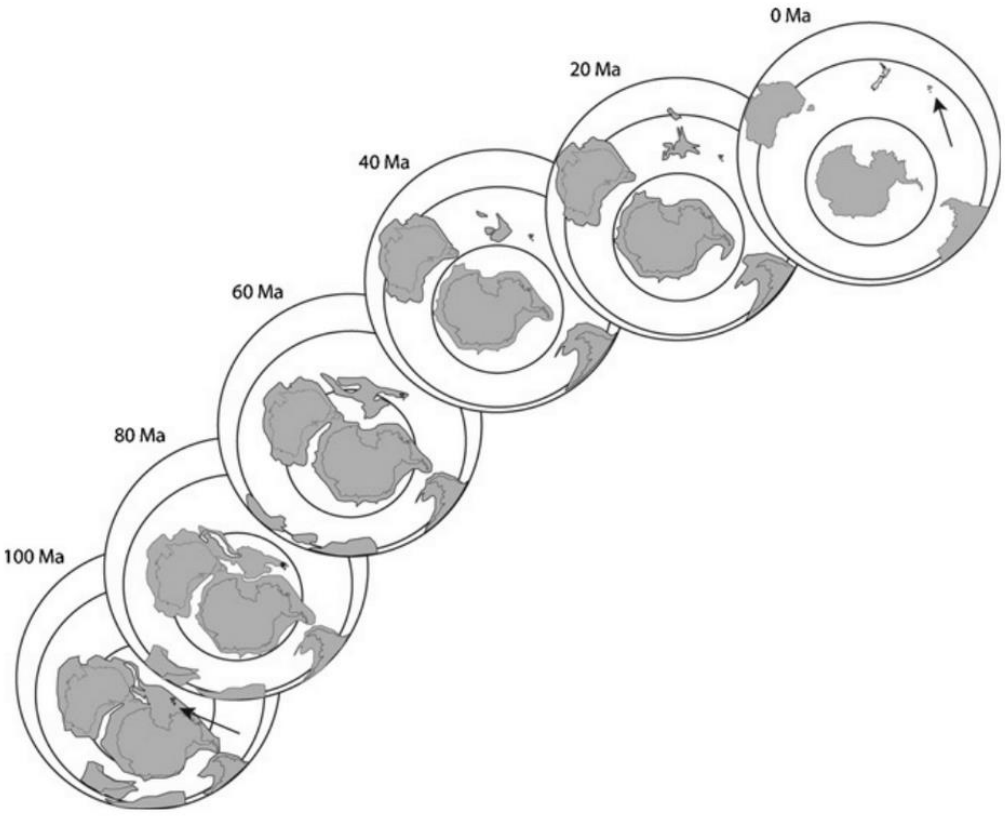

Fig. 3.1: Final break-up of Gondwana. The small, black arrow marks the Chatham Islands as reference point. (from Stilwell and Consoli, 2012)

3.2 - Regional effects of the global thermohaline circulation

The most important water circulation effecting surface and deep-water masses is the THC. It evolved due to the opening and closing of influencing gateways causing significant changes in the global water circulation, illustrated in Fig. 3.2. The THC forms in marginal or shallow shelf areas when water temperature decreases by ice formation or cooling. The dense of the water is now higher and it evolves to deep water, which is fed into the ocean and flows parallel to large-scale bathymetry. Small-scale features like seamounts and ridges can interrupt and accelerate these bottom currents. (Rebesco et al., 2014)

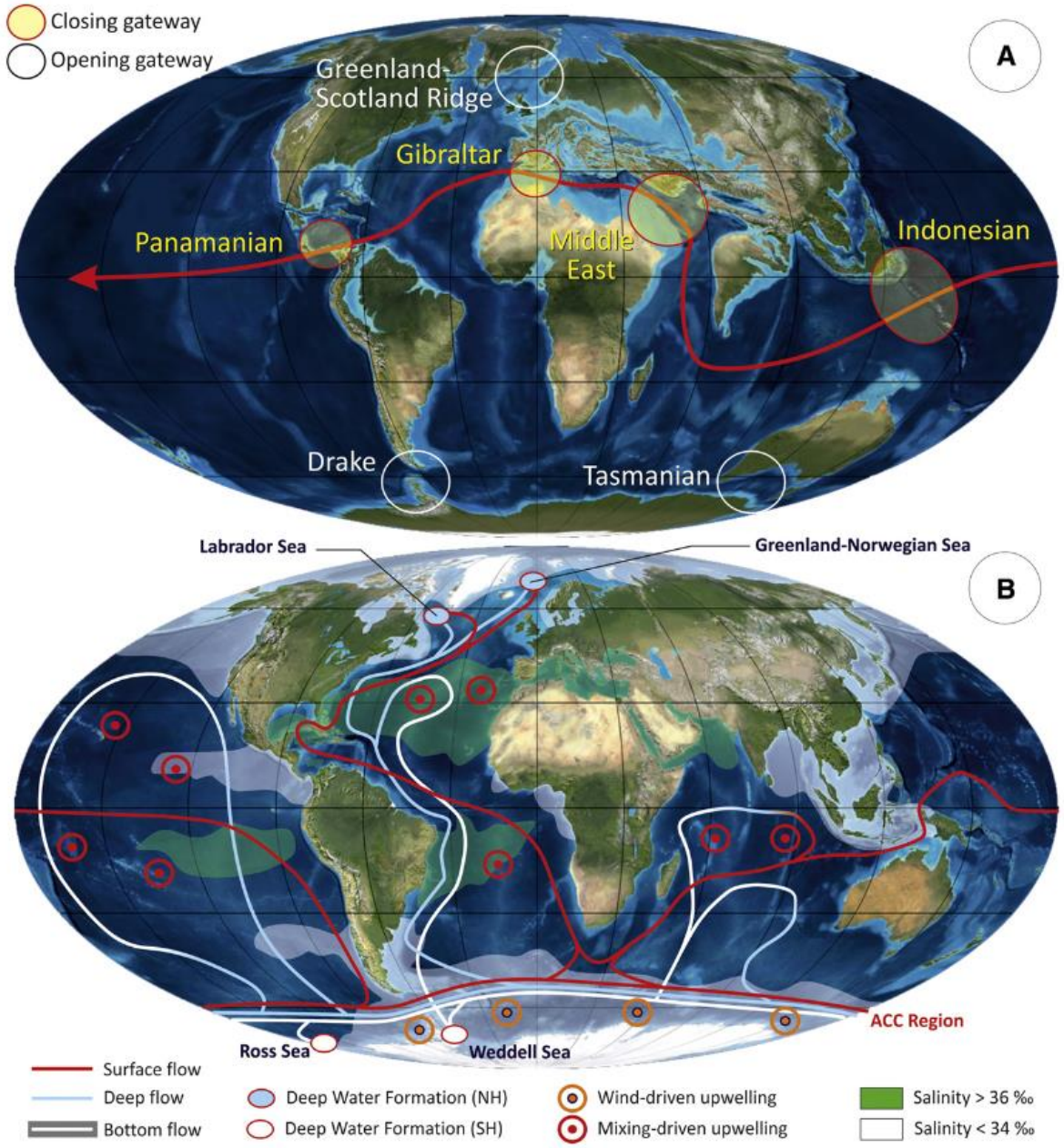

Fig. 3.2: Development of the THC after the opening and closing of influencing gateways. A) illustrates the plate and marine basin distribution including closing (Panamanian, Gibraltar, Middle East and Indonesian) and opening gateways (Greenland-Scotland Ridge, Drake, Tasmanian) in the Eocene. B) shows the pathway of the THC today. (from Rebesco et al., 2014)

3.3 - Oceanographic evolution: Eastern New Zealand Oceanic Sedimentary System

After the opening of the Tasmanian Gateway, which developed due to the diverging of the Tasman Plateau and Antarctica, surface water was able to pass through in the early Oligocene (Carter and McCave, 1994). The on-going process of rifting allowed deeper waters to pass through the Tasmanian Gateway in the mid-Oligocene. As the gap was widened the ACC and the DWBC developed (Carter and McCave, 1994). The DWBC representing the main deep cold-water inflow into the Pacific Ocean is part of the deep-water current system caused by the THC and passes the work area by flowing along the continental margin east of New Zealand (Carter et al., 1996; Horn and Uenzelmann-Neben, 2015). South-east of the Campbell

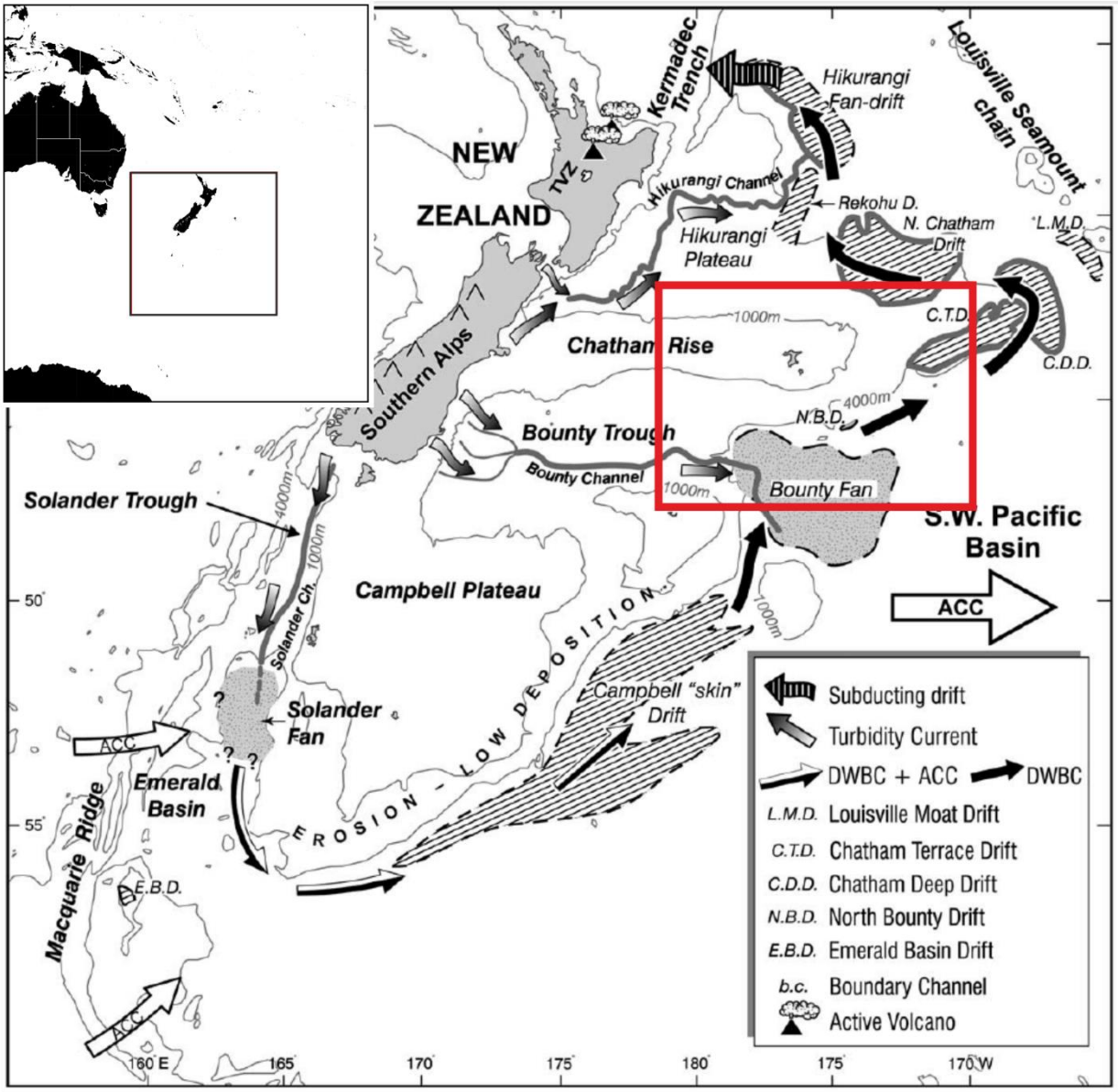

Fig. 3.3: Illustration of the 'ENZOSS model'. The position of sediment drifts described by Carter et al. (2004) are illustrated by dashed areas. The red box shows the location of the work area. (modified from Carter et al., 2004)

Plateau it is accompanied by the ACC, which uncouples at the mouth of Bounty Trough as shown in Fig. 3.3. The DWBC continues its way rounding the eastern flank of the Chatham Rise and diverting northwards along the eastern edge of the Hikurangi Plateau.

After the inception of the ACC and the DWBC the deposition of sedimentary drifts in the work area intensified (Carter et al., 2004). This was the beginning of the development of the ENZOSS, which is a scenario developed by Carter et al. (Carter et al., 1996) to describe the connection between provenance, transport and deposition of sediments within this system (Fig. 3.3). Therein, it is suggested that sediment from the mountains along the New Zealand plate boundary, which has been transported through deep-sea channel and fan systems, is delivered into the path of the DWBC. Then, it is carried northwards within this current system and deposited as a series of sediment drifts, whose sediments can be reworked and are finally consumed by subduction at the same plate boundary, where it originates in, after a transport of more than 3500 km. (Carter et al., 1996)

3.4 - Sediment drifts in the work area

Carter and McCave (1994) described the formation of bottom current-influenced sediment deposits in the work area that have been recorded by seismic as well as 3.5-kHz sub-bottom profiles and reflect regional variations in bathymetry, sediment supply, as well as the tectonic and volcanic framework. Those sediment drifts rest on a widespread erosional surface, which Carter and McCave (1994) interpret to mark the inception of the DWBC after the opening of the Tasmanian Gateway in the Late Oligocene. During the early Miocene, drift construction initiated due to maximum flooding of a low relief New Zealand (Carter et al., 2004). These drifts were mainly composed of biogenic carbonate and reworked sediment, caused by the absence of submarine channel delivery systems (Carter et al., 2004). This period of drift accumulation was disrupted by another period of erosion that concurred with the expansion of the East Antarctic Ice Sheet and increased bottom water production in Antarctica in the late Miocene (Carter and McCave, 1994; Carter et al., 2004). In the Plio-Pleistocene, deposition continued as a result of the injection of large amounts of sediments from the rapidly rising landmass of New Zealand (Carter and McCave, 1994). The sediment supply mostly originated from debris flows and turbidity currents that were transported downslope to the continental rise, but also some reworked pelagic sediments have produced drifts of mainly calcareous material (Carter and McCave, 1994). The channels responsible for the main sediment supply are called Solander, Bounty and Hikurangi channel, which as a result formed the Solander and Bounty Fans as well as the Hikurangi fan-drift system (Carter et al., 2004). During the Quaternary, oscillations of climate and the sea level regulated the influx of sediment (Carter et al., 2004).

Various sediment drifts, which are spread over a depth range of 2200-5700 m, discovered in the work area are shown in Fig. 3.3 (Carter et al., 2004). A sinuous, linear body with a length of 350 km and a thickness of 320 m, named the “Chatham Terrace Drifts” has been discovered in a water depth of 3000 m along the south flank of the Chatham Rise (Carter and McCave, 2002). The “Chatham Deep Drift”, a 300 km long ridge-like drift of 400 m thickness is located in a water depth of 4500 to 5200 m on the east flank and a widespread apron-shaped drift, called the “North Chatham Drift” is situated on the north flank in 2000 to 4500 m water depth (Carter and McCave, 2002). According to Carter and McCave (2002), drilling at Site 1123 has recovered 587 m of North Chatham Drift sediment, which contained nannofossil ooze and chalk with cyclical amounts of terrigenous detritus and reworked subantarctic microfossils. Since the Early Miocene, an almost continuous deposition was traced (Carter and McCave, 2002).

Huge volumes of reworked sediments are incorporated in deep-sea contourite drifts formed by deposition from DWBCs and represent the impact of the opening of the circum-Antarctic seaway, changes in the thermohaline system of the earth, the development of polar ice sheets and the tectonic evolution of the New Zealand plate boundary (Carter and McCave, 1994; Carter et al., 2004). Additionally, these events are overprinted with effects of orbital forcing on sediment supply, abyssal sedimentation and current flow, which increases the complexity of the ENZOSS (Carter et al., 2004). The investigation of sediment drifts in this area enables a better understanding of these processes and their impacts.

4. Material and methods

4.1 - Work area and data set

The issue of this thesis is based on the data of three seismic reflection profiles, which were collected south east of New Zealand with RV Sonne in year 2016. The expedition SO246 took place between 1st February and 20th March 2016 with Wellington being the starting and ending point. Several standard multi-channel seismic reflection data profiles were taken additionally to the refraction seismic data sets, which were the main subject of the cruise. Furthermore, Parasound and multibeam echosounding data were taken during the whole ship cruise and hence deliver complementary information. The work area is located at the south-eastern flank of the so-called Chatham Rise (Fig. 4.1).

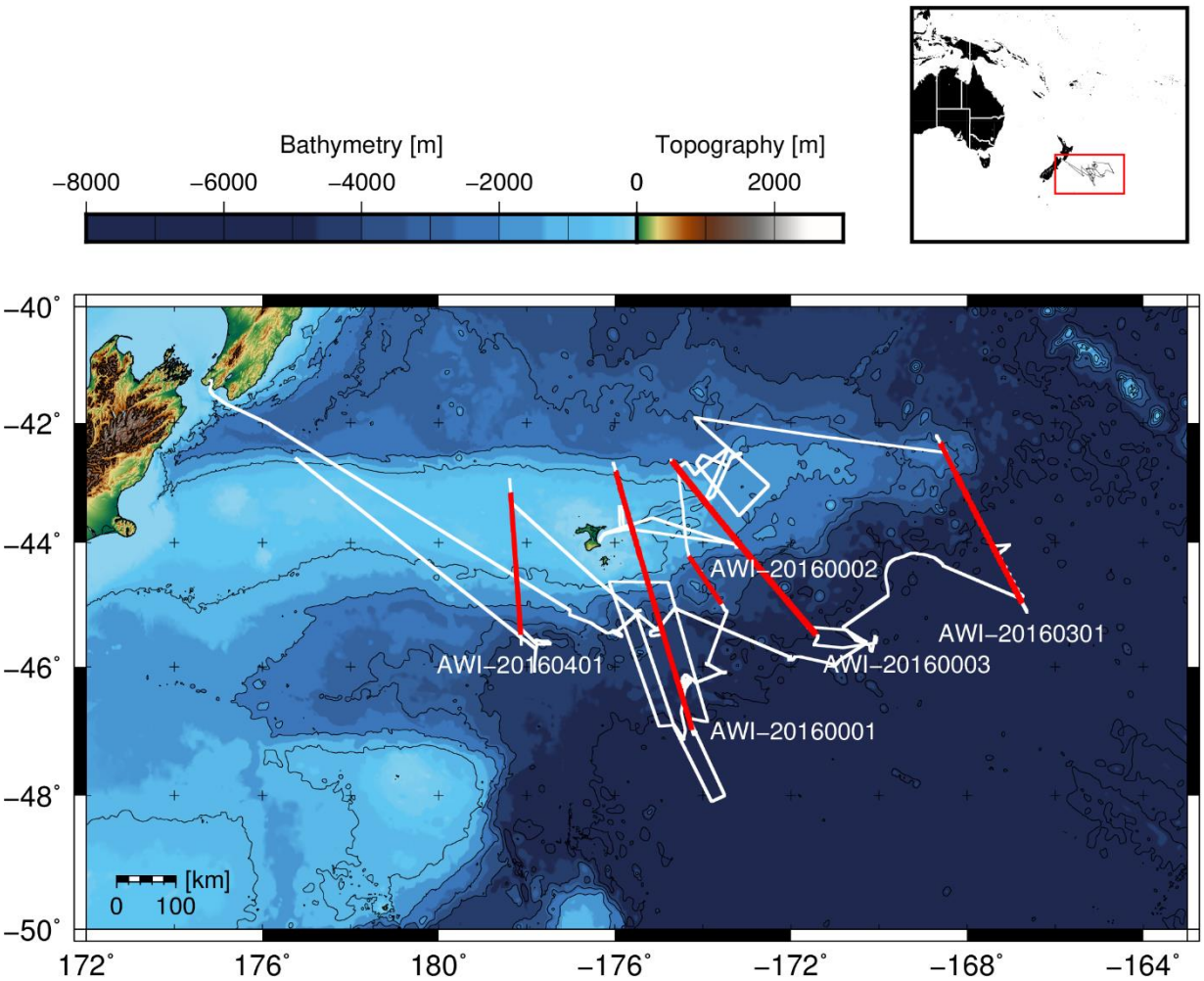

Fig. 4.1: Bathymetric map of the work area. Locations of seismic data profiles from SO246 are represented by red lines and the cruise track is illustrated as white lines in the bathymetric map and black lines in the small overview map.

Since the subject of this thesis is a seismic investigation of sediment structures, with the aim to reconstruct ocean bottom currents in the work area, the first method to gain useful material was the processing of the seismic reflection data, which has been done in the Geophysics group of the Alfred Wegener Institute. The profiles collected on the cruise SO246 (shown in Fig. 4.1) are called AWI-20160401, AWI-20160001, AWI-20160002, AWI-20160003 and AWI-20160301 and are striking north to south or north-west to south-east. Water depths are ranging between approx. 300 to 5300 m. As profile AWI-20160401 only covers shallow water depths, which are not relevant for the reconstruction of deep-water currents, this profile will not be considered in the further processes. Properties of the remaining four profiles are listed in Tab. 4.1. The profile AWI-20160002, which has already been processed and analyzed in a bachelor thesis by Dennis Flenner, will also be used for the further interpretation, but will not be processed again.

Tab. 4.1: Length and approx. water depth range of seismic profiles from SO246.

Profile name	Length [km]	Approx. water depth range [m]
AWI-20160001	467	300 - 5000
AWI-20160002	106	2100 - 3600
AWI-20160003	404	1100 - 4900
AWI-20160301	334	2600 - 5300

Additionally to the seismic reflection data collected on the cruise SO246, 10 already processed seismic profiles from New Zealand (shown in Fig. 4.2) will be used to extend the seismic reflection data set. The profiles tan0207-bt2, tan0207-cr1, tan0207-cr2, tan0207-cr3, tan0207-cr4 and tan0207-cr5a are located along the southern flank of Chatham Rise and are oriented almost in the same direction as the profiles collected on cruise SO246. The profiles cr5 and cr6 are crossing the eastern edge of the Chatham Rise in north-south (cr5) and west-east (cr6) orientation, while profile hkdc12 starts at the eastern flank of Chatham Rise and extends into a northern direction. Since profile tan0207-bt1 is located south of the Bounty Trough on the eastern slope of the Campbell Plateau, which probably reflects a different sedimentation regime, it will not be considered in the following chapters.

Between 1st of February and 20th of March, Parasound as well as bathymetric data were collected supplementary to the seismic reflection data and cover the cruise SO246 area off the Territorial Seas of New Zealand. Parasound data from selected sections of the profiles deliver additional information about subsurface sediment structures and give a more detailed insight into the uppermost layers. Bathymetric data from SO246, as well as bathymetric data provided from New Zealand will be utilized for the better understanding of the expanse of sediment drifts

and the connection between structures occurring in several profiles. Furthermore, the connection of borehole and seismic data from Site 1122 (Carter et al., 1999a), collected on the Ocean Drilling Program Leg 181 (Carter et al., 1999b) will serve to establish a stratigraphic correlation.

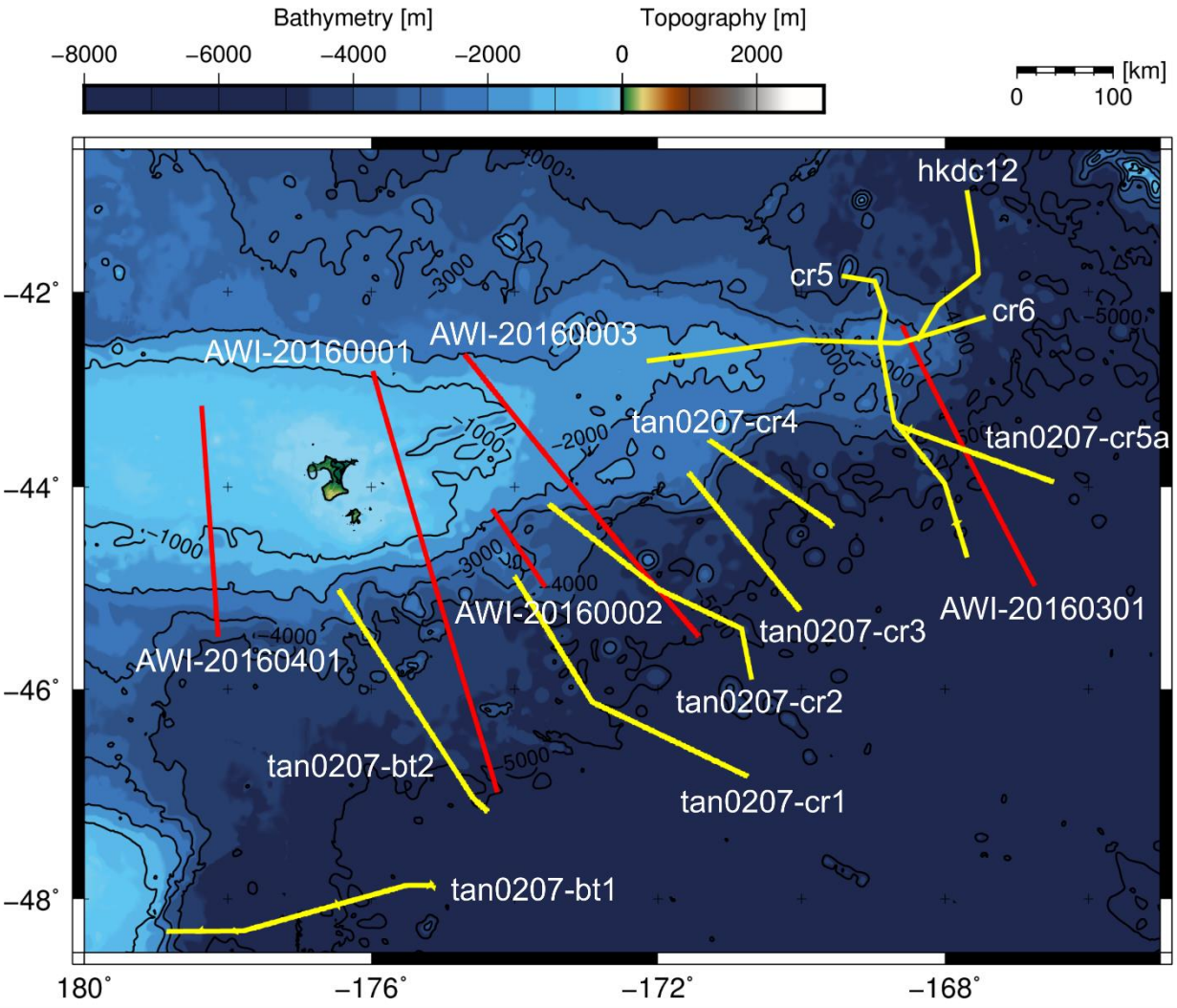

Fig. 4.2: Seismic data profiles from Cruise SO246 (red) and New Zealand seismic data profiles (yellow).

4.2 - Software tools used

Several software tools were used during the work with the data. Geographic maps, illustrating bathymetric data were produced with *GMT 5.3.1* and partly completed with *CorelDRAW X6*, which was used for the complementation of most of the other figures as well. The processing of seismic reflection data as well as the time-to-depth conversion were done with *Paradigm Echos 15.5* and the seismic interpretation, including the definition of different horizons and units with *Paradigm Epos 15.5*. Both programs were used to produce figures of the seismic reflection data. The program *SENT* served to illustrate and create bitmaps of significant sections of the Parasound data.

4.3 - Multi-channel seismic reflection data

Data acquisition

The data were collected with a standard multi-channel seismic reflection technique with the aim to illustrate the outline and reflectivity character of sediment and basement structures. During the data acquisition, the RV Sonne had a vehicle speed of 5 knots equating to 9,26 km/h. A seismic source was towed behind the ship to send an acoustic signal, which was then reflected by the seafloor and sediment layers in the subsurface. The reflected signal was received by a recording system called “streamer” and transmitted to the ship, where it was stored. The setup of the equipment is illustrated in Fig. 4.3.

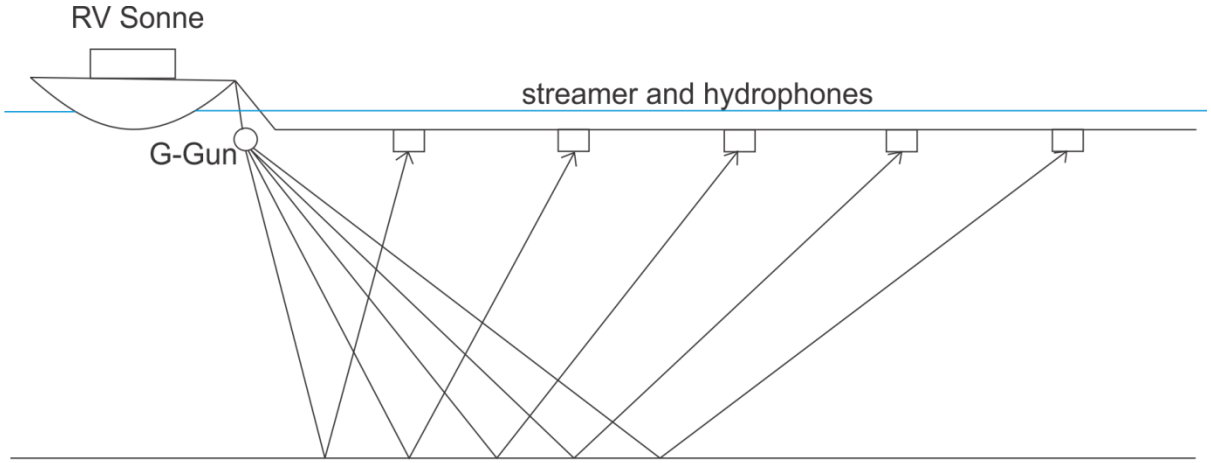

Fig. 4.3: Schematic of data acquisition.

Three of the thereby recorded profiles will be processed and analyzed in the following chapters. The length of these profiles vary between 334 and 467 km (Gohl and Werner, 2016). Detailed profile parameters are listed in Tab. 4.2.

Tab. 4.2: Detailed parameters of the profiles processed during this work. (Gohl and Werner, 2016)

Profile #	Start/End	Date (UTC)	Time (UTC)	Coordinates Latutude	Longitude	Shot #	Record length [s]	Sample rate [ms]	Shot interval [s]	Profile length [km]	G-Gun array
AWI-20160001	start	09.02.2016	16:28	-46.99043	-174.24231	1	15	1	20	467	6 x 520 in³
	end	11.02.2016	19:04	-42.96710	-175.92074	9112					
AWI-20160003	start	24.02.2016	21:00	-42.70846	-174.62425	1	15	1	20	404	6 x 520 in³
	end	26.02.2016	17:00	-45.50253	-171.40743	7027					
AWI-20160301	start	06.03.2016	16:43	-45.02136	-166.72112	1	15	1	60	334	8 x 520 in³
	end	08.03.2016	4:52	-42.35049	-168.60015	2170					

Seismic source

Profile AWI-20160001 as well as profile AWI-20160003 were acquired with an array of 6 G-Guns (51 l / 3120 in³) using a shot interval of 20 s. The easternmost profile AWI-20160301 was recorded by an array of 8 G-Guns with a shot interval of 60 s. For the data acquisition, the G-

Gun arrays were towed behind the ship at an adjusted depth of 6 m. A combined electric trigger-clock system was used to synchronize the firing signal of the seismic source with the time-control of the seismic data recording system. UTC date and time were provided by a *Meinberg GPS*, mounted on the upper deck of the RV Sonne. (Gohl and Werner, 2016)

Multi-channel recording system

For the recording of the multi-channel seismic reflection data a digital solid seismic streamer was used in combination with a high-resolution marine seismic data acquisition system consisting of *SERCEL Sentinel* and *SEAL* to integrate the on-board and in-sea equipment. The streamer is 3000 m long and contains a 240-channel array with a group interval of 12.5 m including 8 hydrophones per group. 12 *DigiBirds* were mounted on the streamer to adjust the water depth. The data collected by the streamer were transferred to the on-board equipment via a fiber optic tow leader and a deck lead. Afterwards the seismic data passed different converting processes. (Gohl and Werner, 2016)

4.4 - Seismic data processing

With the help of so-called jobflows partly being based on each other while performing different tasks, the data quality can be improved significantly. The aim of the data processing is to illustrate the subsurface as good as possible. Since seismic reflection data can be very diverse, the style of processing and determination of single parameters is crucial and has to be developed individually. Hereto, the seismic data processing software *Paradigm Echos 15.5*

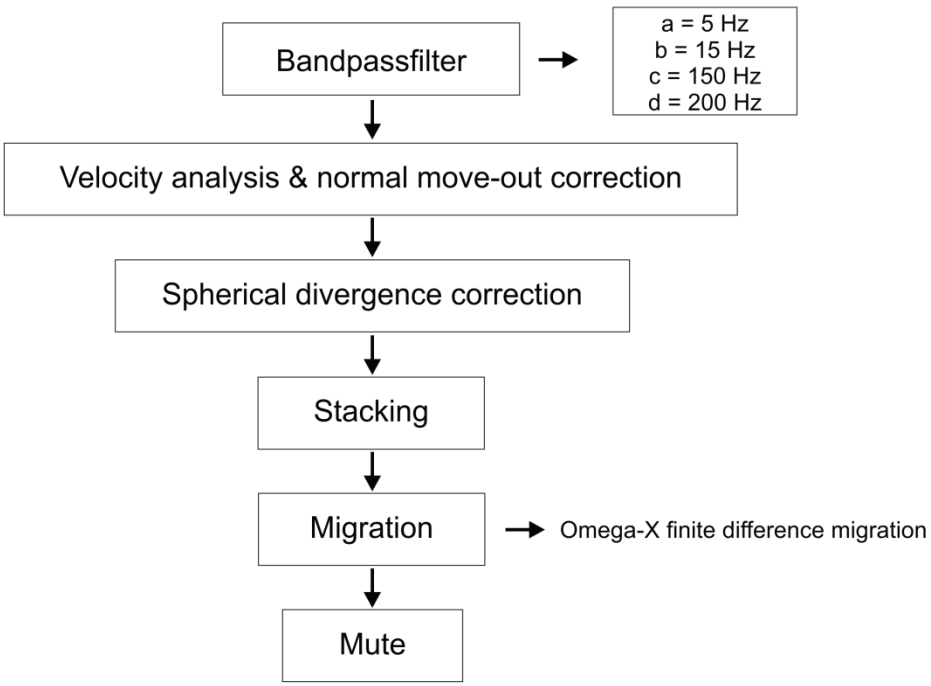

Fig. 4.4: Flowchart of processing steps applied to the seismic reflection data profiles AWI-20160001, AWI-20160003 and AWI-20160301 during this work.

was used. Fig. 4.4 summarizes the processes, which have been applied to the data within this thesis and will be explained hereafter.

Preprocessing

The preprocessing of the data has already been done on board of the RV Sonne during the expedition SO246. This is the first step, which has to be performed before the processing of the data and includes the set-up of the geometry and binning of traces. The geometry set-up is an important step to make sure that all values are correct in the end of the processing. Hereto, it is crucial to know the geometrical array of the equipment during the data acquisition. This includes the position of the G-Gun, the streamer and the GPS, as well as date and time of the recording. The next step is to sort the data from shot to common mid-point (CMP) domains (Veeken and van Moerkerken, 2013). By the binning of traces with several mid-points, which are summarized thereby, the noise can be reduced. Fig. 4.5 illustrates the geometric concept of CMPs.

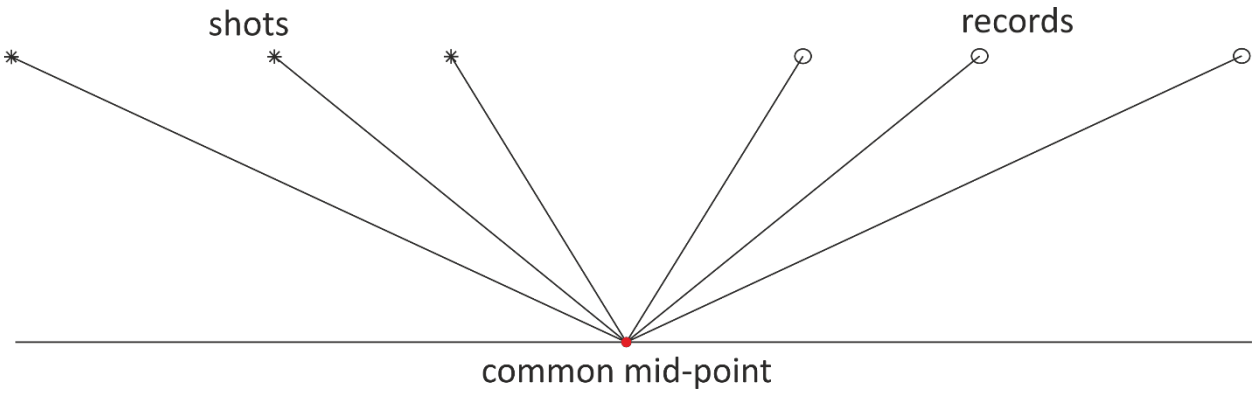

Fig. 4.5: Geometric concept of CMPs.

Bandpassfilter

The bandpassfilter is used to delete frequencies, which are not relevant for the result and could worsen the data quality. The aim of this method is the improvement of the signal-to-noise ratio. Noise can be subdivided into random noise, which is generated for instance by the movement of the ship, wind, waves as well as rain and coherent noise generated by the source. The bandpassfilter uses four frequencies, as shown in Fig. 4.6. All frequencies smaller than the lowermost frequency (a) and bigger than the highest frequency (d) will be eliminated. While the chosen middle-frequencies are representing the used signal frequency, all frequencies below the lower one (b) and above the upper frequency (c) are faded out.

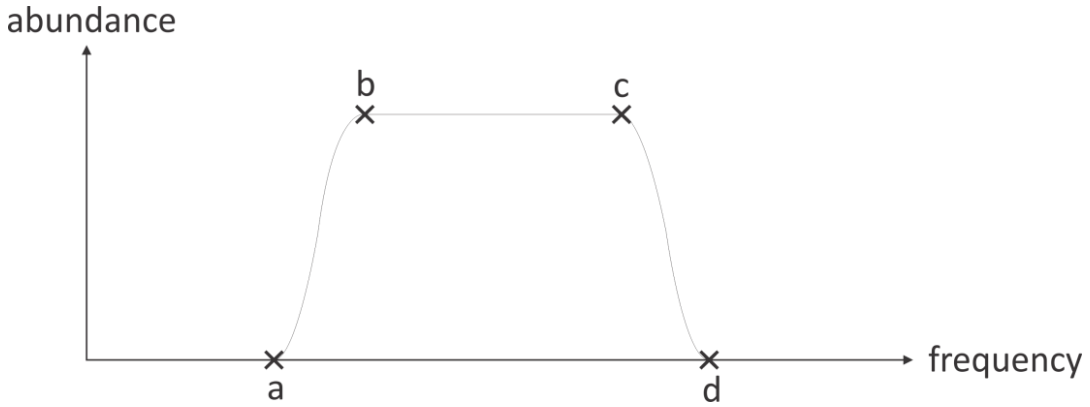

Fig. 4.6: Theoretical example for a bandpassfilter.

Since the source signal was around 50 Hz the following frequencies were chosen as parameters for the bandpassfilter to eliminate all noises that are not in between the range of expected record frequencies:

a = 5 Hz

b = 15 Hz

c = 150 Hz

d = 200 Hz

Fig 4.7 shows the effect of a bandpassfilter with the chosen parameters on the profile AWI-20160001, taken on the cruise SO246. The noise was reduced successfully, so that the received source signal can be imaged very well.

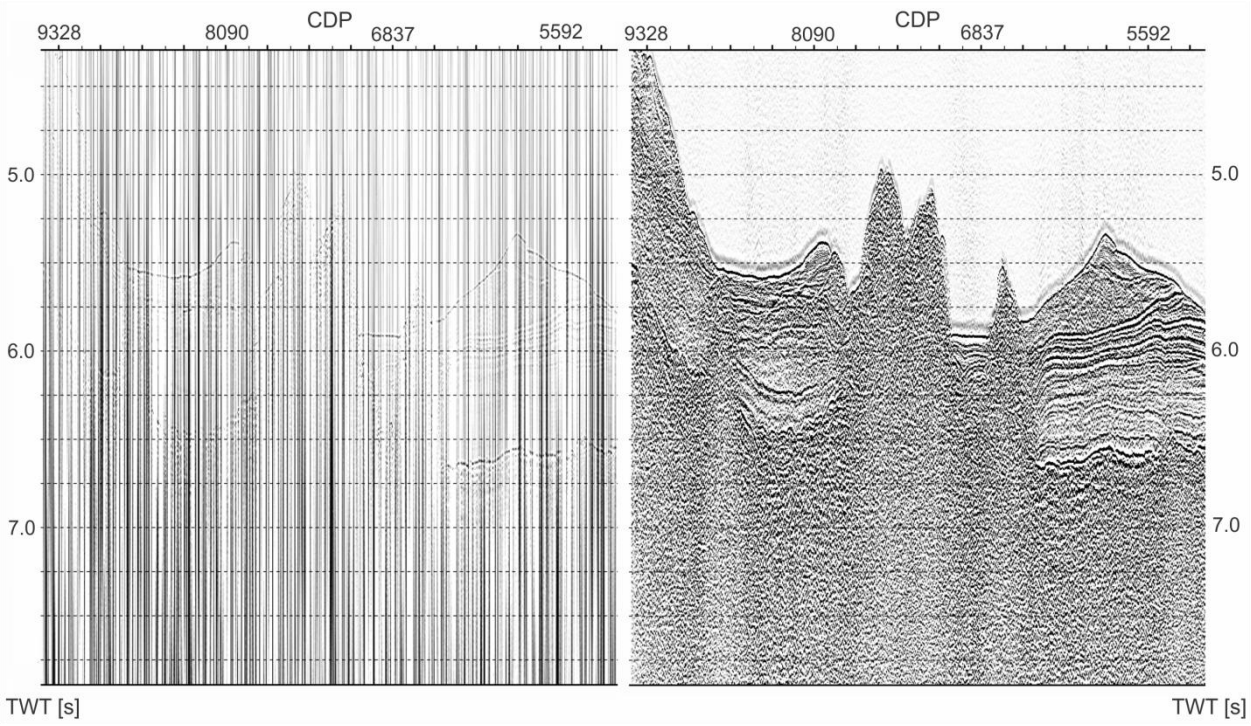

Fig. 4.7: Cutout from profile AWI-20160001 before (left) and after (right) applying the bandpassfilter. The Y-axis shows the two-way-traveltime (TWT), while the X-axis shows the common depth-point (CDP).

Velocity analysis and normal move-out

The velocity analysis is an important and the most time-intensive step of the seismic data processing. It serves to correct the normal move-out (NMO), which is the effect on the travel-time produced by the distance between source and receiver. To compensate this delay, reflections of different traces of same common mid-points are tried to be aligned in one line. The time difference Δt, which is formed by the NMO can be described for the seafloor with the following formula (x represents the offset, v the velocity and t_0 the start time):

$$\Delta t = \frac{x^2}{2v^2 t_0}$$

To determine the NMO for the layers below the seafloor, it is necessary to do a velocity analysis beforehand. At this step, the root-mean-square velocities of strong reflections were picked (Fig. 4.8). After the NMO correction primary reflectors should be illustrated in a horizontal row (Fig. 4.9). Another feature of this adaption is the reduction of the influence of multiples, which originate in a second reflection of the signal at the sea surface.

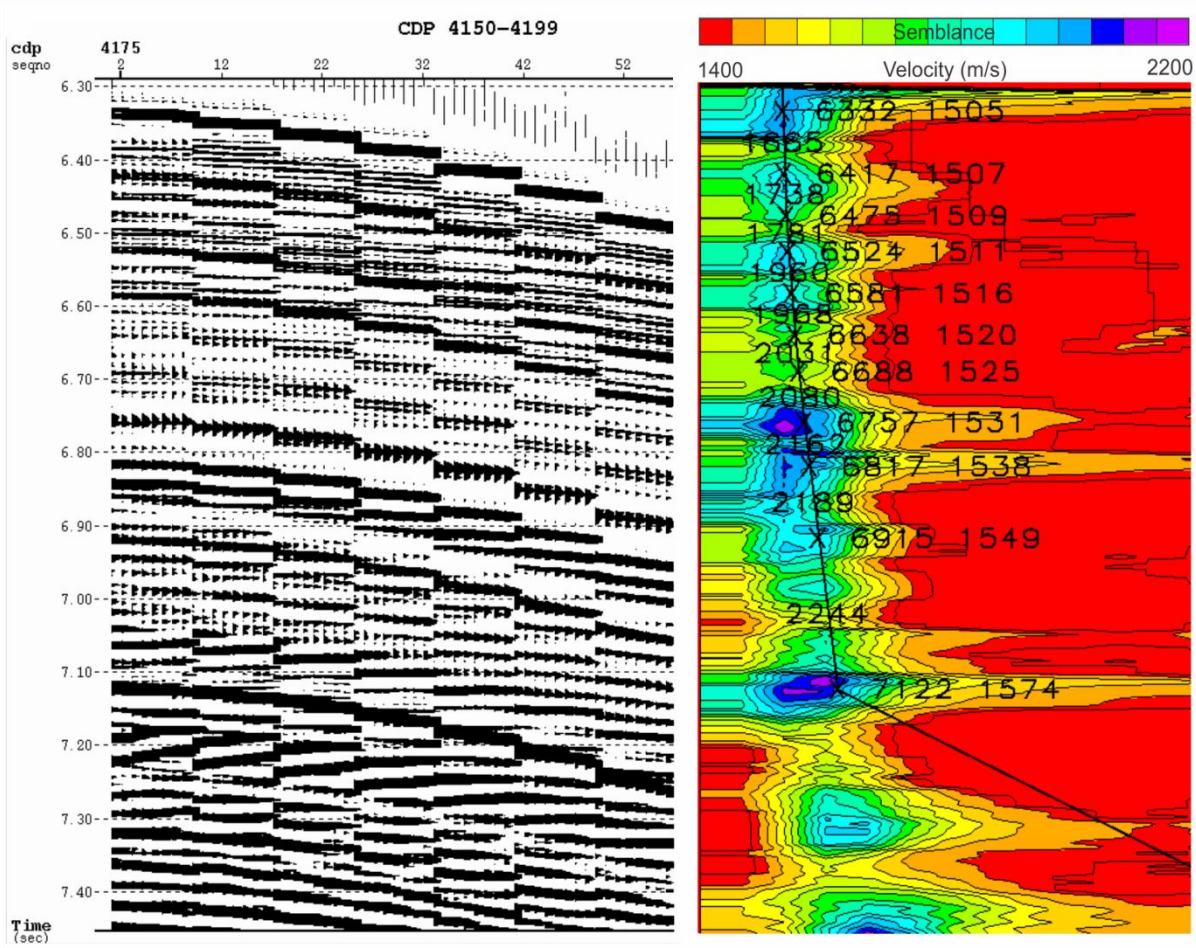

Fig. 4.8: Example for the picking of velocities with Paradigm Echos 15.5.

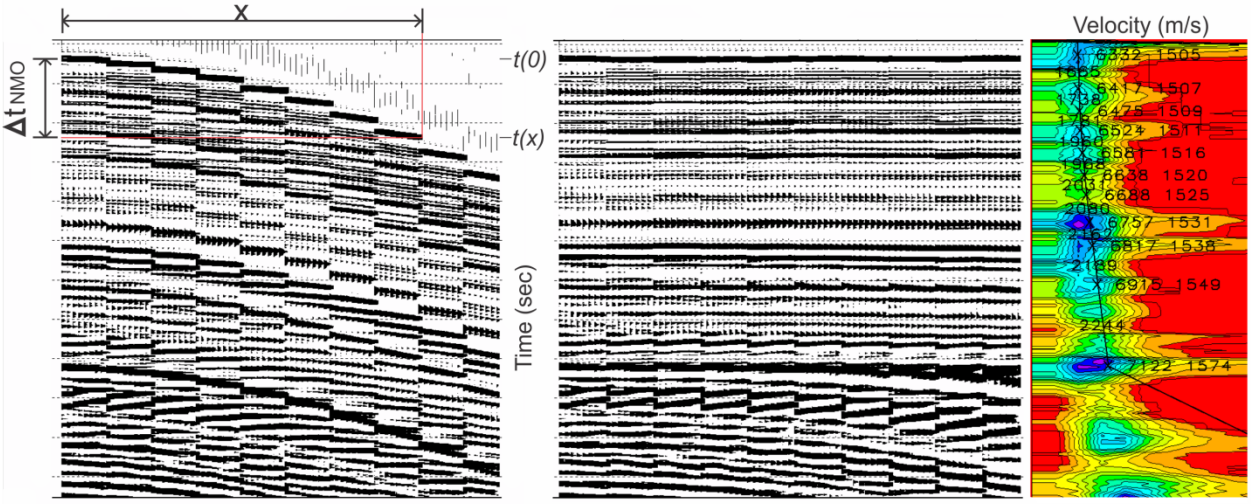

Fig. 4.9: Example for the NMO correction.

For the picking of velocities with *Paradigm Echos 15.5* single job-flows were created for the three profiles. These job-flows contained three modules. The first one is the DSIN-module, which included the loading of the CDP sorted data, a setup of the time range of the TWT and a selection of the CDP-range. Additionally, the number of CDPs in each picking-window and the increment between these picking-windows were defined. These were varying in relation to parts of interest in the single profiles. Profile AWI-20160301 was picked with an increment of 50 CDPs and a number of 50 CDPs from CDP 2650 to 5499. Regions of steep slopes were picked with an increment and number of 10 CDPs to illustrate more details. Profile AWI-20160003 was also picked with an increment of 50 CDPs and a number of 50 CDPs from CDP 9200 to 16249, while profile AWI-20160001 was picked with an increment of 100 CDPs and a number of 50 CDPs from CDP 100 to 10599. The second job-module was a bandpassfilter, which used the parameters already mentioned, while the last one was the VELDEF-module, used to determine the filename to store the picked velocities. After running the job, as much continuous reflectors as possible, starting with the seafloor and ending in the basement were picked in each window. The picked velocities for the seafloor were varying between 1507 m/s in sedimentary areas up to 1567 m/s in areas of seamounts. The subsurface reflectors showed velocities of 1509 m/s in the uppermost parts to more than 2400 m/s in the lowermost parts. The resulting velocity model was then loaded into the migration job-flow. Uncertainties during the velocity picking occurred because of a bug in the display of the semblance, which should help the geophysicist to find areas of importance and sometimes did not work. Another error origins in the graphical resolution of *Paradigm Echos 15.5* on the used screen and results in an error of 2 m/s for the picking of velocities.

Spherical divergence

The spherical divergence correction serves to compensate the amplitudes of single traces. It adjusts the loss of energy of the seismic signal with increasing travel-time to better illustrate the deeper layers of the underground. For this adaption the GAIN-module of *Paradigm Echos 15.5* was utilized.

Stacking

With the 'stacking', traces of one common-mid-point are summarized in one trace to improve the signal-to-noise ratio by the reduction of the noise of single channels. Furthermore, the data volume is being reduced.

Migration

The migration is the correction of the scattering of waves at edges and coarse surfaces etc., which can lead to the occurrence of diffraction hyperbolas as shown in Fig. 4.10. The aim of this step is to reconstruct the true subsurface position of reflectors to get a better spatial resolution (Yilmaz, 2001). With the module MIGFX of *Paradigm Echos 15.5* a finite difference migration in the Omega-X domain has been performed on the data. This function can process both lateral and vertical velocity variations and can improve the data quality. Since there were less diffraction hyperbolas in the data the effect of the migration is rather low, but enhances the differentiation between reflectors (see Fig. 4.11).

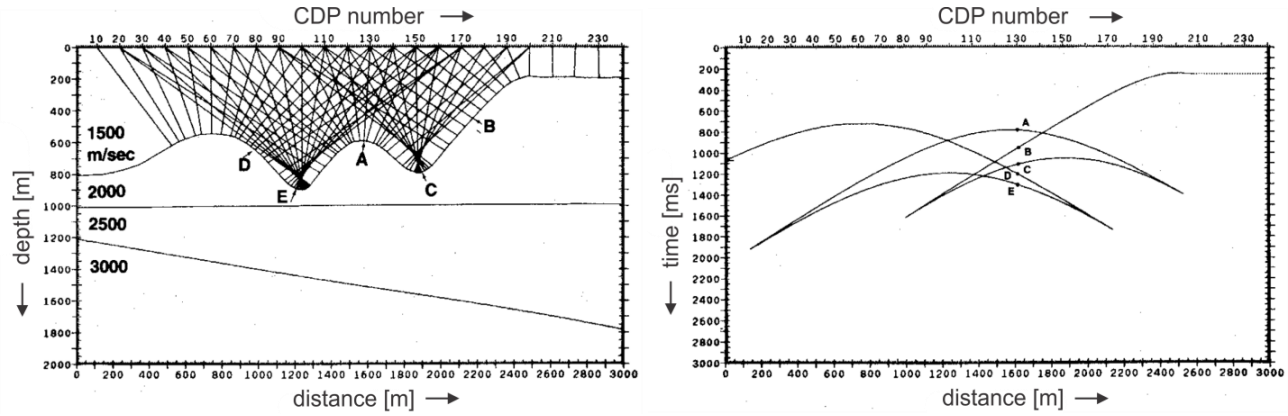

Fig. 4.10: Geometric concept of diffraction hyperbolas. (from Yilmaz, 2001)

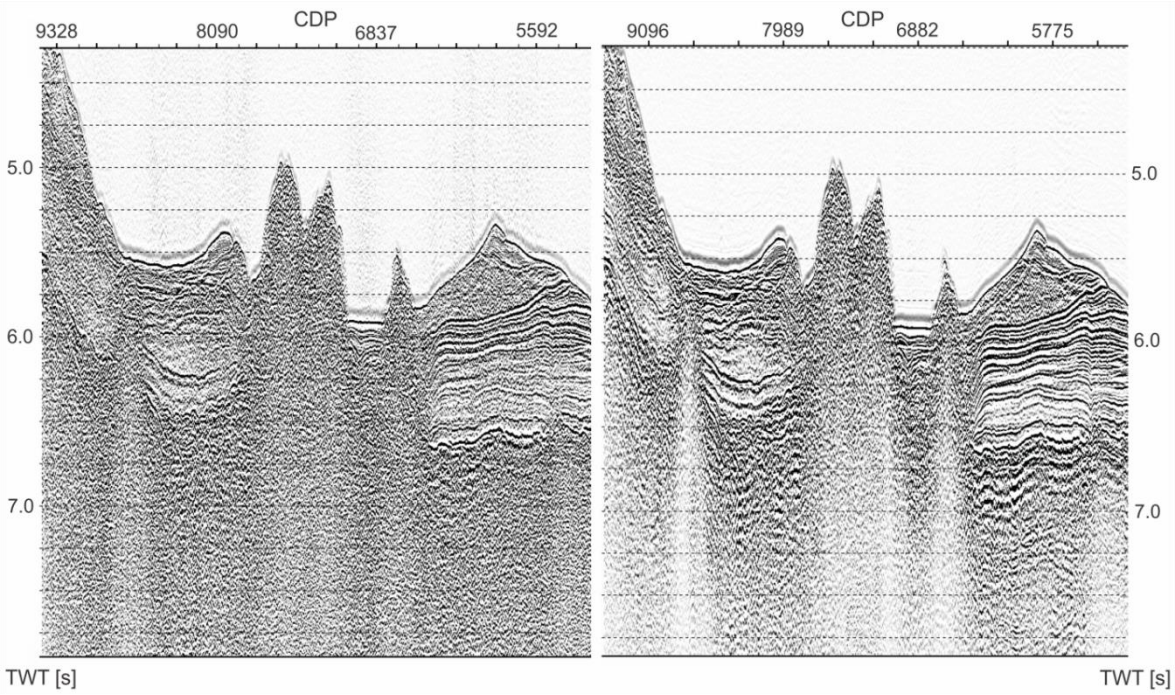

Fig. 4.11: Cutout from profile AWI-20160001 before (left) and after (right) the migration.

Mute

Finally, the MUTE-module of *Paradigm Echos 15.5* was used to clear the data from all signals, which occur in the water column. The data produced during the migration were illustrated and a MUTE-file was created by picking along the seafloor. This file was loaded into the migration-jobflow with the MUTE-module to display the water-column as white-colored area. Fig. 4.12 shows a cutout of Profile AWI-20160001 before and after this procedure.

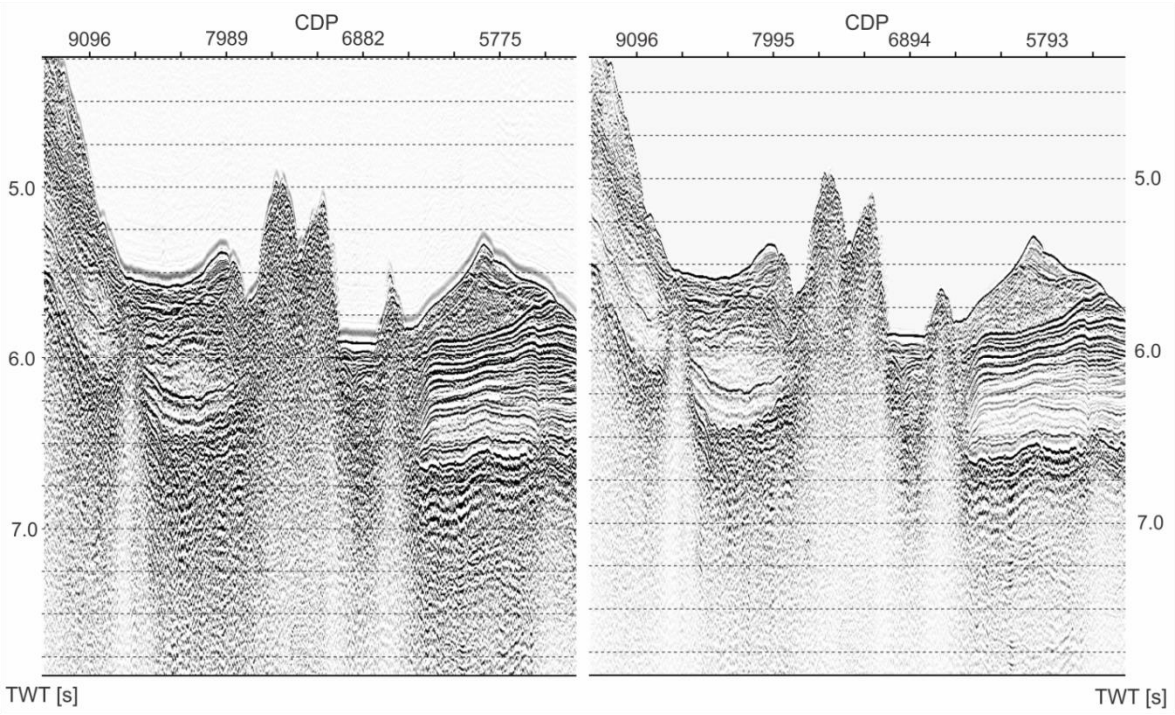

Fig. 4.12: Cutout from profile AWI-20160001 before (left) and after (right) applying the MUTE-module.

4.5 - Additional data

Parasound data

A sediment parametric echosounding system called *Parasound DS III-P70* was used for a better resolution of the uppermost layers of sediment (Gohl and Werner, 2016). It consists of a transmitter, a receiver and a transducer. The Parasound system generates two primary frequencies, which lead to the so-called 'Parametric Effect' and create two secondary frequencies as a result of the non-linear acoustic water behavior. The lower primary frequency can be selected between 18 kHz and 23.5 kHz and the produced secondary frequencies are the difference and the sum of the two primary ones. The primary frequencies used for the data acquisition were 20 kHz and 24 kHz, leading to secondary frequencies of 4 kHz and 44 kHz (Gohl and Werner, 2016). Depending on sediment conditions, these frequencies can allow a sub-bottom penetration of up to 100 m and a vertical resolution of about 30 cm. A higher frequency leads to a lower penetration depth and better resolution, while a lower frequency causes a deeper penetration depth, but a lower resolution. The Parasound sediment-echosounding is characterized by a very high lateral resolution, caused by a sediment-penetrating pulse generated within the narrow beam of the primary frequencies. (Gohl and Werner, 2016)

A software package consisting of *ATLAS HYDROMAP CONTROL* and *ATLAS PARASTORE-3* was used to control the Parasound system (Gohl and Werner, 2016). With *ATLAS HYDROMAP CONTROL* an operator can run the system, while *ATLAS PARASTORE-3* is used for the on-line visualization and processing of received data, data storage in different output formats (PS3 and SEG-Y) and printing. *HYDROMAP SERVER* functions as a database server and is not visible on the monitor. Later on, PS3 data was loaded in and visualized by the program SENT, where TWT can be converted to water depth. (Gohl and Werner, 2016)

Bathymetric data

For the detailed bathymetric mapping of the seafloor on SO246 a hull-mounded multibeam echosounder called *Kongsberg Simrad EM122* was deployed (Gohl and Werner, 2016). This system delivers information about the horizontal behavior of bathymetric structures like seamounts, ridges and even elevations of sediment drifts. The *EM122* works with a frequency ranging from 10.5 kHz to 13 kHz. The transducer arrays are arranged in a hull-mounted Mills Cross configuration, which means that receiver and transmitter are mounted vertically to each other. The opening angle was 65° to both sides to obtain a wide field of surveyed data, while keeping good quality in the outer beams. The width of the 'footprint' depends on the distance of the system to the seafloor, whereby the approximate swath width is 4.4 times the water depth (see Fig. 4.13). For the processing and cleaning of the bathymetric data a program called *Caris HIPS* was utilized. (Gohl and Werner, 2016)

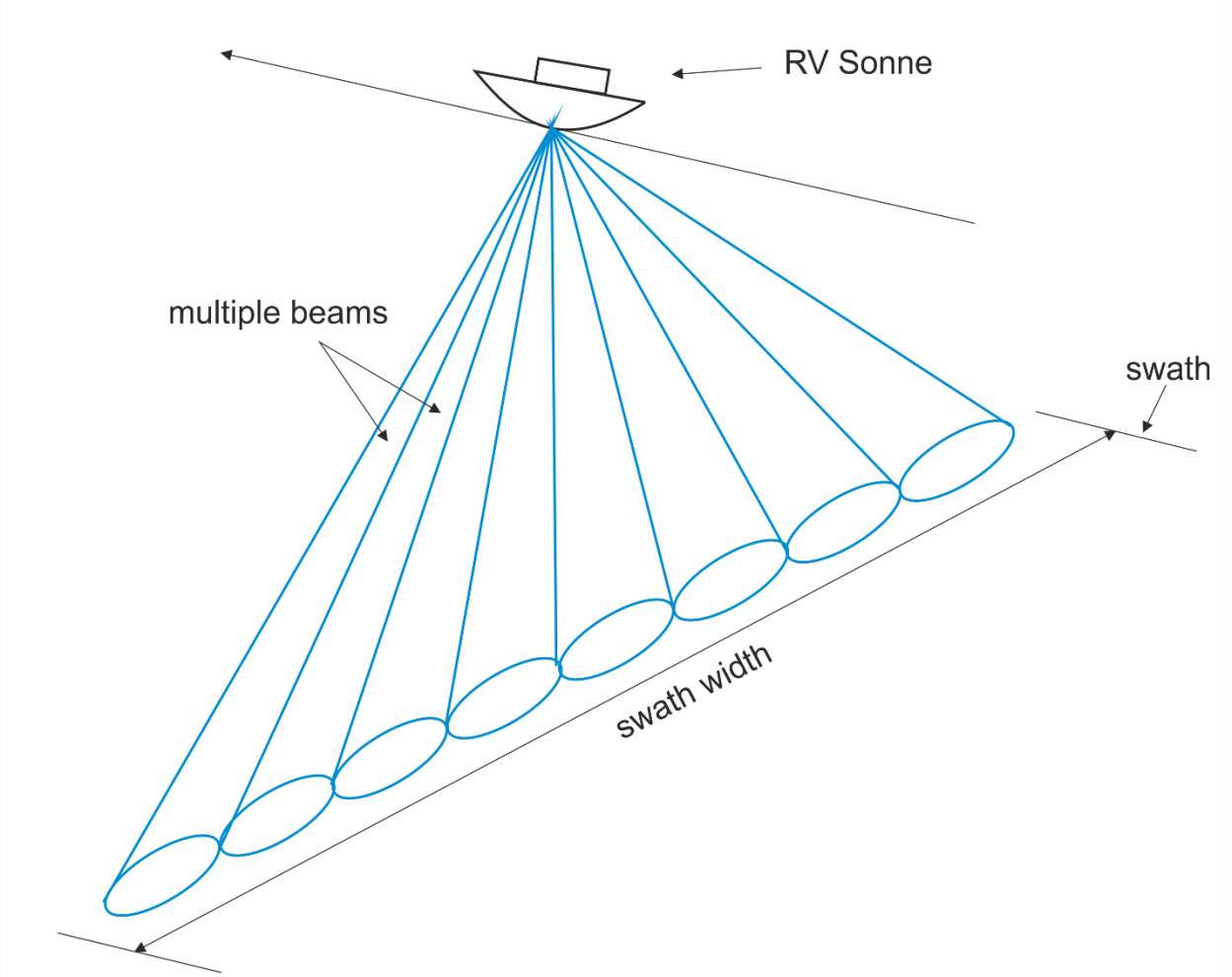

Fig. 4.13: Graphical illustration to explain the functioning of a multibeam echosounder.

5. Results

5.1 - Seismic reflection data results from SO246

The successful processing of the seismic reflection profiles AWI-20160001, AWI-20160002, AWI-20160003 and AWI-20160301 enables an insight into the subsurface of the seafloor. Different units were defined in each profile and combined with units of the other profiles to create a 3D-understanding of the work area. Four main units, as well as four main horizons, which are separating these units from each other, were discovered between basement and seafloor in the seismic data profiles. The location of the acoustic basement was determined with the help of velocity models from refraction seismic data processed by Florian Riefstahl. Since there are no drill core data existing in the work area, it is not possible to distinguish the crystalline basement from metasediments, which were recrystallized by metamorphism. In the following subchapters, these seismic profiles and the selected horizons will be presented and

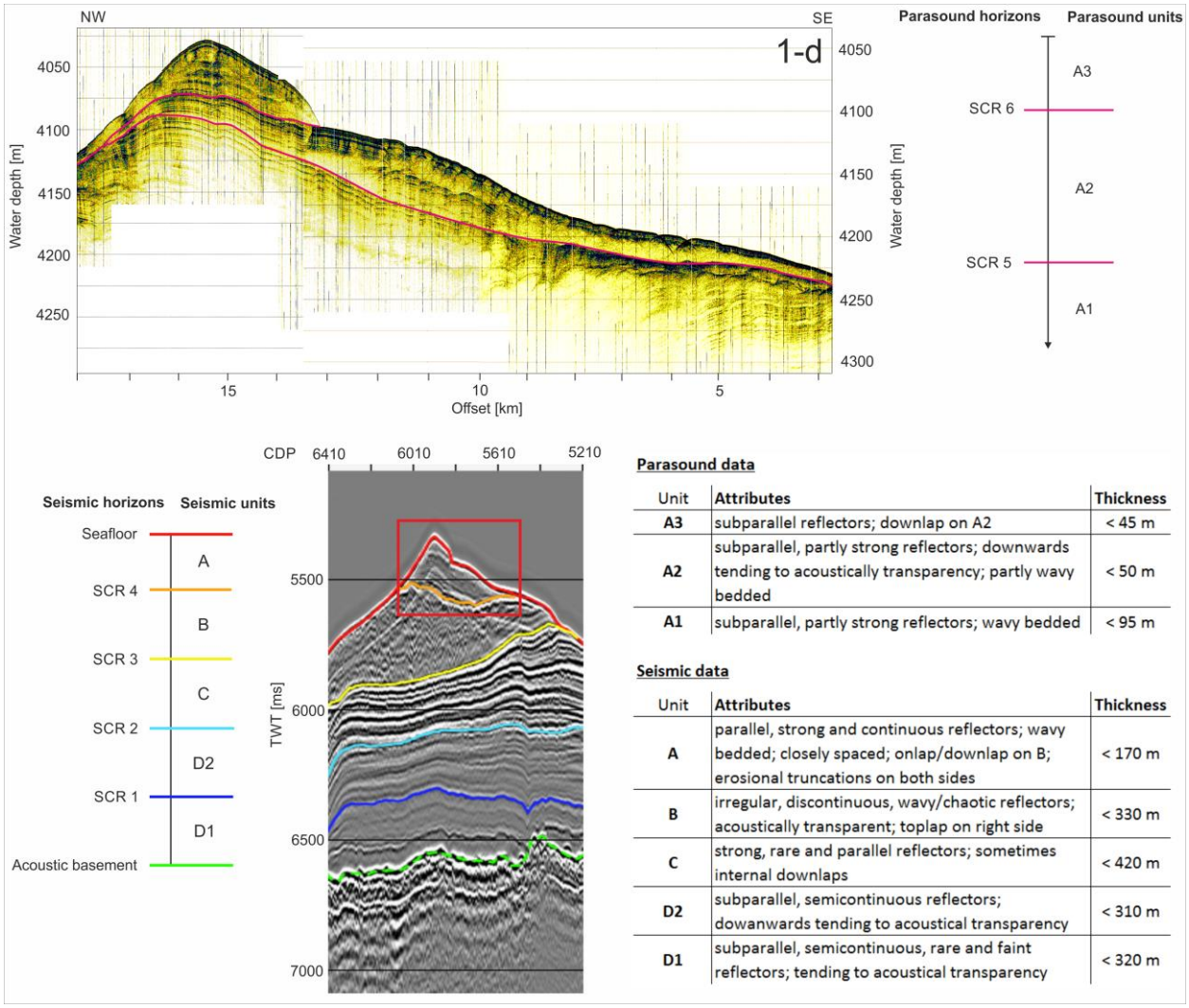

Parasound data

Unit	Attributes	Thickness
A3	subparallel reflectors; downlap on A2	< 45 m
A2	subparallel, partly strong reflectors; downwards tending to acoustically transparency; partly wavy bedded	< 50 m
A1	subparallel, partly strong reflectors; wavy bedded	< 95 m

Seismic data

Unit	Attributes	Thickness
A	parallel, strong and continuous reflectors; wavy bedded; closely spaced; onlap/downlap on B; erosional truncations on both sides	< 170 m
B	irregular, discontinuous, wavy/chaotic reflectors; acoustically transparent; toplap on right side	< 330 m
C	strong, rare and parallel reflectors; sometimes internal downlaps	< 420 m
D2	subparallel, semicontinuous reflectors; dowanwards tending to acoustical transparency	< 310 m
D1	subparallel, semicontinuous, rare and faint reflectors; tending to acoustical transparency	< 320 m

Fig. 5.1: Stratigraphic reference and attributes of seismic units in a chosen section of profile AWI-20160001, shown in the illustration below. A section of the Parasound data with interpretation is shown above.

described. Additionally, Parasound records will be utilized as supplementary information about the uppermost layers. The Parasound data expose up to three subdivisions of the topmost unit in specific parts of the profiles. A typical vertical section with classification of horizons and units and their attributes is shown in Fig 5.1. Horizons were named SCR (South Chatham Rise) 1 to 6 upwards from the basement and can be identified by an allocated color, which is presented in Fig. 5.1 and will be used in the following figures. Main units were named A to D from the seafloor downwards and Subunits A1 to A3 and D1 to D2 from the bottom of the unit upwards. Enlarged figures of all seismic reflection (Appendix A and B) and Parasound (Appendix C) profiles can be found in the appendix.

Profile AWI-20160001

Profile AWI-20160001 (Fig. 5.2) extends from the northern flank of Chatham Rise (water depth of around 1000 m) southwards downslope the Chatham Rise to a water depth of more than 5000 m. The total profile length amounts to 467 km, but a cutout from CDP 66 to 9200 was chosen to focus only on sediment structures, which will be significant for the interpretation. The seafloor water depths are ranging between a minimum of 4350 ms and a maximum of 6750 ms TWT, generally decreasing from north to south. Four main units disrupted by seamount structures were identified above the assumed acoustic basement, which reaches down to a maximum depth of 1300 ms TWT below seafloor. It is characterized by a strong but discontinuous reflector, which underlies the sediment bodies. At CDP 3500 to 3700, 6500 to

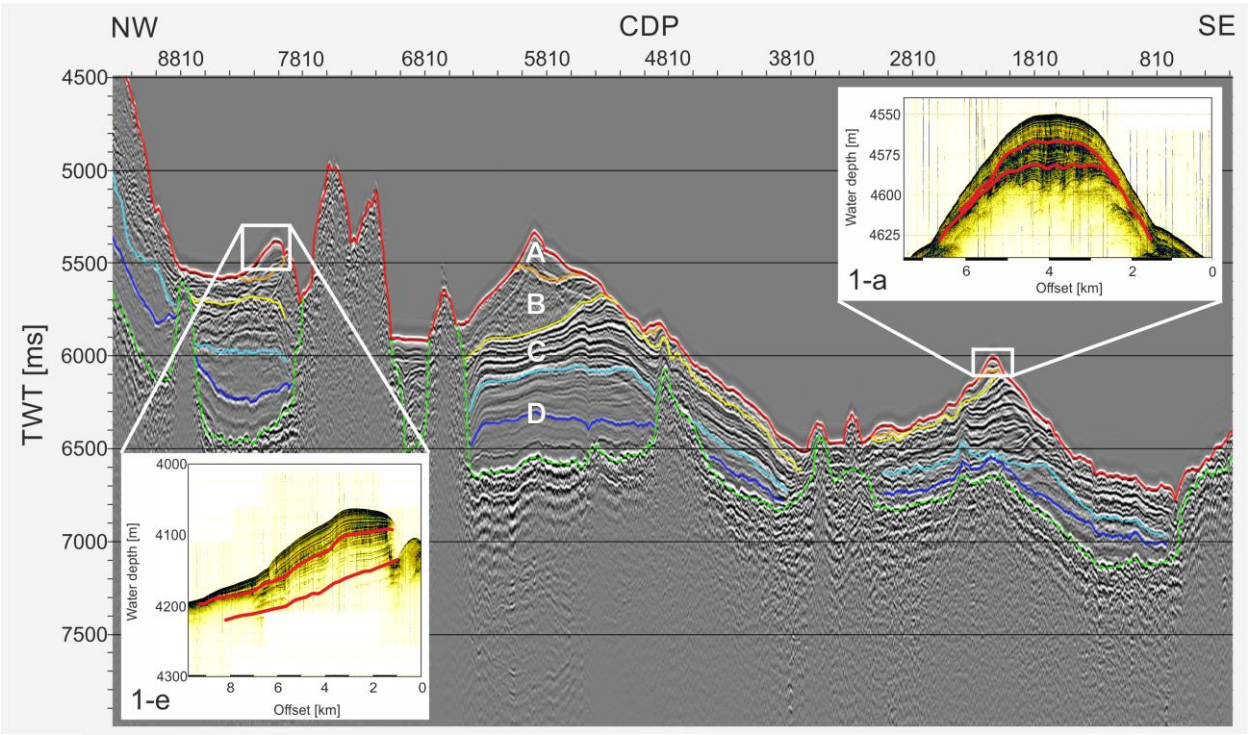

Fig. 5.2: Seismic reflection profile AWI-20160001, additionally Parasound profiles 1-a and 1-e. An explanation of the seismic interpretation (horizon colors and unit classification) can be adopted from Fig. 5.1.

6750 and 7050 to 7800 it outcrops as seamounts. Unit D is the lowermost horizon detected in this profile and overlies the assumed basement. It can be traced from CDP 750 to 2000, 3900 to 4550, 4900 to 6450, 7900 to 8700 and 8900 to 9200. The thickness ranges from 200 ms to 500 ms TWT. Unit D can be subdivided into two Subunits, D1 and D2, which are both characterized by subparallel, discontinuous reflectors and in some cases acoustic transparency. They are separated by a comparatively strong reflector (SCR 1), which distinctly appears from CDP 7900 to 8700 and 8900 to 9200. From CDP 4900 to 6450 it occurs in a less continuous, sometimes transparent character. Unit C overlies Unit D, showing onlap (CDP 1300 to 1700) and downlap (CDP 5100 to 5300) structures on reflector SCR 2. Erosional truncations can be found where Unit C outcrops (CDP 1800 to 2000 and 5100 to 5250). It is characterized by strong reflectors, which are losing intensity downwards. From CDP 4900 to 6450 reflectors are bedded parallel, whereas in other cases, like for example from CDP 7900 to 8700 they are less continuous. The thickness reaches up to 400 ms TWT. At CDP 2350 Unit C shows an erosional truncation on the overlying Unit B, which is separated by a strong reflector called SCR 3. It distinguishes by chaotic, discontinuous, wavy bedded reflectors with lower amplitude and extends from CDP 2100 to 3200, 3700 to 5000, 5300 to 6600 and 7900 to 8700. The thickness highly varies from less than 20 ms at CDP 2850 to 400 ms TWT at CDP 6000. Erosional truncations can be found at CDP 2400 and 5400. An unconformity (SCR 4) marks the border to Unit A, which overlays Unit B with onlap (CDP 2100, 4900 and 8000) and downlap (CDP 2100 and 3000) structures. It occurs as small depositions at CDP 2100 (Fig. 5.2, 1-a), 3000 (1-b, appendix: Fig. C.4) and 4900 (1-c, appendix: Fig. C.6), whose internal reflectors cannot be resolved by multi-reflection seismic, but by Parasound. Two bigger depositions, which are located at CDP 5500 to 6100 (1-d, appendix: Fig. C.8) and 8050 to 8400 (Fig. 5.2, 1-e) show closely spaced, weak but continuous and subparallel reflectors, which are wavy bedded. Parasound data exposes an internal separation of three subunits, separated of each other by reflectors SCR 5 and SCR 6 and often show onlaps. Unit A reaches a thickness of 200 ms at CDP 5900. Enlarged figures 1-a to 1-e can be found in the appendix.

Profile AWI-20160002

The profile length of the profile AWI-20160002 (Fig. 5.3) amounts 106 km and the water depth ranges between 2100 and 3600 m, generally decreasing from northwest to southeast. It is located at the southern flank of Chatham Rise central between the profiles AWI-20160001 and AWI-20160003. Profile AWI-20160002 is interrupted by a data gap, occurring from CDP 2600 to 2750. The acoustic basement, which irregularly shows up as high-amplitude reflectors, wavy extends with varying water depths and builds a seamount from CDP 400 to 650. It is overlain by Unit D, which occurs from the beginning of the profile until CDP 3300, but is disrupted by several basement highs (at around CDP 600, 1200 and 1500). Unit D is characterized by wavy

and discontinuous low amplitude reflectors and partly acoustic transparency. From CDP 1220 to 3300 a discontinuous reflector (SCR 1) occurring sometimes with low and sometimes with high amplitude, divides the unit into D1 and D2. D2 appears more homogenous, while D1 shows areas of acoustic transparency (CDP 2800 to 3300) and also areas with chaotic high amplitude reflectors (CDP 2400 to 2600). The thickness of D1 varies between 100 to 500 ms TWT. D2 shows thicknesses from 200 to 450 ms TWT, but since SCR 1 could not be traced in the sediment deposition at the beginning of the profile and the exact basement depth is unknown, thicknesses are probably higher. A light and wavy reflector (SCR 2) marks the boundary to Unit C, which is distinguished from Unit D by wavy, subparallel, partly discontinuous reflectors of mostly high amplitude. Unit C extends from CDP 4100 downslope until the end of the profile with varying thicknesses of 100 to 600 ms TWT. It shows erosional truncations at the boundary (SCR 3) to Unit B (CDP 2300 to 2500), which on its part shows an onlap at this point. The overlying Unit B occurs in three disconnected depositions extending downslope from CDP 3100 to 4100, as a horizontal deposition from CDP 1100 to 3000 and from the beginning of the profiles to CDP 360. These sections show similar characteristics of wavy bedded, discontinuous and chaotic reflectors of low amplitude. In the lower part high-amplitude reflectors can also be found in small areas (e.g. CDP 2100 to 2300). Erosional truncations (CDP 3100 to 3220, CDP 2800 to 3000 and CDP 150 to 250) mark the boundary to Unit A, which is characterized by subparallel, sometimes wavy bedded and mostly continuous reflectors. From CDP 1150 to 3500 it shows thicknesses of 100 to 300 ms TWT,

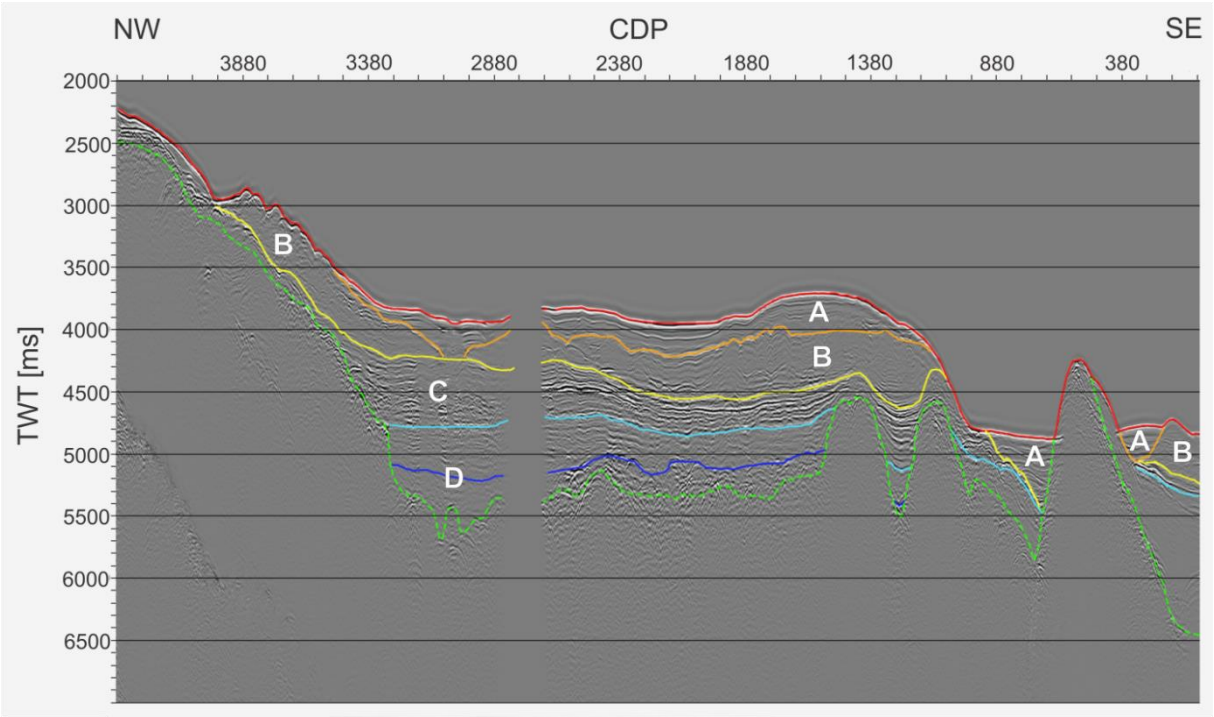

Fig. 5.3: Seismic reflection profile AWI-20160002. An explanation of the seismic interpretation (horizon colors and unit classification) can be adopted from Fig. 5.1.

partly onlaps on Unit B (e. g. CDP 2300 to 2400, 3100 to 3200) and an erosional truncation from CDP 1200 to 1400. From CDP 150 to 360 and 650 to 900 Unit A occurs as basin fill, onlapping at the boundary to Unit B (CDP 150 to 360), the boundary to Unit C and the uprising basement (CDP 650 to 900).

Profile AWI-20160003

The profile AWI-20160003 (Fig. 5.4) extends over 404 km from the northern flank of Chatham Rise in a water depth of around 2400 m southeast downslope the southern flank of Chatham Rise to a water depth of around 5000 m. It has been analyzed from CDP 9200 to CDP 16300, where water depths are ranging between 4500 to 6600 ms TWT, generally decreasing from north to south. In this profile the same units identified in profile AWI-20160001 and AWI-20160002 could be found, but differences in the appearance were recognized. The acoustic basement shows high amplitudes and a ragged behavior from CDP 10000 to 11300, then rises up as a seamount until CDP 13000 and can only be traced by rarely appearing high-amplitude reflectors to the end of the profile. It is overlain by large sediment depositions, which can be found from CDP 9500 to the end of the profile and are disrupted by the mentioned seamount. Unit D with a thickness of up to 750 ms TWT extends from CDP 9750 to the end of the profile and is characterized by acoustic transparency in the lowermost layers and partly strong, sometimes wavy reflectors in the uppermost layers (CDP 10500 to 11300), which are losing

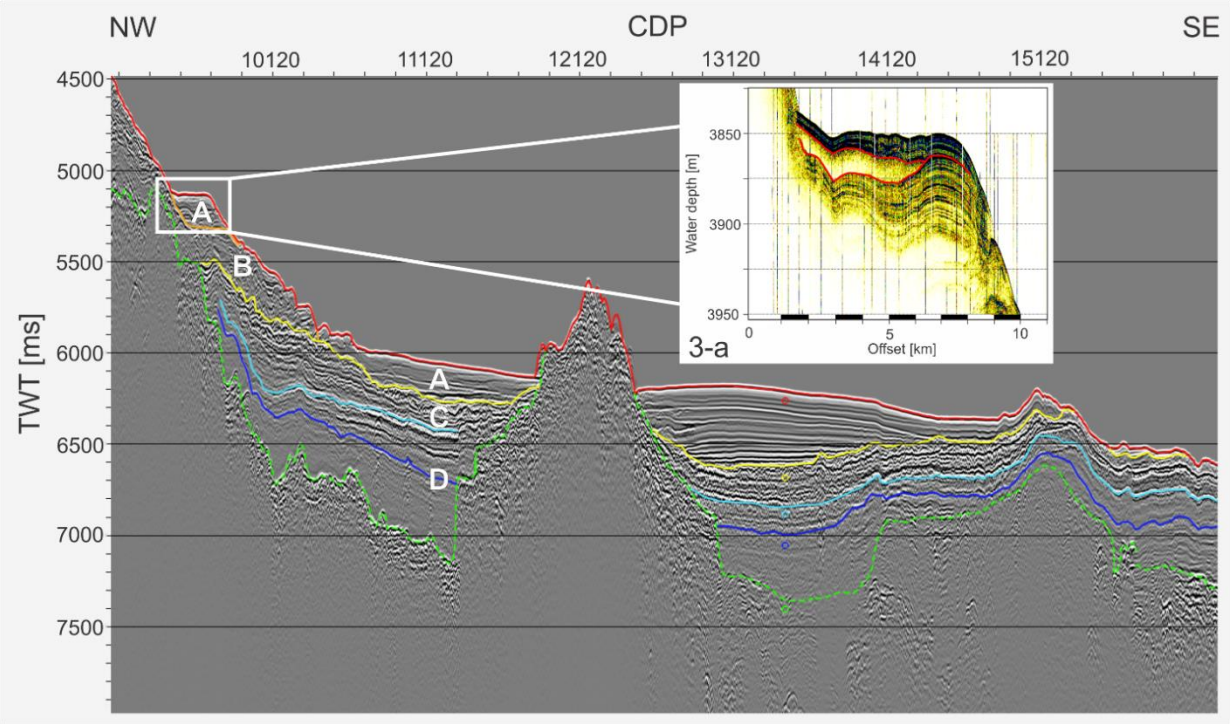

Fig. 5.4: Seismic reflection profile AWI-20160003, additionally Parasound profile 3-a. An explanation of the seismic interpretation (horizon colors and unit classification) can be adopted from Fig. 5.1. Little, colored circles mark the intersection points with horizons from profile tan0207-cr2.

intensity downwards. A distinct reflector (SCR 1) separates Unit D into D1 and D2. D1 mostly appears acoustically transparent with partly strong discontinuous internal reflectors (CDP 13000 to 15000). In D2 reflectors are partly strong and partly tending to acoustic transparency (CDP 10500 to 11300). A strong reflector (SCR 2) marks the boundary to Unit C, which overlies Unit D and has a thickness of around 200 ms TWT. From CDP 1000 to 11300 it has a wavy but continuous character, while from CDP 12600 onwards it appears more chaotic. Unit C is featured by strong, discontinuous reflectors from CDP 10500 to 11500 and strong, but very chaotic reflectors from CDP 12600 to the end of the profile. Its upper boundary (SCR 3) is characterized by a sharp unconformity with erosional truncations (CDP 10500 to 11300). Unit B occurs from CDP 9400 to 10400, showing very chaotic, discontinuous reflectors. It reaches a maximum thickness of 280 ms TWT. The uppermost Unit A occurs as four single depositions and has a very variable thickness, ranging between 100 to 450 ms TWT. The first section is located from CDP 9500 to 9800 and shows discontinuous wavy reflectors in the lower part. The upper part can better be resolved by the Parasound (Fig. 5.4, 3-a), where it can be subdivided into three subunits. A1 shows subparallel, wavy reflectors and is overlain by the highly transparent layer A2. The top forms Subunit A3, which shows closely spaced reflectors with very high amplitude. From CDP 10700 to 11800 the so-called “ghost”, which appears when the already by sediments reflected signal is again reflected by the sea surface before it is received by the hydrophones, cuts reflectors in the seismic data. This effect doesn’t appear in the Parasound data, where Unit A can again be divided into three subunits (3-b, appendix: Fig. C.14). This time Subunits A1 and A2 are transparent and limited by wavy low-amplitude reflectors (SCR 4, SCR 5 and SCR 6). The uppermost Subunit A3 is characterized by subparallel, to the south out-thinning reflectors, which show a downlap on A2. From CDP 12500 to 15250 the uppermost layers of Unit A can be subdivided into two packages, based on Parasound data. A1 shows widely-spaced subparallel reflectors with low amplitudes and A2 closely-spaced reflectors with high amplitudes (3-c, appendix: Fig. C.16). A very small deposition of Unit A occurs from CDP 15600 to 16000, where internal reflectors show a wavy character (3-d, appendix: Fig. C.17). Enlarged figures of Parasound profile 3-a as well as 3-b, 3-c and 3-d can be found in the appendix.

Profile AWI-20160301

The profile AWI-20160301 (Fig. 5.5) has a total length of 334 km and is located at the eastern edge of the Chatham Rise, where it extends in southeastern direction. The water depths are ranging between 2600 to 5300 m. AWI-20160301 has been observed from CDP 2650 to 5450, starting in a water depth of more than 5000 ms TWT and generally decreasing to a water depth of 6700 ms TWT. Four main units, occurring in two sediment drift bodies (CDP 2650 to 4500 and 4650 to 5350) have been detected between the seafloor and the acoustic basement, which

is mostly characterized by a discontinuous reflector of high amplitude. It is disrupted by many faults, causing elevations and depressions in the basement reflector. The acoustic basement is overlain by Unit D, which extends from CDP 2650 to 4500 and 4650 to 5350. From CDP 2650 to 4500 sediment thicknesses of Unit D are highly fluctuating because of the faulted basement structure. It shows acoustic transparent areas (CDP 3900 to 3950 and 2850 to 2900) as well as chaotic, discontinuous, strong reflectors in other parts (CDP 3600 to 3800). The upper boundary of Unit D is represented by a wavy reflector (SCR 2) with varying amplitude. From CDP 4650 to 5350 Unit D, which occurs mostly acoustically transparent is subdivided into D1 and D2 by a discontinuous, low amplitude reflector (SCR 1). Both subdivisions show a maximum thickness of around 350 ms TWT. The upper boundary is marked by a semi-continuous wavy reflector (SCR 2). The overlying Unit C shows a very small thickness of 50 to 100 ms TWT from CDP 2650 to 4500 and a slightly higher thickness of around 200 ms from CDP 4650 to 5350. It is characterized by a chaotic occurrence of alternating acoustically transparent areas (CDP 3900 to 3950) and reflectors of high amplitudes (CDP 3400 to 3600). At CDP 3630 and 4950 Unit C shows toplaps and at CDP 5200 to 5400 erosional truncations at the boundary to Unit B, which is defined by a high-amplitude reflector (SCR 3). Thicknesses of Unit B are ranging around 150 ms TWT and reflectors are closely spaced, subparallel and of low amplitude from CDP 2650 to 3150, where most of them end up in an onlap to SCR 3. From CDP 3900 to 4350 Unit B is characterized by discontinuous reflectors, starting from an erosional truncation and ending in a downlap on SCR 3. Chaotic and discontinuous reflectors can be found from CDP 4900 to 5350. Erosional truncations mark the boundary to Unit A, which is defined by a low-amplitude discontinuous reflector (SCR 4). Unit A shows an onlap at CDP 5300 and erosional truncations on both flanks of the elevation of the sediment body. Internal reflectors are wavy bedded and subparallel with varying amplitude. From CDP 2650 to 4500 reflectors of Unit A appear with a wavy character and are partly disrupted by diffraction hyperbolas. Another artefact was produced by the ‘ghost’, which partly disrupts or interferes reflectors (e.g. CDP 3750). An elevation of Unit A is located at CDP 4100. Internal reflectors are partly downlapping and partly onlapping from CDP 4400 to 4500. The thickness of Unit A ranges around 300 ms TWT.

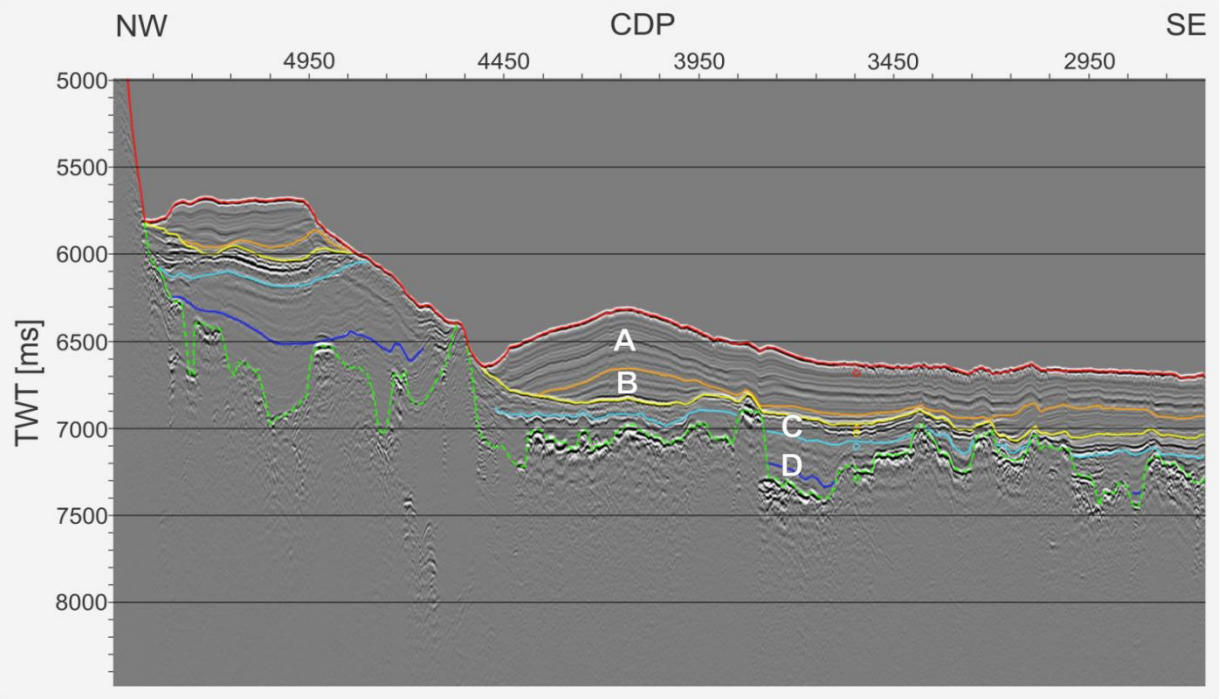

Fig. 5.5: Seismic reflection profile AWI-20160301. An explanation of the seismic interpretation (horizon colors and unit classification) can be adopted from Fig. 5.1. Little, colored circles mark the intersection points with horizons from profile tan0207-cr5a.

Summary of unit characteristics of seismic reflection profiles from SO246

Tab. 5.1: Unit characteristics of seismic reflection profiles from SO246.

	AWI-20160001	AWI-20160002	AWI-20160003	AWI-20160301
A3	closely spaced, weak, continuous, wavy bedded reflectors; onlaps on underlying subunits	subparallel, partly wavy bedded, mostly continuous reflectors, onlaps on B; erosional truncations	closely/widely spaced, subparallel reflectors with high amplitude	wavy bedded, subparallel reflectors of varying amplitude; onlap/downlap on B; erosional truncations; faulted
A2			acoustically transparent, partly strong discontinuous reflectors	
A1			subparallel, wavy reflectors, partly	
B	chaotic, discontinuous, wavy bedded reflectors with low amplitude; erosional truncations	wavy bedded, discontinuous, chaotic low-amplitude reflectors; partly higher amplitudes; erosional truncations to A ;onlap on C	strong, widely spaced reflectors; onlap on C	closely spaced, subparallel, low-amplitude reflectors/ discontinuous reflectors; onlap/downlap on C; erosional truncations to A
C	strong reflectors losing intensity downwards, partly bedded paralle; partly discontinuous/faulted onlap/downlap on D; erosional truncations at outcrops; toplap on B	wavy, subparallel, partly discontinuous reflectors with mostly high amplitude; erosional truncations to B	strong discontinuous reflectors, partly chaotic; erosional truncations	partly high-amplitude reflectors, partly acoustically transparent; toplap on B
D2	subparallel, discontinuous reflectors, partly acoustical transparency	wavy, discontinuous, low-amplitude reflectors, partly acoustical	strong, discontinuous reflectors, partly acoustically transparent	partly acoustically transparent, partly chaotic, discontinuous, strong reflectors
D1		wavy, discontinuous, low-amplitude reflectors, partly acoustical	acoustically transparent, partly strong discontinuous reflectors	

5.2 - Depth conversion

A time-to-depth conversion with the DEPCON-module of *Paradigm Echos 15.5* was applied to the three previously processed profiles AWI-20160001, AWI-20160003 and AWI-20160301. This module enables to convert the TWT into depth, based on the velocity model generated during the velocity analysis (see chapter 4.4). As an example, the profile AWI-20160001 converted into depth is shown in Fig. 5.6. Enlarged figures of all three profiles can be found in the appendix (Fig. A.3, Fig. A.8 and Fig. A.11).

The result of this procedure shows a depth range of the profile AWI-20160001 between 3150 m and 5180 m. In comparison with the same profile illustrated in TWT the Units A and B look quite similar and are reaching maximum thicknesses of 170 m (Unit A) and 330 m (Unit B). The underlying Units C and D, which are reaching maximal thicknesses of 420 m (Unit C) and 940 m (Unit D) show a modified shape of internal reflectors. This is clarified especially from CDP 5900 to 6200, where reflectors are increasing from southeast to northwest instead of decreasing as in Fig. 5.2. The top of the sediment body at CDP 5900 shows a water depth of ~ 4030 m. This can be confirmed by Parasound profile 1-d (Fig. 5.1), which shows the same depth. However, as most of the seismic reflection profiles regarded in the discussion can only be displayed in TWT, all profiles are described in TWT.

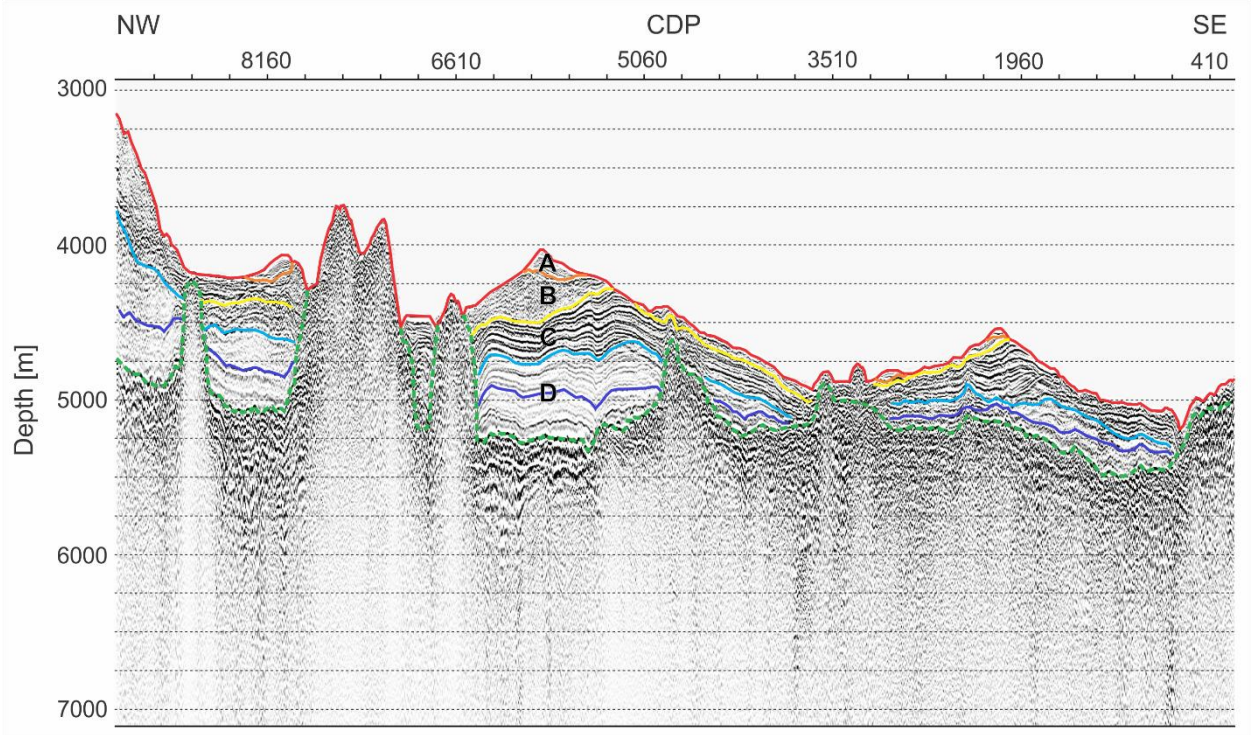

Fig. 5.6: Seismic reflection profile AWI-20160001 illustrated in depth. An explanation of the seismic interpretation (horizon colors and unit classification) can be adopted from Fig. 5.1.

5.3 - Pre-existing seismic reflection profiles

Additional seismic reflection data from New Zealand delivered complementary information to extend the understanding of oceanographic and sedimentary processes. The same units and horizons discovered in seismic reflection data from SO246 could be detected. The stratigraphic reference can be adopted from Fig. 5.1. Due to the high similarity of sediment depositions found in the following data and data from SO246, profiles will be presented briefly.

Profile tan0207-bt2

The western-most profile in the work area, tan0207-bt2 (Fig. 5.7), extends downslope of the southern flank of Chatham Rise in north-west to south-eastern direction. It shows very similar stratigraphic sequence and attributes as the profile AWI-20160001 (Fig. 5.2), which is located nearby. The sediment drift at CDP 6000 to 12500 in Fig. 5.7 is comparable to a sediment drift of AWI-20160001 from CDP 4900 to 6450 (Fig. 5.2). Another sediment deposition with the same stratigraphic sequence and attributes can be traced from CDP 18500 to 20900 (Fig. 5.7). Unit C whose upper boundary is defined as SCR 3, shows erosional truncations to the overlying Unit B. Unit B terminates in an erosional truncation as well and Unit A occurs as two basin fills with onlaps to the flanks (CDP 20200 to 20500 and 20700 to 20900).

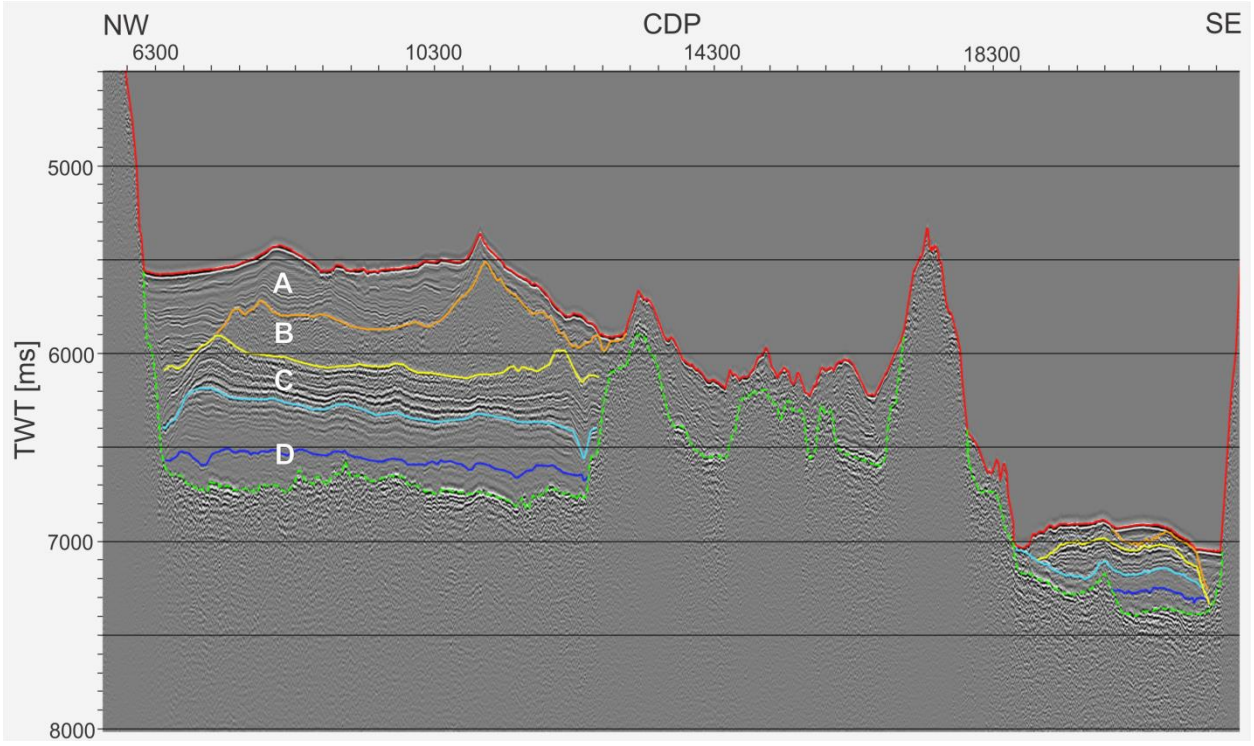

Fig. 5.7: Seismic reflection profile tan0207-bt2. An explanation of the seismic interpretation (horizon colors and unit classification) can be adopted from Fig. 5.1.

Profile tan0207-cr1

Tan0207-cr1 (Fig. 5.8) is oriented in the same direction as the profile AWI-20160002 and can be considered as a south-west shifted extension of this profile. Since tan0207-cr1 consists of

four single profiles (tan0207-cr1a to -cr1d), which extend outside of the area of interest, only the northernmost part, comprising tan0207-cr1d and half of tan0207-cr1c have been observed. From the beginning of the profile to CDP 30000 a sediment deposition with comparative stratigraphic sequence and attributes to AWI-20160002 can be found. From CDP 19200 to 28250, reflectors of the sedimentary Units D to C are extending wavily and show erosional truncations (e.g. CDP 22000; 24400 to 24800). The overlying Unit A is bedded almost horizontally (CDP 22000 to 23000; 24200 to 25200; 26300 to 28250), whereby internal reflectors have a wavier character downwards of the unit.

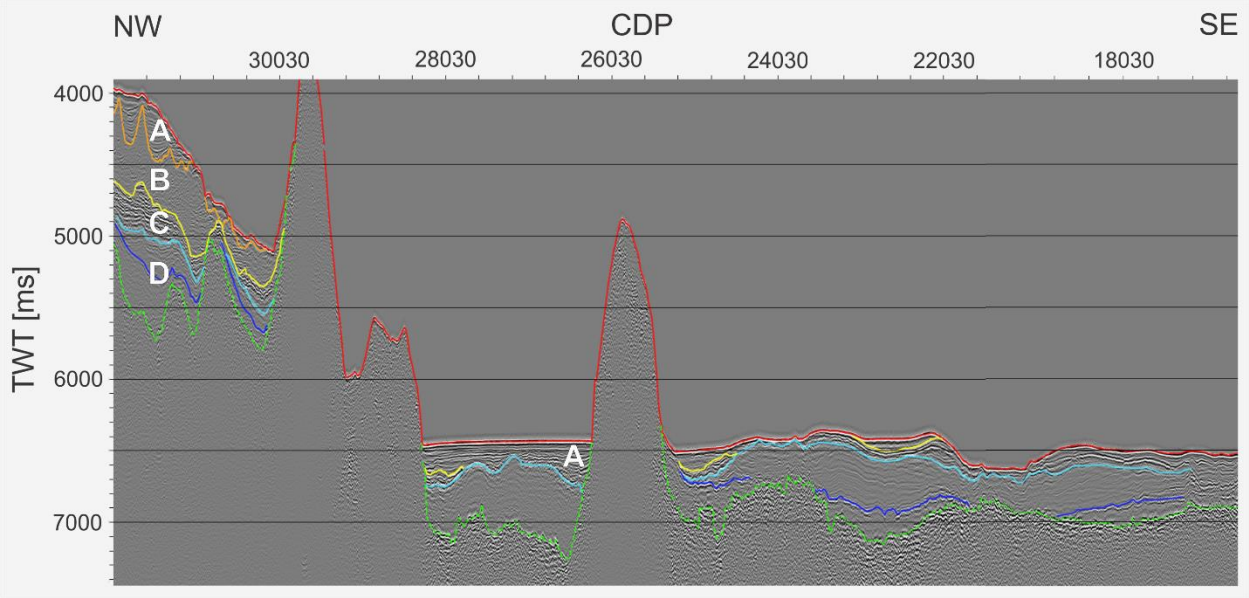

Fig. 5.8: Seismic reflection profile tan0207-cr1. An explanation of the seismic interpretation (horizon colors and unit classification) can be adopted from Fig. 5.1.

Profile tan0207-cr2

The profile tan0207-cr2 (appendix, Fig. B.6) crosses AWI-20160003 and therefore shows the same stratigraphic sequence and attributes. The intersection points can be located by little circles, which are marking the horizons in the respectively other profile.

Profiles tan0207-cr3 and tan0207-cr4

The profiles tan0207-cr3 (Fig. 5.9) and tan0207-cr4 (Fig. 5.10) are located nearby each other at the south-eastern flank of Chatham Rise and extend in south-eastern direction. Sediment depositions are primarily consisting of Unit D, which extends from CDP 11000 on tan0207-cr3 and CDP 4000 on tan0207-cr4 until the end of the profiles. On tan0207-cr4, two seamounts are disrupting the sediments. Unit D can only be subdivided into D1 and D2 on tan0207-cr3, where D1 shows a higher amplitude of internal reflectors than D2. An erosional truncation of the upper boundary of Unit D can be found in both profiles (tan0207-cr3: CDP 9300 to 10400; tan0207-cr4: CDP 10500 to 11100). Unit C is situated further south-eastwards on the profiles, initially occurring at CDP 4700 on tan0207-cr3 and CDP 6300 on tan0207-cr4 and showing

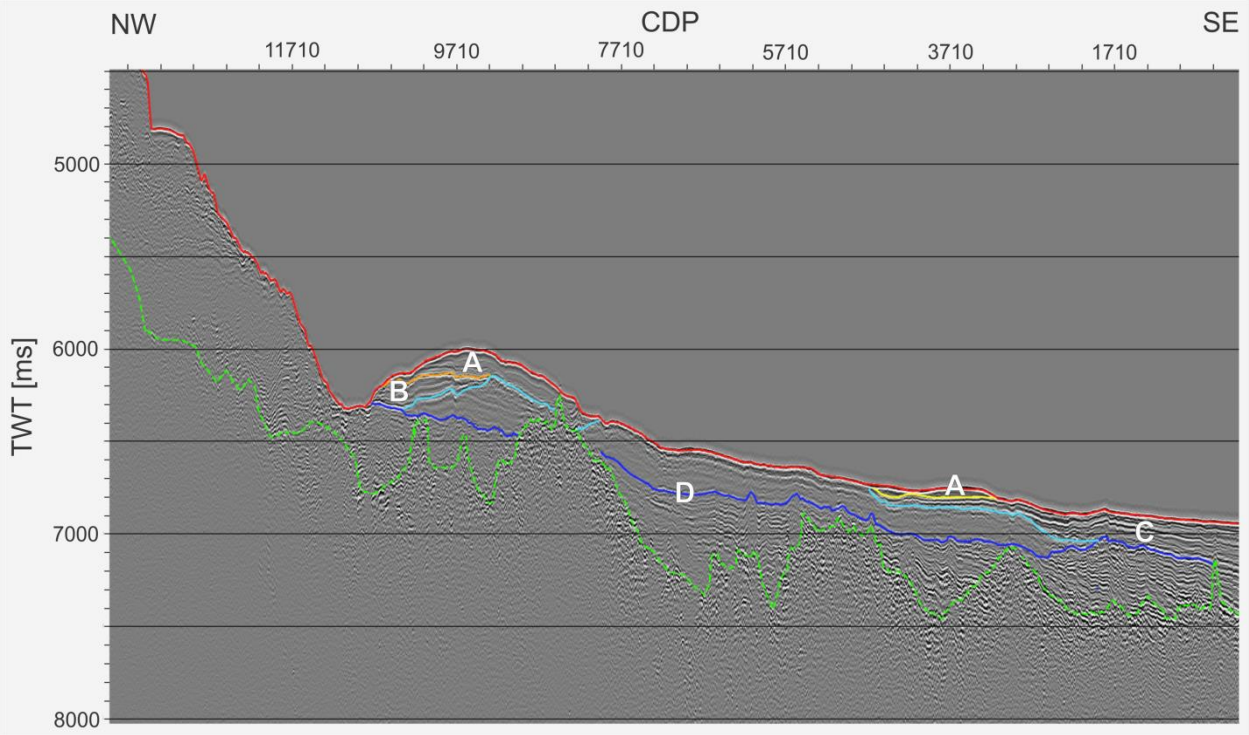

Fig. 5.9: Seismic reflection profile tan0207-cr3. An explanation of the seismic interpretation (horizon colors and unit classification) can be adopted from Fig. 5.1.

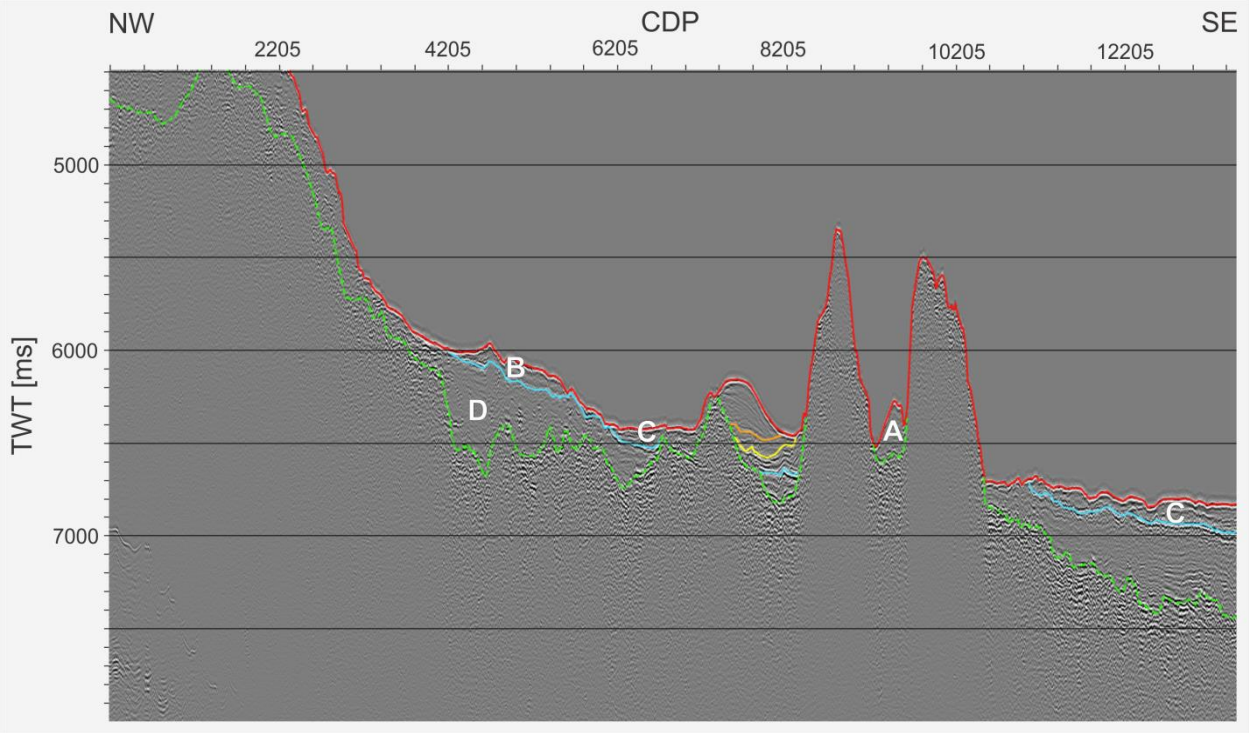

Fig. 5.10: Seismic reflection profile tan0207-cr4. An explanation of the seismic interpretation (horizon colors and unit classification) can be adopted from Fig. 5.1.

onlaps on Unit D as well as erosional truncations at its upper boundary (tan0207-cr3: CDP 200 to 2500; tan0207-cr4: CDP 6300 to 7100). Small depositions of Unit B as well as Unit A can be found in both profiles and are showing erosional truncations (tan0207-cr3: CDP 10000 to

11000; tan0207-cr4: CDP 7400), Unit B on tan0207-cr3 a toplap to Unit A (CDP 9300 to 9700) and Unit A on tan0207-cr4 a downlap to Unit B (CDP 7800 to 8200).

Profiles cr5, tan0207-cr5a, cr6 and hkdc12

Sediment depositions of the profiles cr5, tan0207-cr5a, cr6 and hkdc12 show very similar characteristics to those of the nearby profile AWI-20160301 and will therefore be summarized in this subchapter. Profile cr5 is located westwards and mostly parallel to profile AWI-20160301 and is only shown from the intersection with profile tan0207-cr5a on southwards in Fig. B.12, which can be found in the appendix B. Profile tan0207-cr5a crosses AWI-20160301 in west-northwest to southeast-east direction (Fig. 5.11). The circles in Fig. 5.11 represent intersections of picked horizons in profile AWI-20160301. Profile cr6 (appendix, Fig. B.16) extends along the eastern slope of Chatham Rise and is illustrated from the intersection with AWI-20160301 eastwards, while profile hkdc12 (appendix, Fig. B.18) extends downslope the northeastern flank of Chatham Rise, first northeastwards and then northwards.

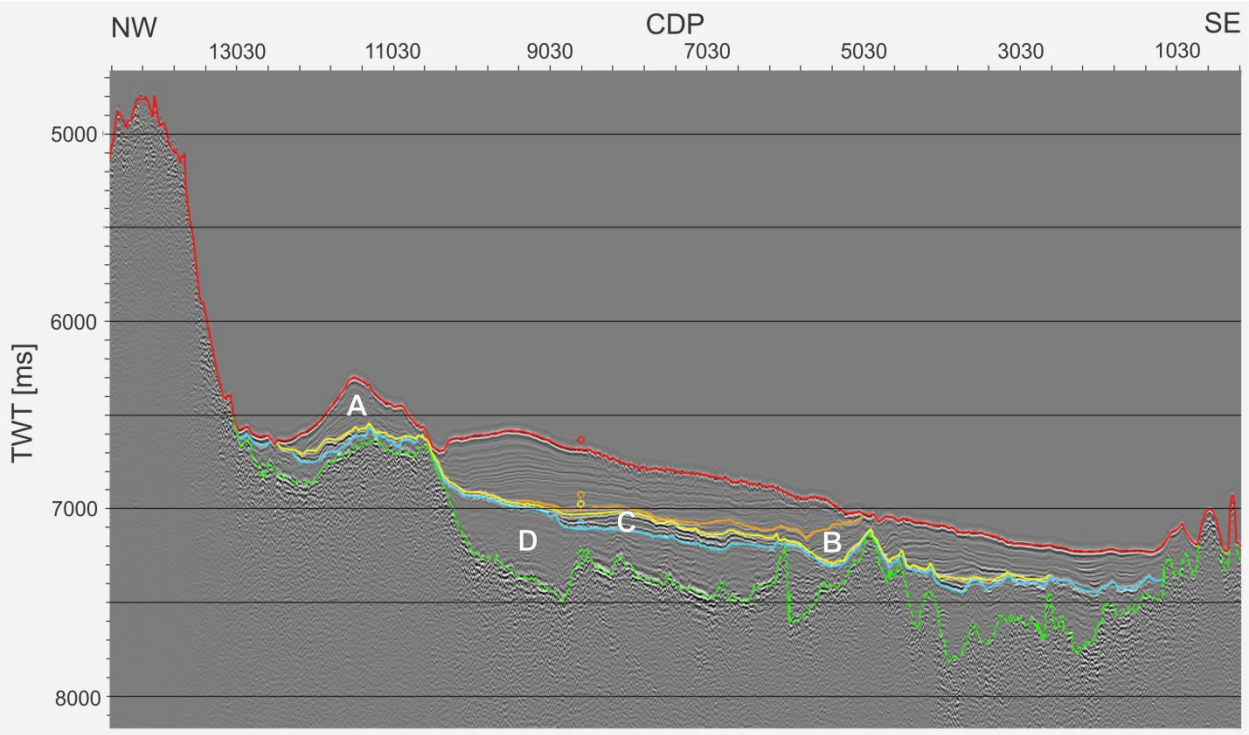

Fig. 5.11: Seismic reflection profile tan0207-cr5a. An explanation of the seismic interpretation (horizon colors and unit classification) can be adopted from Fig. 5.1. Little, colored circles mark the intersection points with horizons from profile AWI-20160301.

In all profiles the basement has a very faulted occurrence and sometimes disrupts sediment units (e.g. cr5: CDP 1500 to 2500; tan0207-cr5a: CDP 4500 to 5300; hkdc12: CDP 7900 to 8800). Unit D shows mostly discontinuous reflectors, alternating between high amplitudes and areas of acoustic transparency. In the profiles cr6 and hkdc12, Unit D can be subdivided into D1 and D2 by a discontinuous reflector of high amplitude (SCR 1). Especially in tan0207-cr5a, cr6 and hkdc12, the overlying Unit C has a very small thickness and shows an erosional

surface in all four profiles. Internal reflectors of a very high amplitude occur in tan0207-cr5a at CDP 4200 to 7500, cr6 at CDP 2100 to 2400 and hkdc12 at CDP 5200 to 7100. Unit B as well as Unit A are characterized by subparallel, wavy bedded internal reflectors (e.g. cr5: CDP 3100 to 6300, hkdc12: 8800 to 10800). They show onlaps (e.g. cr5: CDP 900 to 1500; CDP 3900 to 4700; tan0207-cr5a: CDP 9500 to 10500) and downlaps (e.g. cr5: CDP 900 to 1500; cr6: CDP 1800 to 2100; tan0207-cr5a: CDP 10600 to 11200; hkdc12: CDP 10200 to 11000, CDP 2600 to 3600) to the respectively underlying unit. Erosional truncations can be found in tan0207-cr5a at CDP 10800 to 11300 as well as CDP 11600 to 12300 and in hkdc12 at CDP 8200 to 8600.

6. Discussion

6.1 - Stratigraphic classification of sedimentary units in the work area

A stratigraphic classification of the sedimentary units is essential for a time-dependent reconstruction of current and accumulation conditions. Since there are no drill core data existing in the work area, a correlation of seismic units in the work area with seismic stratigraphy developed by Horn & Uenzelmann-Neben (2015) (Fig. 6.1) as well as Carter et al. (1994) has been done. These are based on the ODP Site 1122 located in the Bounty Trough (Carter et al., 1999a) and oil exploration wells. A map with the location of the ODP Site 1122 can be found in the appendix (Fig. E.1). Tab. 6.1 shows the resulting stratigraphic age model for the sedimentary units described in this work.

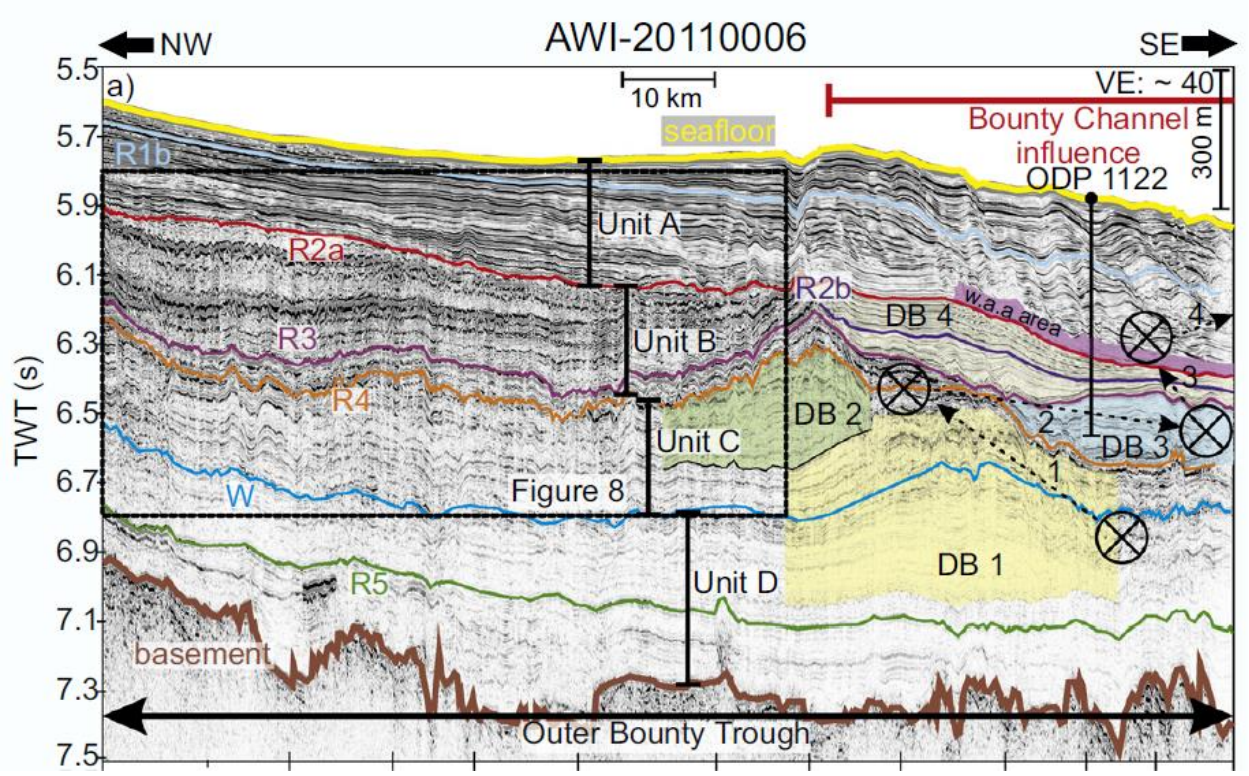

Fig. 6.1: Profile AWI-20110006 with interpretation of Horn & Uenzelmann-Neben (2015). (from Horn and Uenzelmann-Neben, 2015)

The Units A to D identified in this work are assumed to represent the Units A to D (Fig. 6.1) determined in Horn & Uenzelmann-Neben (2015). The uppermost Units A and B have been drilled at ODP Site 1122 and were described by Carter et al. (1999a). Unit A is comparable with Unit I from Carter et al. (1999a), dated from the early Pleistocene to recent times and consists of terrigenous sediments, which have been transported by turbidity currents via the Bounty Channel (Horn and Uenzelmann-Neben, 2015). At Site 1122 this unit shows

subparallel, strong reflections onlapping the underlying unit (Horn and Uenzelmann-Neben, 2015). After Horn & Uenzelmann-Neben (2015) the following Unit B can be linked to Unit II and Unit III from Site 1122 (Carter et al., 1999a), which are dated from the middle Miocene to middle Pleistocene by Horn & Uenzelmann-Neben (2015). Unit II contains bioturbated, pelagic and hemipelagic sediments, interbedded with current-laminated deposits (Carter et al., 1999a). A hiatus dated at 10.4 to 5 Ma defines the boundary to Unit III, which shows the same lithology but a coarser grainsize (Horn and Uenzelmann-Neben, 2015). Horn & Uenzelmann-Neben (2015) describe Unit B as chaotic in the Outer Sill, with subparallel medium amplitude reflections in the Outer Bounty Trough. A hiatus from Eocene to middle Miocene age, called the 'Marshall Paraconformity' separates Unit B from Unit C by a strong amplitude erosional unconformity (Horn and Uenzelmann-Neben, 2015). Units C and D, which have not been drilled at Site 1122 have been dated by correlation to oil exploration wells from the Canterbury Basin and the Great South Basin (Carter et al., 1994; Horn and Uenzelmann-Neben, 2015). There, Unit C comprises hemi- and biopelagites (Carter et al., 1994). Horn & Uenzelmann-Neben (2015) date this unit, which is characterized by medium amplitude equally spaced reflectors, from Paleocene to Eocene age. Carter et al. (1994) describe Unit D as non-marine breccia-conglomerates with thick immature coal measure sequences. This unit is characterized by medium amplitude reflectors in the upper part to almost reflection free sections in the lower part and dated from Cretaceous to Paleocene age (Horn and Uenzelmann-Neben, 2015). The upper part is interpreted to represent Unit D2, while the lower part is comparable to Unit D1 of this work. The boundary between both subunits is probably represented by reflector R5 from Horn & Uenzelmann-Neben (2015), which they describe as a reflector of continuous varying amplitude, dated to 65 Ma.

Since there were no seismic lines available for Site 1123, which is located north of Chatham Rise close to profile hkdc12 (see appendix: Fig. E.1), a direct stratigraphic correlation with this drill hole was not possible. The following table shows the stratigraphic classification of sedimentary units found in the work area, based on seismic stratigraphy by Horn & Uenzelmann-Neben (2015).

Tab. 6.1: Stratigraphic age model of sedimentary units in the work area.

Unit	Age (Ma)	Seismic characteristics
A	recent - 1.7	subparallel closely spaced reflectors, onlapping underlying unit
B	1.7 - 19.5	chaotic reflectors
C	33.7 - 56	high amplitude equally spaced reflectors
D2	56 - 65	medium amplitude reflectors to acoustically transparent zones
D1	65 - 80	

6.2 - Implications for bottom current conditions from 80 to 19.5 Ma

Carter et al. (1994) describe sediments accumulated during the time before the opening of the Tasmanian Gateway as post-rift or rift-fill sediments. Sedimentary units found in the work area occur as a typical sedimentary drape, which suggests a post break-up accumulation. Fig. 6.2 and Fig. 6.3 show an interpolated distribution of the Units C and D based on a comparison of seismic and bathymetric data. Additionally, an interpolation between these areas only based

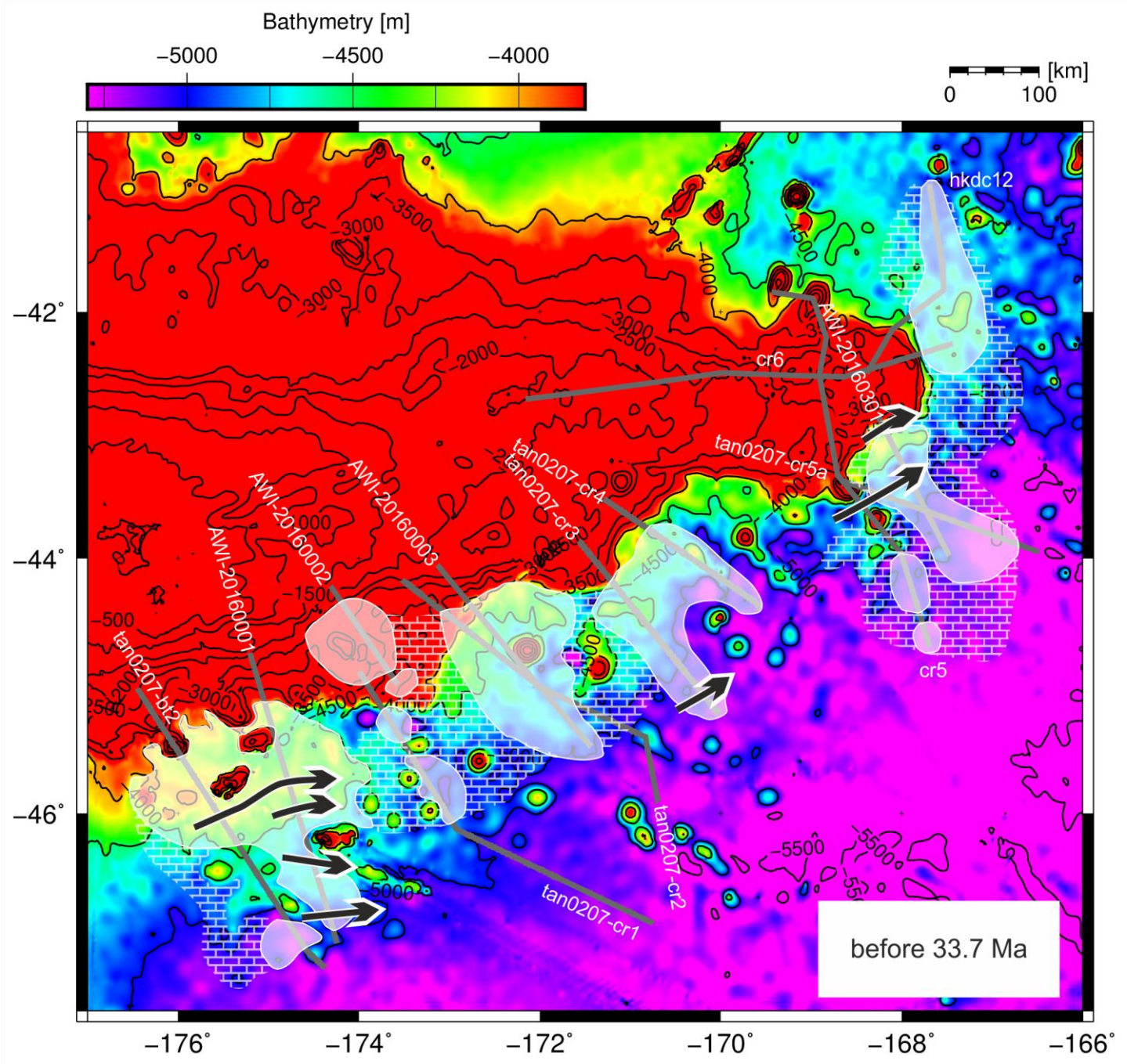

Fig. 6.2: Interpolated locations of sediment depositions of Unit C and D before the opening of the Tasmanian Gateway are illustrated by white areas. Dashed-white areas represent interpolations between those areas. Suggested current locations of a Proto-DWBC are illustrated by arrows. Profile lines are shown in grey.

on bathymetric data illustrates a broadly sediment-covered area, that might have existed before the opening of the Tasmanian gateway and thereby induced sediment dislocation. Currents, which are assumed to have influenced these sediment depositions during their accumulation before the opening of the Tasmanian Gateway are illustrated in Fig. 6.2, while Fig. 6.3 shows the assumed current distribution after the opening of the Tasmanian Gateway.

Based on a numerical simulation by Sijp et al. (2011), Horn & Uenzelmann-Neben (2015) suggest the occurrence of a Proto-DWBC, which has existed at around 56 Ma and passed the work area in north-eastern direction. Sijp et al. (2011) describe a southern hemisphere subpolar circulation with a clockwise rotation in the south-west Pacific Ocean prior to the opening of the Tasmanian Gateway.

Both Units C and D show subparallel reflectors which often follow the basement structure like for example in the profiles AWI-20160001 (Fig. 5.2), AWI-20160003 (Fig. 5.4), cr5 (appendix: Fig. B.12) and cr6 (appendix: Fig. B.16). This indicates an accumulation of the sediments conformed to the post-breakup faulted and folded structure of the basement. Since these layers are bedded regularly in most cases, accumulation conditions must have been smooth and without strong currents, which would have influenced the bedding here. However, in several areas internal discontinuities point to the occurrence of regional bottom current activity before the opening of the Tasmanian Gateway, like in profile AWI-20160001 (Fig. 5.2), where internal onlap (CDP 1800 to 1900) and erosional truncations as well as downlap structures on Unit D (CDP 5100 to 5700) occur. An erosional truncation of Unit D1 to D2 in tan0207-cr3 (Fig. 5.9) indicates an even younger influence of bottom currents. Horn & Uenzelmann-Neben (2015) suggest the existence of a Proto-DWBC driven by cold deep-water flows in the early Paleocene, which could be an explanation for erosional and current-controlled features in the data of this work. Bottom current features such as eddies might have created areas of local erosion as in profile tan0207-cr3. Fig. 6.2 shows that sediment depositions especially in the south-western part of the work area were influenced by a suggested Proto-DWBC.

The opening of the Tasmanian Gateway, which has been dated to 33.5 Ma by Carter et al. (2004) led to the initiation of the ACC and following this, widespread erosion and the formation of the Marshall Paraconformity (Carter et al., 2004). Evidence for this event can be found in all profiles investigated in this work (e.g. Fig. 5.7: tan0207-bt2, CDP 11300 to 12100; Fig. 5.8: tan0207-cr1, CDP 30000 to 32000; Fig. 5.10: tan0207-cr4, CDP 7600 to 8400). Especially downslope areas of the profiles tan0207-bt2 (Fig. 5.7: CDP 18700 to 21500), AWI-20160001 (Fig. 5.2: CDP 400 to 1900) and tan0207-cr1 (Fig. 5.8: CDP 20700 to 30000) show a strong erosional influence of bottom currents with high velocities. Erosional truncations next to seamounts and ridges like in tan0207-bt2 (Fig. 5.7: CDP 18700 to 19400; CDP 21100 to 21500) and AWI-20160001 (Fig. 5.2: CDP 7800 to 8000) indicate high current velocities due

to a diverting of flows around these bathymetric structures and therefore narrowing of the currents. In addition, the profiles tan0207-cr3 and tan0207-cr4 show a highly erosional surface of Unit C (Fig. 5.9: CDP 200 to 1700; Fig. 5.10: CDP 6300 to 7100) and even areas where Unit C was totally eroded and bottom currents effected Unit D (Fig. 5.9: CDP 9300 to 11100; Fig. 5.10: CDP 10500 to 11100). This effect might have been caused by high velocities of bottom currents, which were narrowed by a small branch of the Chatham Rise slope at around 44°S

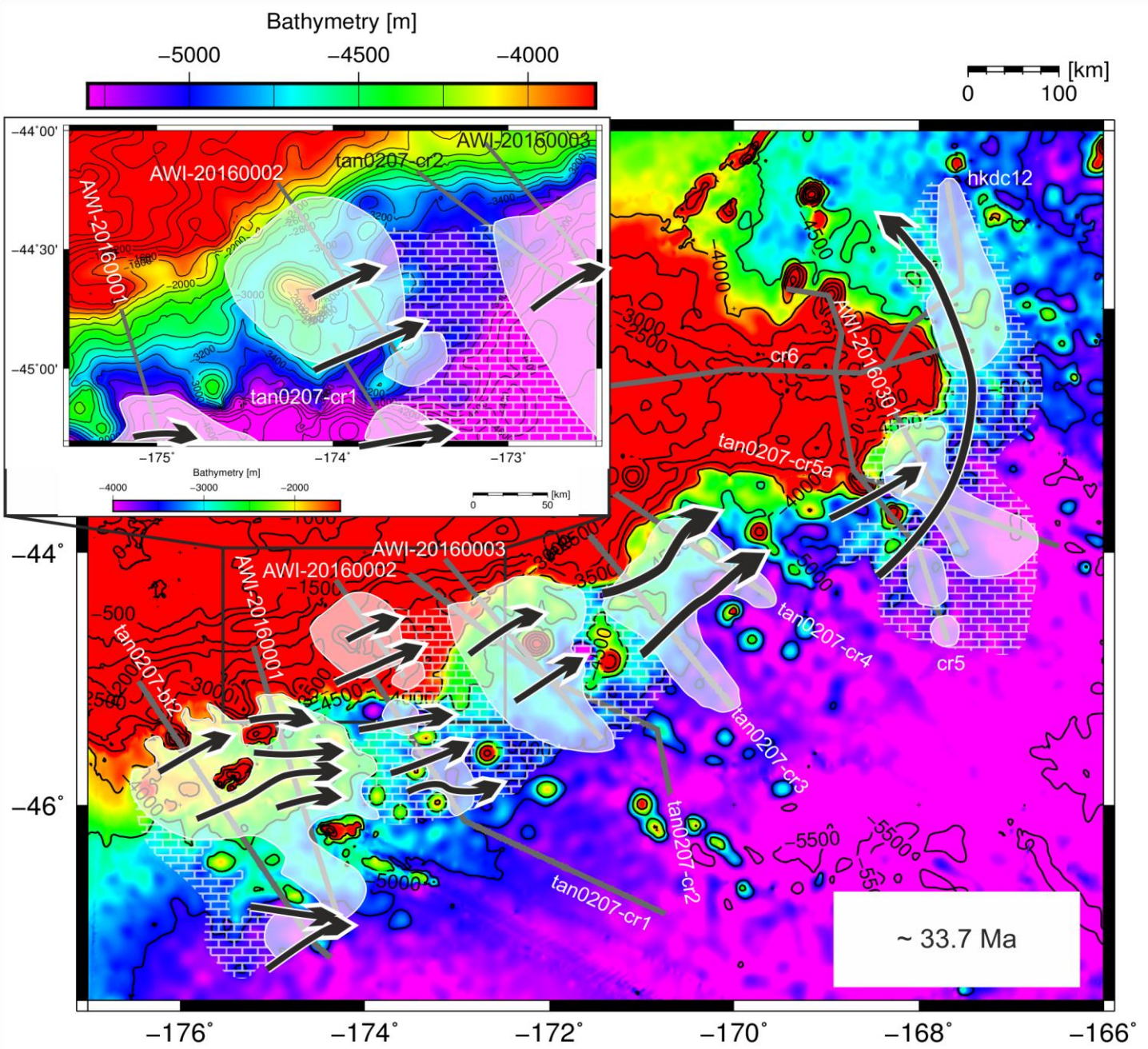

Fig. 6.3: Interpolated locations of sediment depositions of Unit C and D before the opening of the Tasmanian Gateway are illustrated by white areas. Dashed-white areas represent interpolations between those areas. Suggested current locations after the opening of the Tasmanian Gateway are illustrated by arrows. The small detail map serves to better illustrate the more highly located areas of interest with an adjusted depth scale. Profile lines are shown in grey.

to 44.2°S and 171°W to 172°W (see Fig. 6.3). The erosional truncation of Unit D in profile tan0207-cr3 at CDP 9300 to 11100 (Fig. 5.9) implies the evolution of a bottom current channel between the mentioned branch and a seamount ridge at 44.4°S to 45°S and 171°W to 171.6°W. Unit C shows very small thicknesses in the profiles cr5 (appendix: Fig. B.12), tan0207-cr5a (Fig. 5.11), AWI-20160301 (Fig. 5.5), cr6 (appendix: Fig. B.16) and hkdc12 (appendix: Fig. B.18), which lead to the assumption that after the opening of the Tasmanian Gateway current velocities must have been constantly high in the whole area around the eastern flank of the Chatham Rise. This might have been caused by a steep slope in the area of cr5 (appendix: Fig. B.12), tan0207-cr5a (Fig. 5.11) and AWI-20160301 (Fig. 5.5) as shown in Fig. 6.3 and the narrowing of the DWBC between the Chatham Rise and the Valerie Passage (Carter and McCave, 2002).

6.3 - Implications for bottom current conditions from 19.5 to 1.7 Ma

An unconformity of widespread erosion marks the boundary to Unit B, whose youngest layers are dated to an age of 19.5 Ma (Horn and Uenzelmann-Neben, 2015). This unit is distinguished from the underlying units by a different distribution over the work area and different seismic characteristics. Chaotic, wavy internal reflectors in the profiles tan0207-bt2 (Fig. 5.7), AWI-20160001 (Fig. 5.2), tan0207-cr1 (Fig. 5.8), AWI-20160002 (Fig. 5.3), tan0207-cr2 (appendix: Fig. B.6) and AWI-20160003 (Fig. 5.4) indicate often varying current conditions. Uenzelmann-Neben et al. (2009) suggest the occurrence of major modifications in sedimentation processes in the Bounty Trough and refer to internal onlaps, which indicate changes in the sedimentary environment and periods of erosion or non-deposition. Internal onlaps in Unit B can also be found in the profiles AWI-20160001 at CDP 8000 (Fig. 5.2), AWI-20160002 at CDP 2500 to 2600 (Fig. 5.3) and tan0207-cr2 at CDP 2700 to 3500 (Fig. B.6), which points to similar oceanographic conditions in the work area. Probably, sediments have often been reworked by strong bottom currents and accumulated again in temporarily quiescent regions. Distinctly varying thicknesses of Unit B and small areas of non-deposition or erosion next to seamounts in tan0207-bt2 (Fig. 5.7), AWI-20160001 (Fig. 5.2) and AWI-20160002 (Fig. 5.3) might have been caused by a strong influence of bottom currents surrounding these seamounts and therefore acceleration of the flows. Channels of high current-velocities could have existed in tan0207-bt2 at CDP 6300 to 7300, CDP 18600 to 18900 and CDP 21300 to 21600 (Fig. 5.7), in AWI-20160001 at CDP 7700 to 7900 (Fig. 5.2) and in AWI-20160002 at CDP 250 to 400, CDP 650 to 1100 and CDP 3000 to 3100 (Fig. 5.3). These channels as well as further possible current paths, which might have affected the deposition of Unit B are illustrated in Fig. 6.4. Sedimentary structures in these profiles combined with each other and the bathymetry allow an interpolation of depositional areas between the profiles tan0207-bt2 (Fig. 5.7) and AWI-20160001 (Fig. 5.2) and the surrounding area (Fig. 6.4).

The profiles tan0207-cr1 (Fig. 5.8), tan0207-cr2 (appendix: Fig. B.6) and AWI-20160003 (Fig. 5.4) only show depositions of Unit B at the slope (Fig. 5.8: tan0207-cr1, CDP 30000 to 32000; appendix: Fig. B.6, tan0207-cr2 CDP 4000 to 6700; Fig. 5.4: AWI-20160003, CDP 9500 to 10400), which show chaotic internal reflectors and a very erosive surface. It is not possible to exclude that also landslide events have affected those depositions. The non-deposition of Unit B further southwards infers that bottom currents must have been shifted southwards and that current velocities have been very high there. This coincides with the assumption that seamounts, which are rather rare in that area, are disrupting the current flow. An interpolation of deposition distribution together with bathymetric data in Fig. 6.4 clarifies, that Unit B has only been deposited in more highly situated locations and interpolations can possibly be extended along the slope between the profiles. The profiles tan0207-cr3 (Fig. 5.9) and tan0207-cr4 (Fig. 5.10) show very small depositions of Unit B. This indicates that current

velocities must have been high in this area, so either only small volumes of Unit B accumulated or parts of the accumulations have been eroded later on. After a period of drift accumulation, which initiated after the widespread erosion of the Marshall Paraconformity and continued until the early Miocene, Carter et al. (2004) suggest an interruption of drift deposition by several erosional phases, which have coincided with an expansion of the East Antarctic Ice Sheet causing a quickening of the DWBC. The small depositions of Unit B with erosional surfaces in

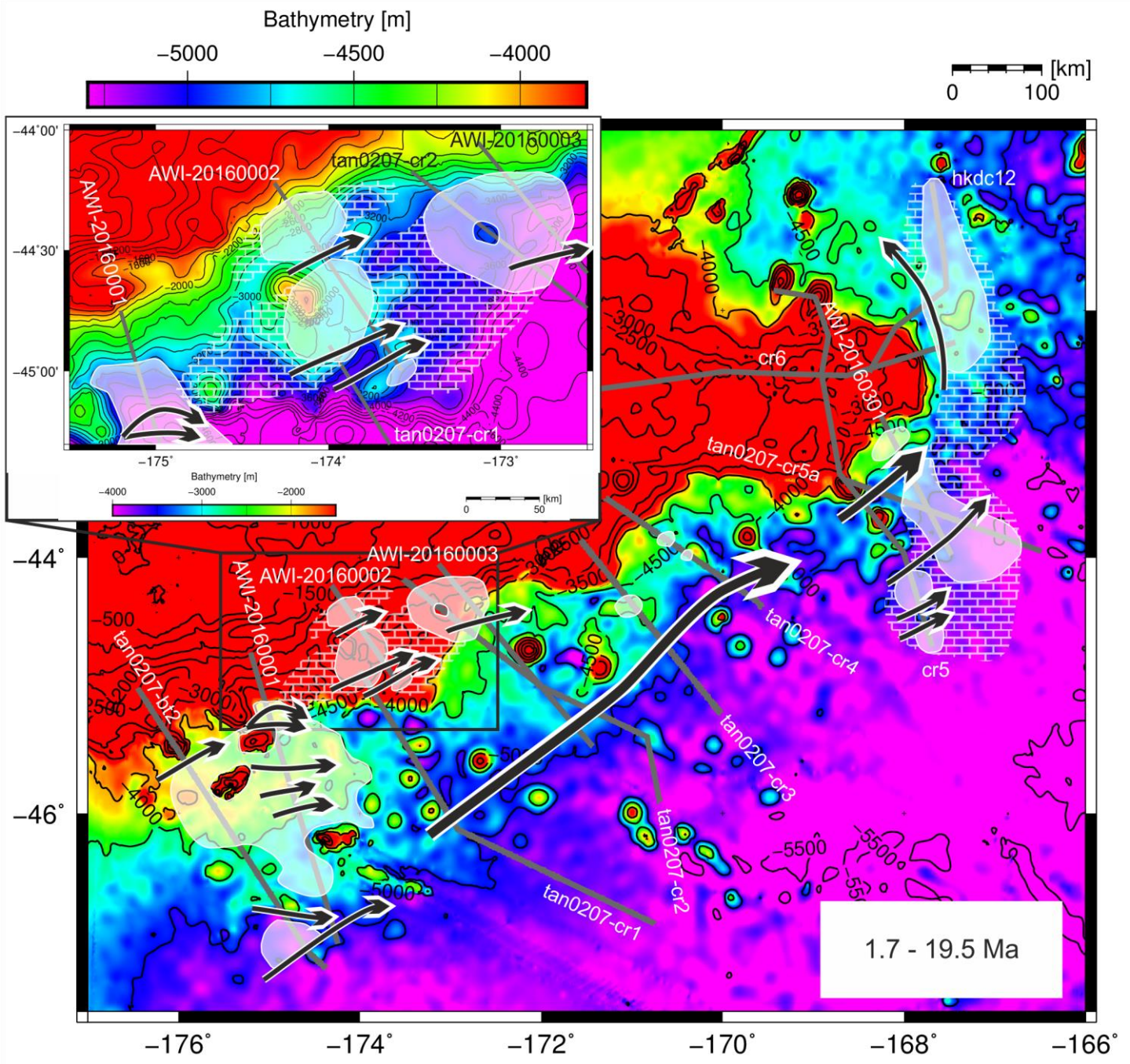

Fig. 6.4: Interpolated locations of sediment depositions of Unit B, illustrated by white areas. Dashed-white areas represent interpolations between those areas. Suggested current locations are illustrated by arrows. The small detail map serves to better illustrate the more highly located areas of interest with an adjusted depth scale. Profile lines are shown in grey.

the profiles indicates that this effect might have been high in this area. Another explanation could be the narrowing of bottom currents due to a branch of the Chatham Rise at 44°S to 44.2°S and 171°W to 172°W (see Fig. 6.4), as explained in the previous subchapter.

Depositions of Unit B in the profiles cr5 (appendix: Fig. B.12), tan0207-cr5a (Fig. 5.11), AWI-20160301 (Fig. 5.5), cr6 (appendix: Fig. B.16) and hkdc12 (appendix: Fig. B.18) show wavy, subparallel internal reflections. This points to a smoother depositional environment than in the previously discussed profiles. Internal onlaps in cr5 at CDP 3300 to 4700 (appendix: Fig. B.12) and tan0207-cr5a at CDP 3600 to 4000 (Fig. 5.11) imply minor, small-scale changes of the current regime, like for example the formation of eddies. Onlaps and downlaps of Unit B to Unit C like in cr5 at CDP 3900 to 5900 (appendix: Fig. B.12), tan0207-cr5a at CDP 5400 to 9500 (Fig. 5.11) and cr6 at CDP 1100 to 1800 (appendix: Fig. B.16) suggest a migration of the sediment body towards the Chatham Rise. Furthermore, all depositions of Unit B found in the profiles cr5 (Fig. appendix: B.12), tan0207-cr5a (Fig. 5.11), AWI-20160301 (Fig. 5.5), cr6 (appendix: Fig. B.16) and hkdc12 (appendix: Fig. B.18) show an upwardly convex geometry, which together with the migration of the sediment bodies are typical characteristics for contour current depositions (Faugères et al., 1999). Horn & Uenzelmann-Neben (2015) identified drift bodies with similar characteristics (convex upward bent reflection pattern) in the Bounty Trough. The comparable structure of sediment depositions of Unit B in the mentioned profiles suggests that bottom currents are rounding the eastern flank of Chatham Rise as illustrated in Fig. 6.4. High velocities can be assumed between the three northernmost seamounts in profile cr5 (appendix: Fig. B.12), where no depositions of Unit B could be detected.

6.4 - Implications for bottom current conditions from 1.7 Ma to recent

After the developments of the Solander channel, Bounty channel and Hikurangi channel (Fig. 3.3) in the Plio-Pleistocene, the accumulation of sediment drifts changed to a terrigenous-dominant sedimentation (Carter et al., 2004). In the work area most of the terrigenous material is delivered to the abyssal floor by turbidity currents along the Bounty channel, which were then transported by a branch of the DWBC (McCave and Carter, 1997). Fig. 6.5 illustrates the interpolated distribution of depositions of Unit A and the recent expected flow of bottom currents in the work area.

A very large deposition of Unit A can be found along the profile tan0207-bt2 (Fig. 5.7: CDP 6100 to 11300) and extended to AWI-20160001 (Fig. 5.2: CDP 5500 to 6100) by comparison with bathymetric data (appendix: Fig. D.2). Many small depositions of Unit A indicate a bottom current influenced sedimentation regime. This is also evidenced by a wavy character of subparallel internal reflectors, which can better be resolved by Parasound profiles 1-a to 1-e (appendix: Fig. C.1 - C.10). Profile 1-a and 1-e clarify that the wavy structure of internal reflectors has decreased from Subunit A1 to Subunit A3 (appendix: Fig. C.2: 4 to 7 km offset, Fig. C.8: Subunit A1 at 2 to 10 km offset and Subunit A3 at 13 to 16 km offset), which is probably attributed to a smoothing of current conditions since times of deposition of Unit B. A ceasing of channel activity is represented by small basin fills, as in tan0207-bt2 at CDP 6100 to 7500, CDP 20100 to 20700 and CDP 21200 to 21600 (Fig. 5.7) as well as AWI-20160002 at CDP 200 to 400 and 650 to 950 (Fig. 5.3). Another huge deposition of Unit A (Fig. 6.5, appendix: Fig. D.4) probably extends along the slope between tan0207-cr1 (Fig. 5.8: CDP 30000 to 32000) and AWI-20160002 (Fig. 5.3: CDP 1150 to 3550). This can be attributed to a ceasing of the channel, which has separated two depositions of Unit B from each other (Fig. 5.3: CDP 3000 to 3100). Small depositions of Unit A in tan0207-cr1 at CDP 22000 to 23000, CDP 24200 to 25200 and CDP 26200 to 28300 (Fig. 5.8), as well as very large depositions of Unit A in tan0207-cr2 (appendix: Fig. B.6, CDP 6300 to 14300) and AWI-20160003 (Fig. 5.4) indicate either a shifting of the current path southwards or a deceleration of the current causing a reduction of the influenced area. However, a small deposition with downlapping, wavy reflectors in tan0207-cr2 at CDP 1800 to 3000 (appendix: Fig. B.6) still points to the existence of along-slope currents in more highly situated regions. This coincides with observations in the Parasound data. The profile 3-c (appendix: Fig. C.16) shows a uniform, subparallel bedding of internal reflectors south of the seamount (Fig. 5.4: CDP 11850 to 12450), while the profiles 3-a (appendix: Fig. C.12) and 3-b (appendix: Fig. C.14) north of it show variations especially of the reflectivity of internal reflectors and the thickness of the Subunits A1, A2 and A3.

The profiles tan0207-cr3 (Fig. 5.9) and tan0207-cr4 (Fig. 5.10) show a less common distribution of Unit A in small mounded depositions. This might be attributed to a narrowing

and therefore strengthening of the bottom currents due to steepening of the slope (Fig. 6.5). Nevertheless, the bathymetry between both profiles (appendix: Fig. D.5) suggests an interpolation between a deposition of Unit A in tan0207-cr3 at CDP 8500 to 10500 (Fig. 5.9) and two depositions in tan0207-cr4 at CDP 7400 to 8200 and CDP 9200 to 9600 (Fig. 5.10), which are separated by a seamount. Erosional truncations next to the slope (e.g. Fig. 5.9: CDP 9700 to 10500, Fig. 5.10: CDP 7400 to 7600) and downlap structures next to seamounts (e.g.

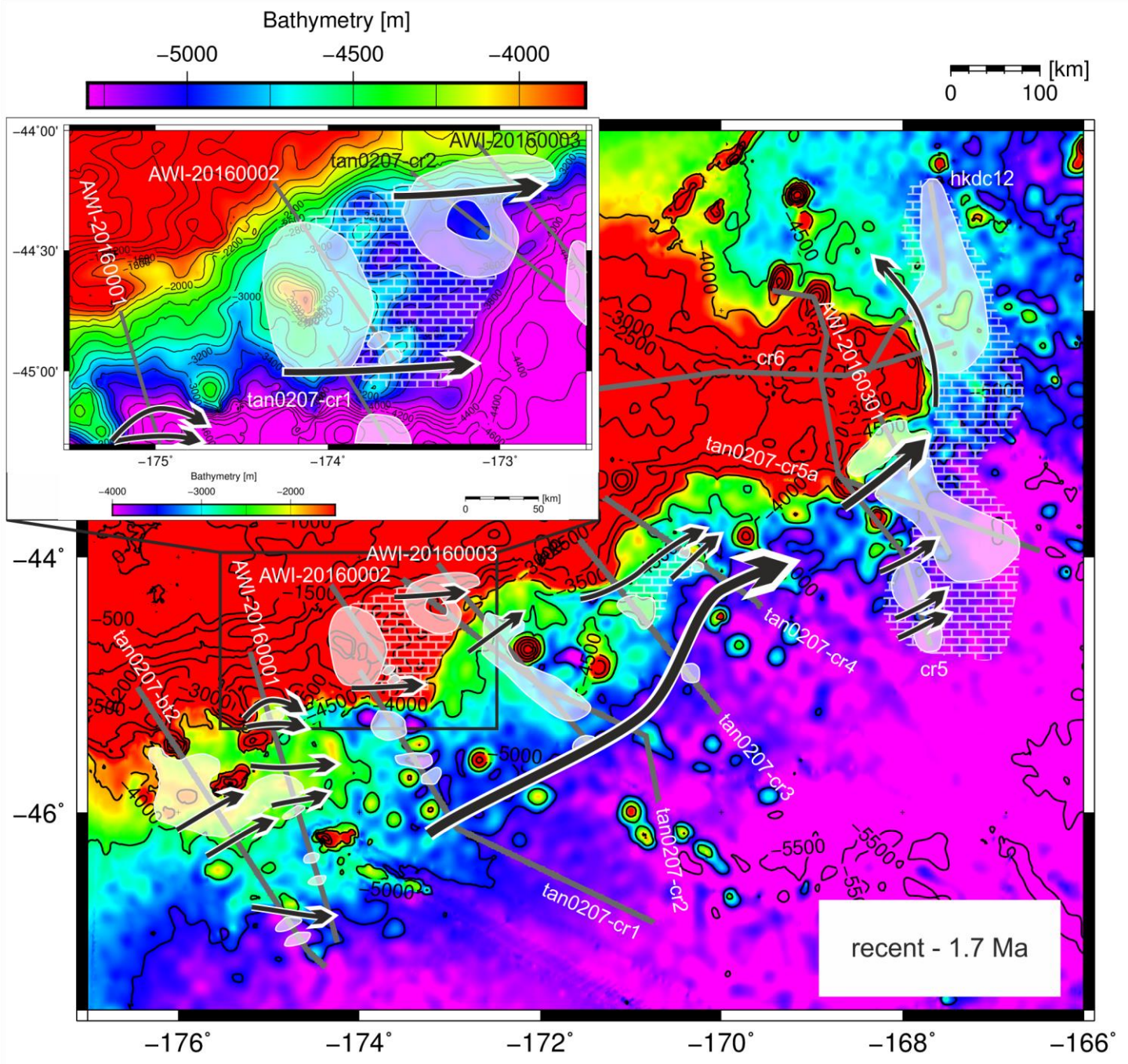

Fig. 6.5: Interpolated locations of sediment depositions of Unit A, illustrated by white areas. Dashed-white areas represent interpolations between those areas. Suggested current locations are illustrated by arrows. The small detail map serves to better illustrate the more highly located areas of interest with an adjusted depth scale. Profile lines are shown in grey.

Fig. 5.10: CDP 7800 to 8200) indicate the existence of an along-slope channel as previously described for this area and a flow of branches around the seamounts, which creates sediment depositions in slipstream areas (Fig. 6.5).

The profiles cr5 (appendix: Fig. B.12), tan0207-cr5a (Fig. 5.11), AWI-20160301 (Fig. 5.5), cr6 (appendix: Fig. B.16) and hkdc12 (appendix: Fig. B.18) show a very similar sedimentation pattern of Unit A. Internal reflectors occur as a sedimentary drape and are wavy, subparallel and closely spaced, as already described in Unit B. This indicates sedimentation conditions similar to the deposition of Unit B. Erosional truncations in tan0207-cr5a at CDP 10300 to 11300 and CDP 11600 to 12300 (Fig. 5.11) and AWI-20160301 at CDP 4400 to 4500 and 4850 to 4950 (Fig. 5.5) suggest high current velocities along the slope. Depressions next to seamounts, like in profile cr5 (appendix: Fig. B.12: CDP 2700 to 3100 and CDP 1300 to 1700) indicate an increase of the current velocity around these. Another indicator for the existence of channels is the mounded geometry of all sediment bodies with depressions next to the slope, as it is described for elongate-mounded contouritic drifts by Faugères et al. (1999). Bathymetric data (appendix: Fig. D.6) suggest an interpolation of Unit A between different profiles and point to the occurrence of large sediment bodies around the eastern flank of Chatham Rise, which might possibly be connected with each other as illustrated by dashed-white areas in Fig. 6.5. This correlates with the description of a large sediment deposition by Carter et al. (2004), which they called ‘Chatham Deep Drift’ (Fig. 3.3). Summarized, a migration of the sediment bodies towards the Chatham Rise can be recognized by a downlap of internal layers as in cr5 at CDP 5900 to 6700 (appendix: Fig. B.12), AWI-20160301 at CDP 4300 to 4500 (Fig. 5.5), cr6 at CDP 1800 to 2100 (appendix: Fig. B.16) and hkdc12 at CDP 10400 to 11000 (appendix: Fig. B.18). This is probably attributed to a westward shifting of the current towards the slope and can be explained by the southern hemisphere Coriolis deflection of the DWBC according to Carter & McCave (1994).

7. Conclusion

The investigation of seismic data results from the RV Sonne expedition SO246 enable a reconstruction of ocean current conditions at the south-eastern Chatham Rise slope in the past 80 My. A classification of different units compared with a lithostratigraphic model from Horn & Uenzelmann-Neben (2015) allowed to create an age model for these units. Additionally, Parasound and bathymetric data delivered complementary information and enabled the development of a reconstruction of the lateral extension of sediment depositions in different time periods. By means of this, it was possible to reconstruct time-dependent current regimes in the work area.

The oldest sedimentary unit was dated to a maximum age of 80 Ma. Accumulations of an age until 33.7 Ma occur in a sedimentary drape, which suggests a post break-up deposition and a mostly regular bedding indicates smooth accumulation conditions at this time. However, internal discontinuities point to the occurrence of bottom current activity prior to the opening of the Tasmanian Gateway, as described by Horn & Uenzelmann-Neben (2015), who suggest a Proto-DWBC, which passed the work area in north-eastern direction. The opening of the Tasmanian Gateway at 33.5 Ma led to the initiation of the ACC, which strongly influenced the further development of the DWBC and caused widespread erosion and the formation of the 'Marshall Paraconformity' (Carter et al., 2004). This is evidenced by a strong discontinuity in the seismic profiles investigated in this work. During the Miocene current conditions in the western part of the work area often changed, which is indicated by chaotic, wavy internal reflectors. Sediments, which have often been reworked by strong bottom currents and accumulated again in temporarily quiescent regions as well as periods of erosion or non-deposition caused internal onlaps. Several erosional phases can possibly be associated with an expansion of the East Antarctic Ice Sheet, leading to an intensification of the DWBC (Carter et al., 2004). In the eastern part of the work area, a migration of sediment bodies towards the Chatham Rise and an upwardly convex geometry of these indicate an along-slope current, rounding the eastern flank of the Chatham Rise since the Miocene until recent times. According to Carter & McCave (1994) a westward shifting of the current towards the slope of Chatham Rise can be explained by the southern hemisphere Coriolis deflection of the DWBC. The development of three main sediment conduits in the Plio-Pleistocene led to a terrigenous-dominant sedimentation (Carter et al., 2004). Many small drift depositions indicate a bottom current influenced sedimentation regime. A wavy, but subparallel and regular bedding of most internal reflectors, as well as many sediment accumulations, which fill previous current channels point to smoother current conditions compared with depositions of the Miocene.

All in all, the successful investigation of seismic and Parasound, as well as bathymetric data enable confirm and extend previous knowledge of oceanographic and sedimentary processes east of New Zealand. The existence of along-slope ocean bottom currents, which are highly influencing the sedimentation conditions could be verified and the ENZOSS model, developed by Carter et al. (1996) extended and refined for the work area. Nevertheless, there still remain gaps of information between the seismic reflection profiles used in this work, as seismic lines were widely-spaced and a direct lithostratigraphic correlation with drill core data was not possible, since no drill sites exist in the work area. 3-D seismic profiles would allow an even more detailed mapping of sediment depositions discussed in this work. Furthermore, new drill core data from the southern Chatham Rise could provide essential information to develop a direct lithostratigraphic correlation with seismic reflection profiles and create a more precise sedimentary age model. Thereby, a small-scale reconstruction of bottom currents in the work area could be developed and the knowledge about sediment drift formation could be extended.

References

Carter, L., and McCave, I.N. (1994). Development of sediment drifts approaching an active plate margin under the SW Pacific Deep Western Boundary Current. Paleoceanography, *9*: 1061–1085.

Carter, L., and McCave, I.N. (2002). Eastern New Zealand Drifts, Miocene-Recent. Geological Society, London, Memoirs, *22*: 385–407.

Carter, L., Carter, R.M., and McCave, I.N. (2004). Evolution of the sedimentary system beneath the deep Pacific inflow off eastern New Zealand. Marine Geology, *205*: 9–27.

Carter, R.M., McCave, I.N., Richter, C., Carter, L., Aita, Y., Buret, C., Di Stefano, A., Fenner, J., Fothergill, P., Gradstein, F., et al. (1999a). Site 1122: tubidites with a contourite foundation. In Carter, R. M., McCave, I. N., Richter, C., Carter, L., et al., Proc ODP, Init. Repts., 181: College Station, TX (Oean Drilling Program), 1–146.

Carter, R.M., McCave, I.N., Richter, C., Carter, L., Aita, Y., Buret, C., Di Stefano, A., Fenner, J., Fothergill, P., Gradstein, F., et al. (1999b). Leg 181 summary: Southwest Pacific paleoceanography. In Carter, R. M., McCave, I. N., Richter, C., Carter, L., et al., Proc ODP, Init. Repts., 181: College Station, TX (Oean Drilling Program), 1–80.

Carter, R.M., Carter, L., and Davy, B. (1994). Seismic stratigraphy of the Bounty Trough, south-west Pacific Ocean. Marine and Petroleum Geology, *11*: 79–93.

Carter, R.M., Carter, L., and McCave, I.N. (1996). Current controlled sediment deposition from the shelf to the deep ocean: the cenozoic evolution of circulation through the SW pacific gateway. Geologische Rundschau, *85*: 438–451.

Davy, B., Hoernle, K., and Werner, R. (2008). Hikurangi Plateau: Crustal structure, rifted formation, and Gondwana subduction history. Geochemistry Geophysics Geosystems, *9*: 1–31.

Faugères, J.-C., Stow, D.A.V., Imbert, P., and Viana, A. (1999). Seismic features diagnostic of contourite drifts. Marine Geology, *162*: 1–38.

Gohl, K., and Werner, R. (2016). The Expedition SO246 of the Research Vessel SONNE to the Chatham Rise in 2016, Berichte zur Polar- und Meeresforschung = Reports on polar and marine research. Bremerhaven, Alfred Wegener Institute for Polar and Marine Research, 698.

Horn, M., and Uenzelmann-Neben, G. (2015). The Deep Western Boundary Current at the Bounty Trough, east of New Zealand: Indications for its activity already before the opening of the Tasmanian Gateway. Marine Geology, *362*: 60–75.

McCave, I.N., and Carter, L. (1997). Recent sedimentation beneath the Deep Western Boundary Current off northern New Zealand. Deep Sea Research Part I, *44*: 1203–1237.

Mitchell, J.S., Mackay, K.A., Neil, H.L., Mackay, E.J., Palletin, A., and Notmann, P. (2012). Undersea New Zealand, 1:5,000,000. NIWA Chart, Miscellaneous Series No. 92. https://www.niwa.co.nz/our-science/oceans/bathymetry/download-the-data.

Press, F., Siever, R., and Grotzinger, J. (2011). Allgemeine Geologie. Spektrum, Akademischer Verlag, 709.

Rebesco, M., Hernández-Molina, F.J., Van Rooij, D., and Wåhlin, A. (2014). Contourites and associated sediments controlled by deep-water circulation processes: State-of-the-art and future considerations. Marine Geology, *352*: 111–154.

Sijp, W.P., England, M.H., and Huber, M. (2011). Effect of the deepening of the Tasman Gateway on the global ocean. Paleoceanography, *26*: 1–18.

Stilwell, J.D., and Consoli, C.P. (2012). Tectono-stratigraphic history of the Chatham Islands, SW Pacific—The emergence, flooding and reappearance of eastern ‘Zealandia.’ Proceedings of the Geologists' Association, *123*: 170–181.

Uenzelmann-Neben, G., Grobys, J., Gohl, K., and Barker, D. (2009). Neogene sediment structures in Bounty Trough, eastern New Zealand: Influence of magmatic and oceanic current activity. Geological Society of America Bulletin, *121*: 134–149.

Veeken, P.C.H., and van Moerkerken, B. (2013). Seismic Stratigraphy and Depositional Facies Models. Academic Press, 360.

Wobbe, F., Gohl, K., Chambord, A., and Sutherland, R. (2012). Structure and breakup history of the rifted margin of West Antarctica in relation to Cretaceous separation from Zealandia and Bellingshausen plate motion. Geochemistry Geophysics Geosystems, *13*: 1–19.

Yilmaz, Ö. (2001). Seismic data analysis. Society of Exploration Geophysicists, 2028.

Acknowledgement

I would like to thank all the people who supported me, while writing my Master thesis.

First of all, many thanks to Dr. Karsten Gohl for being my first evaluating supervisor and for all the helpful advises, given during the whole formation process of my thesis.

Also, I would like to thank Dr. Tilmann Schwenk for agreeing to be my second evaluating supervisor.

Furthermore, I would like to thank the Geophysics group of the Alfred Wegener Institute for their help with the program tools I used to work with the data. Many thanks to Florian Riefstahl for teaching me how to handle the software *GMT* and *Paradigm Echos* as well as *Paradigm Epos*. I want to thank Dr. Estella Weigelt and Dr. Katharina Hochmuth for their advises during the work with the *Paradigm* software. Moreover, I would like to thank Dr. Catalina Gebhardt for providing the software and knowledge to work with the Parasound data and Dr. Jan Erik Arndt for the help with gridding the NIWA bathymetric data.

Last but not least, many thanks to my friends Philipp Kelm, Janna-Lina Heuser, Florentina Münzner and Verena Nickel for their advises during the last phase of finishing my work. I would also like to thank my family for their support during my studies.

List of figures

List of tables

List of abbreviations

DWBC	Deep Western Boundary Current
ENZOSS	Eastern New Zealand Sedimentary System
ACC	Antarctic Circumpolar Current
THC	Global Thermohaline Circulation
CMP	Common Mid-point
TWT	Two-way-traveltime
CDP	Common depth-point
NMO	Normal move-out

Appendix

A. Seismic reflection profiles from SO246

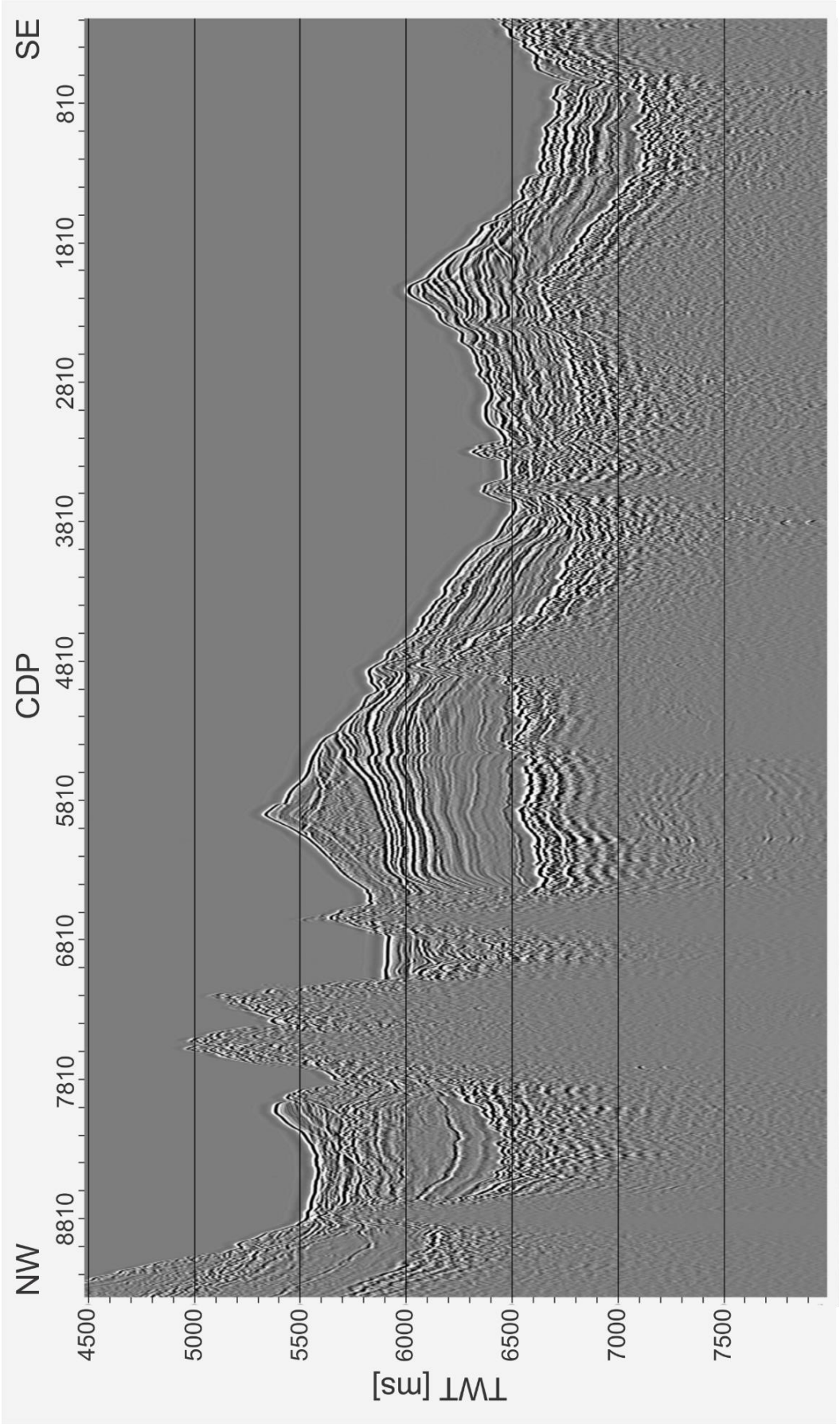

Fig. A.1: Processed seismic reflection profile AWI-20160001

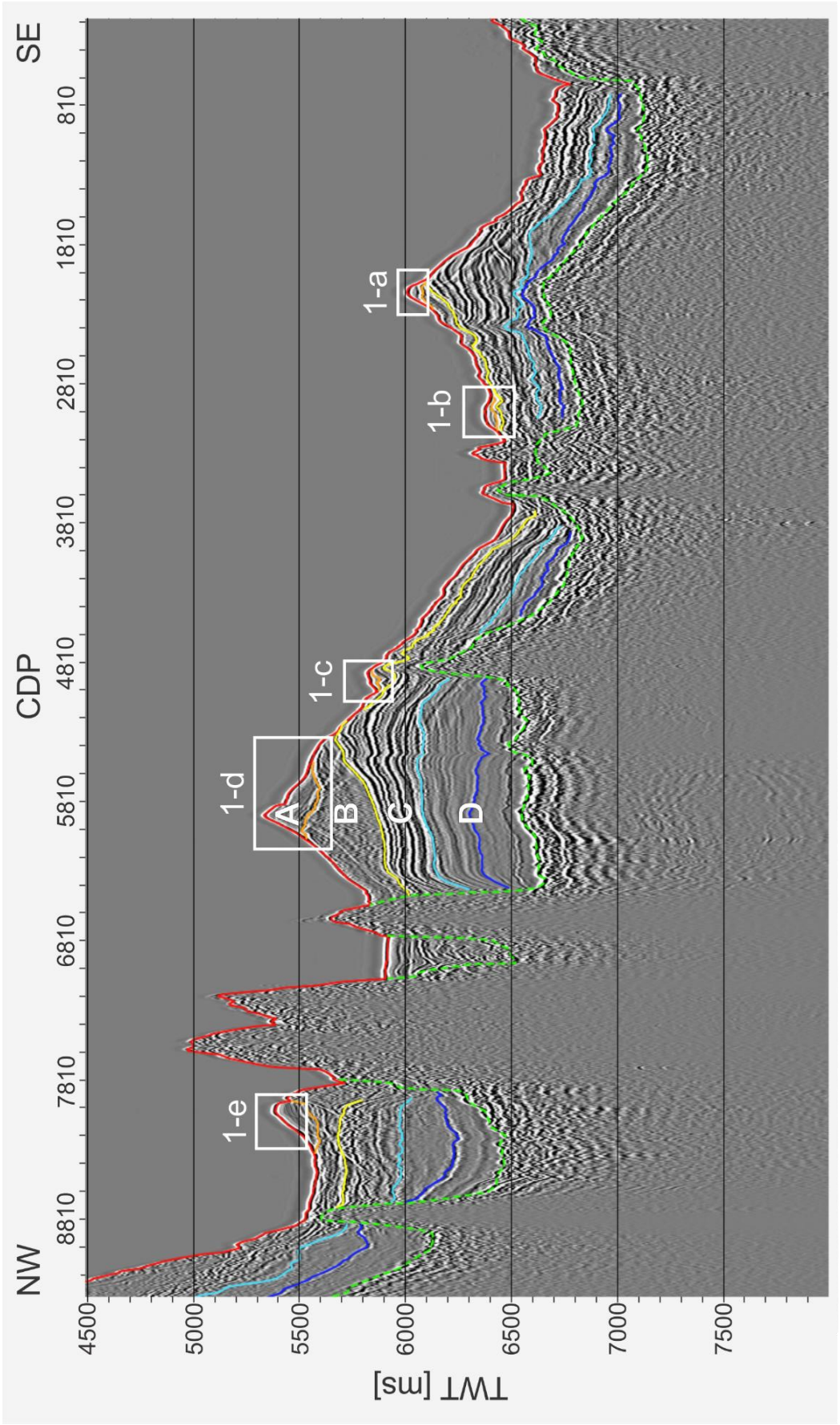

Fig. A.2: Processed seismic reflection profile AWI-20160001 with seismic interpretation, white boxes show locations of Parasound profiles

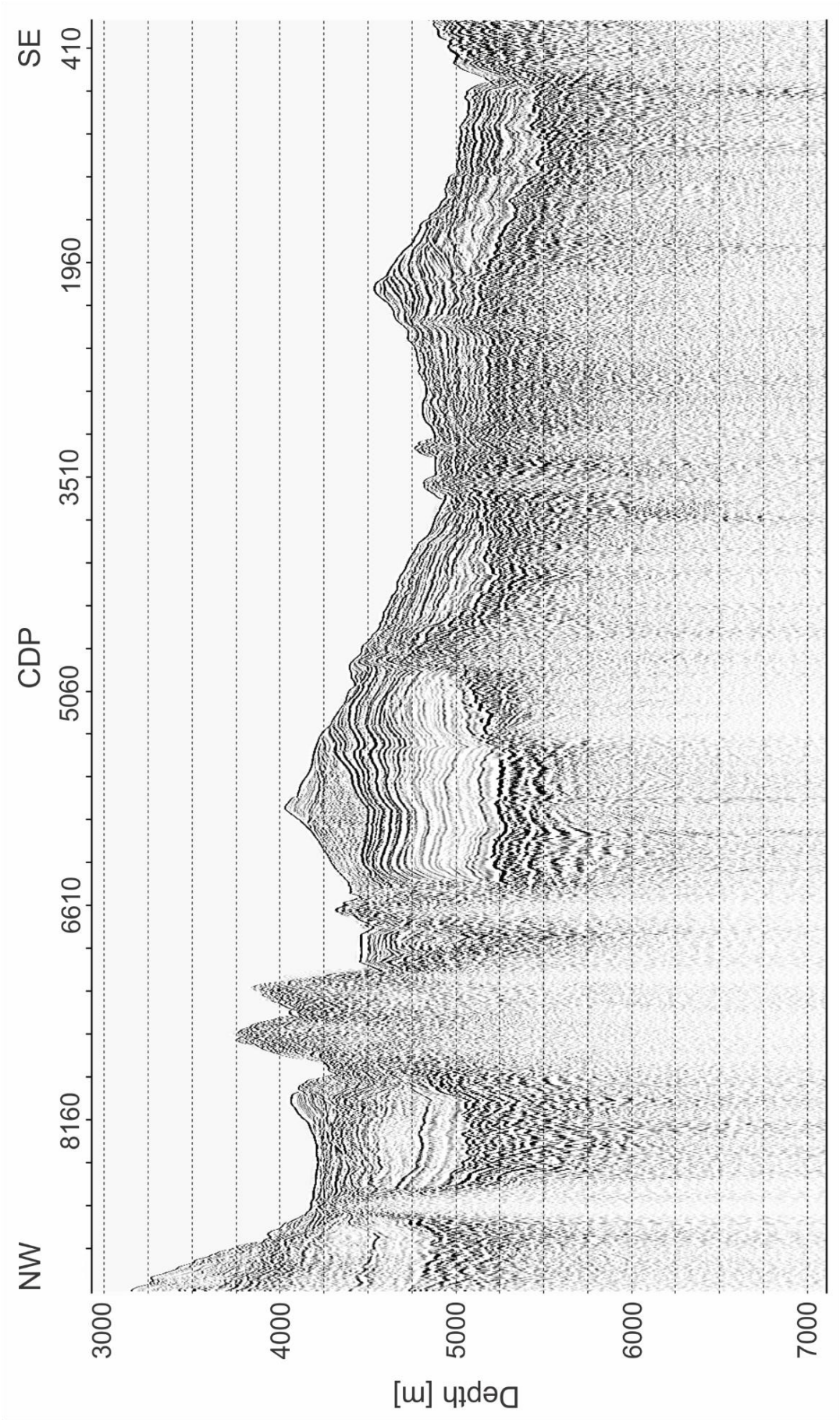

Fig. A3: Processed seismic reflection profile AWI-20160001 converted to depth

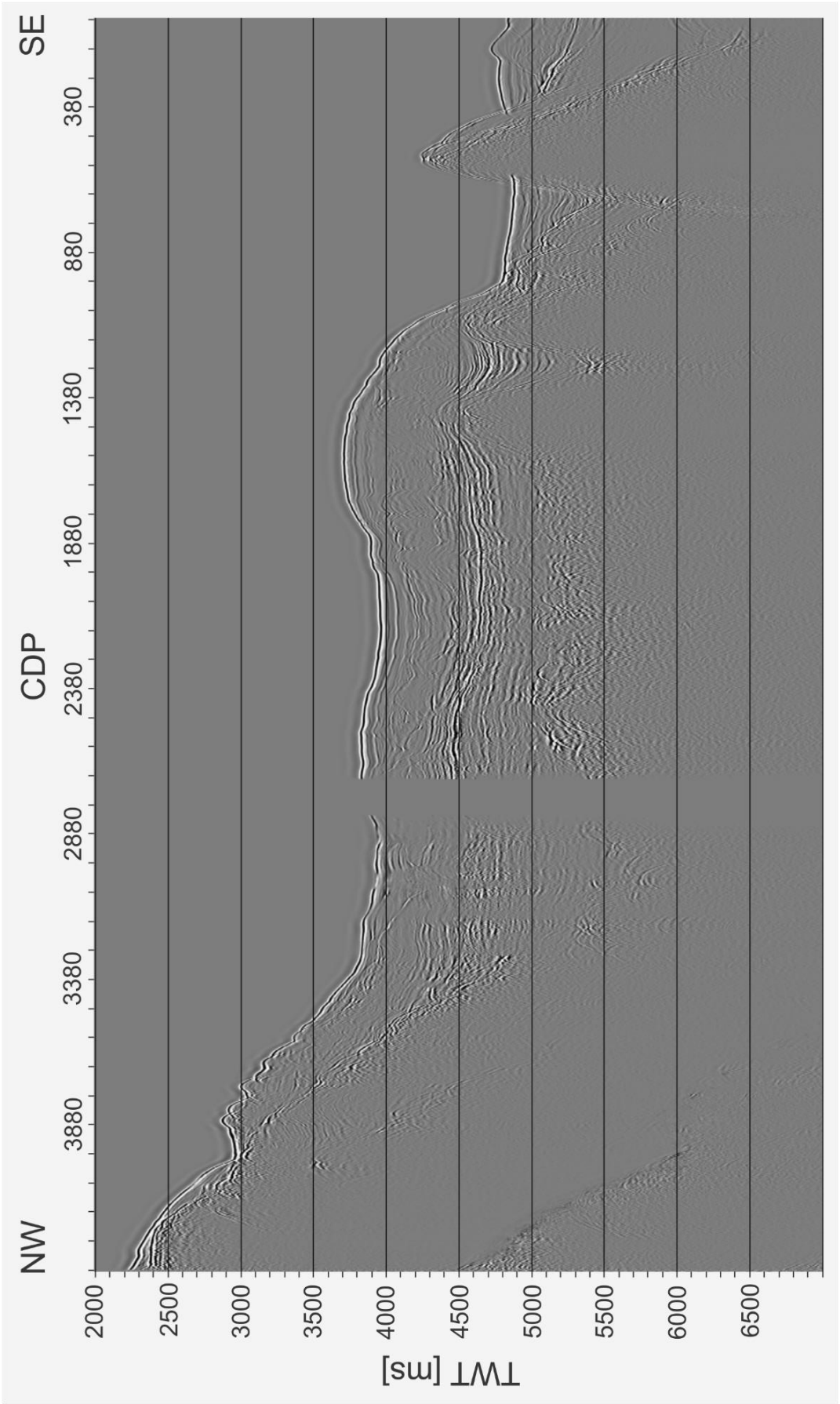

Fig. A.4: Processed seismic reflection profile AWI-20160002

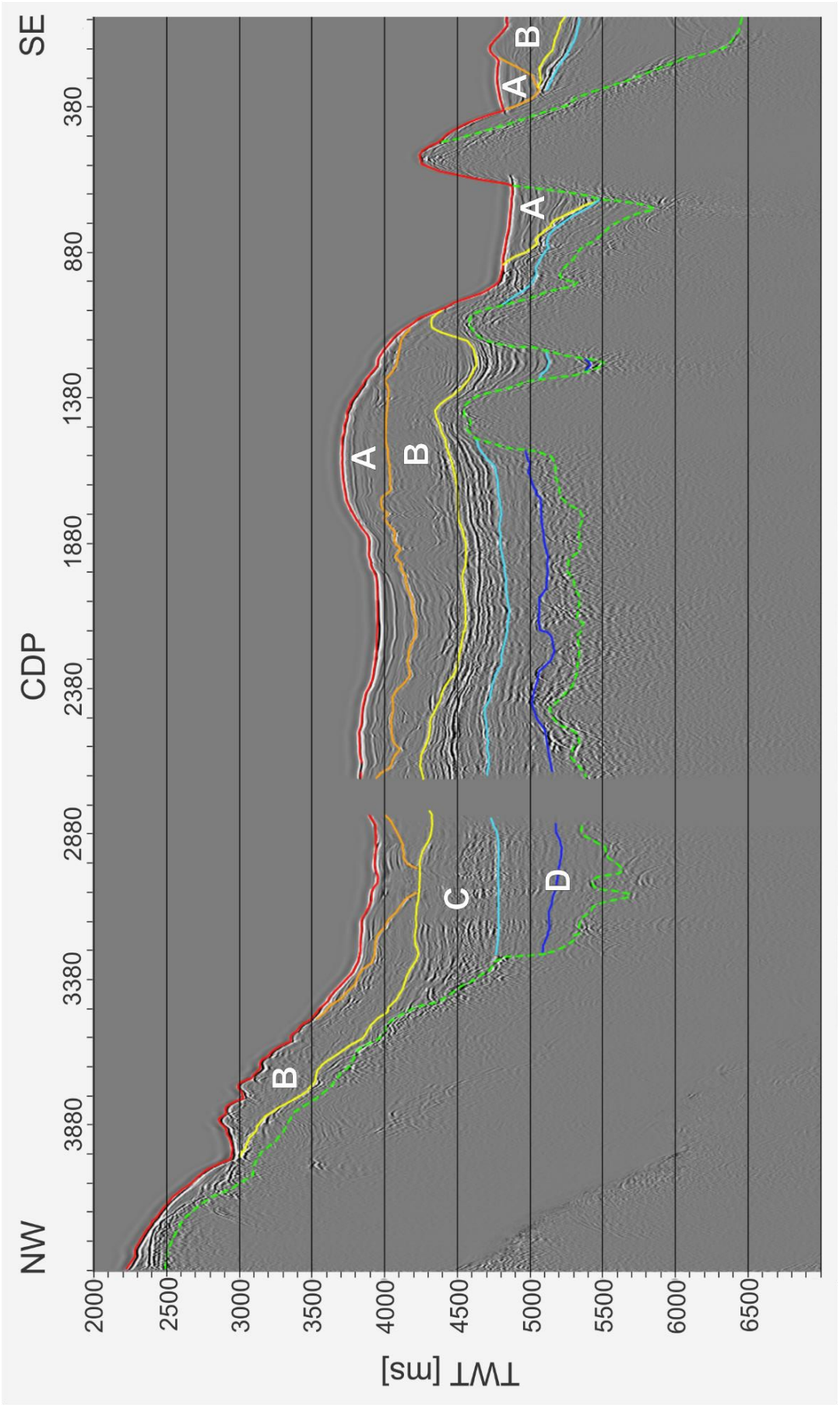

Fig. A.5: Processed seismic reflection profile AWI-20160002 with seismic interpretation

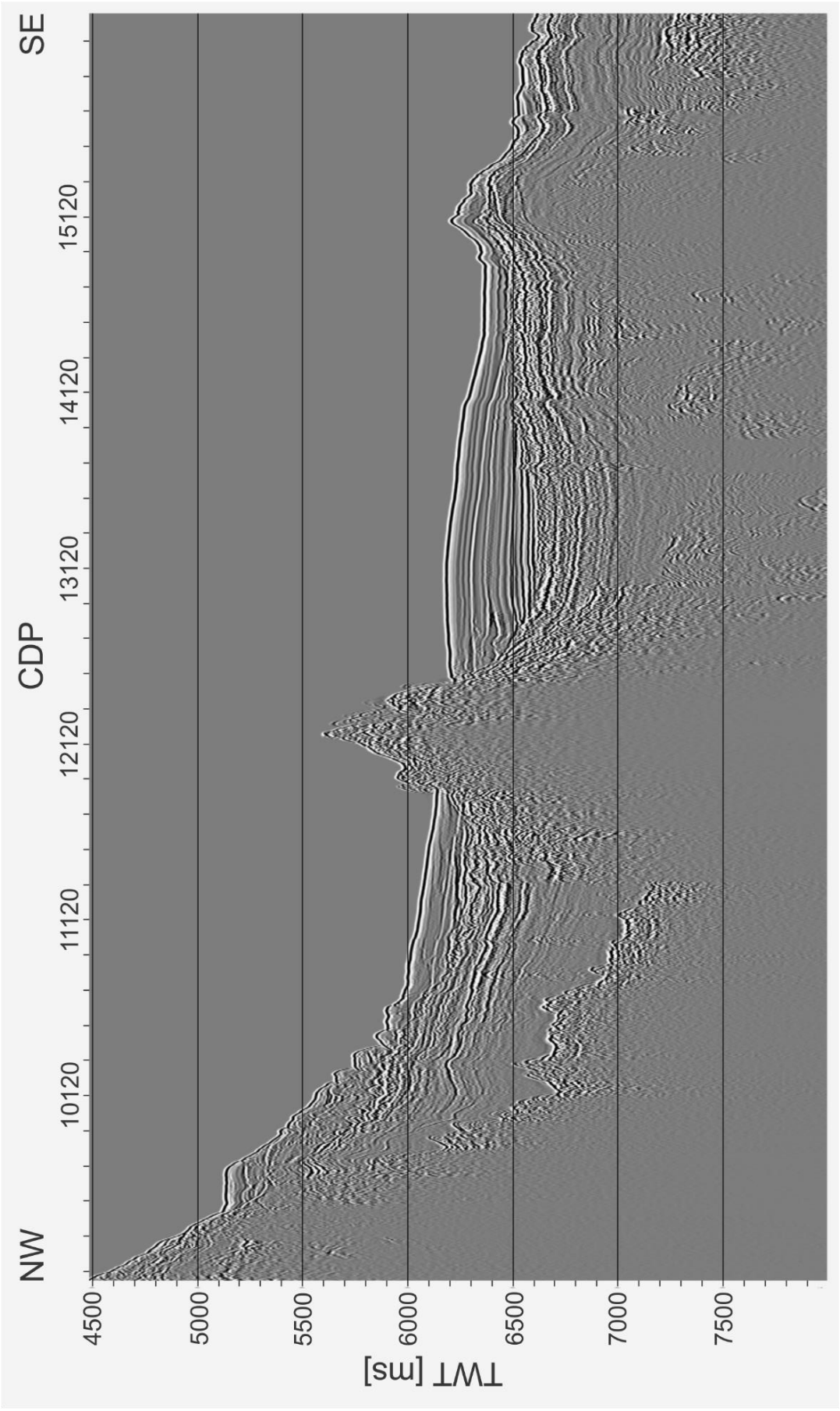

Fig. A.6: Processed seismic reflection profile AWI-20160003

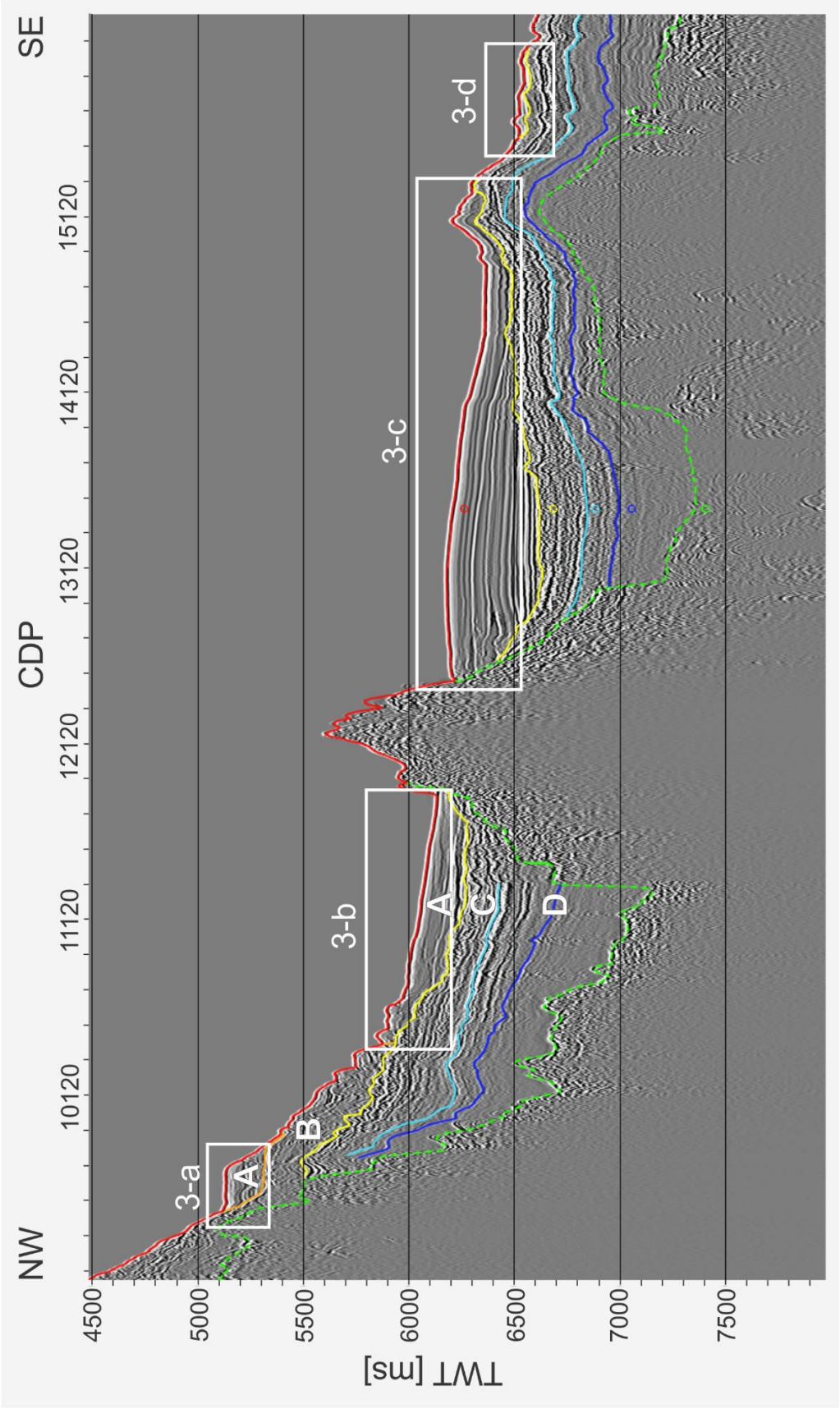

Fig. A.7: Processed seismic reflection profile AWI-20160003 with seismic interpretation, white boxes show locations of Parasound profiles. Little, colored circles mark the intersection points with horizons from profile tan0207-cr2.

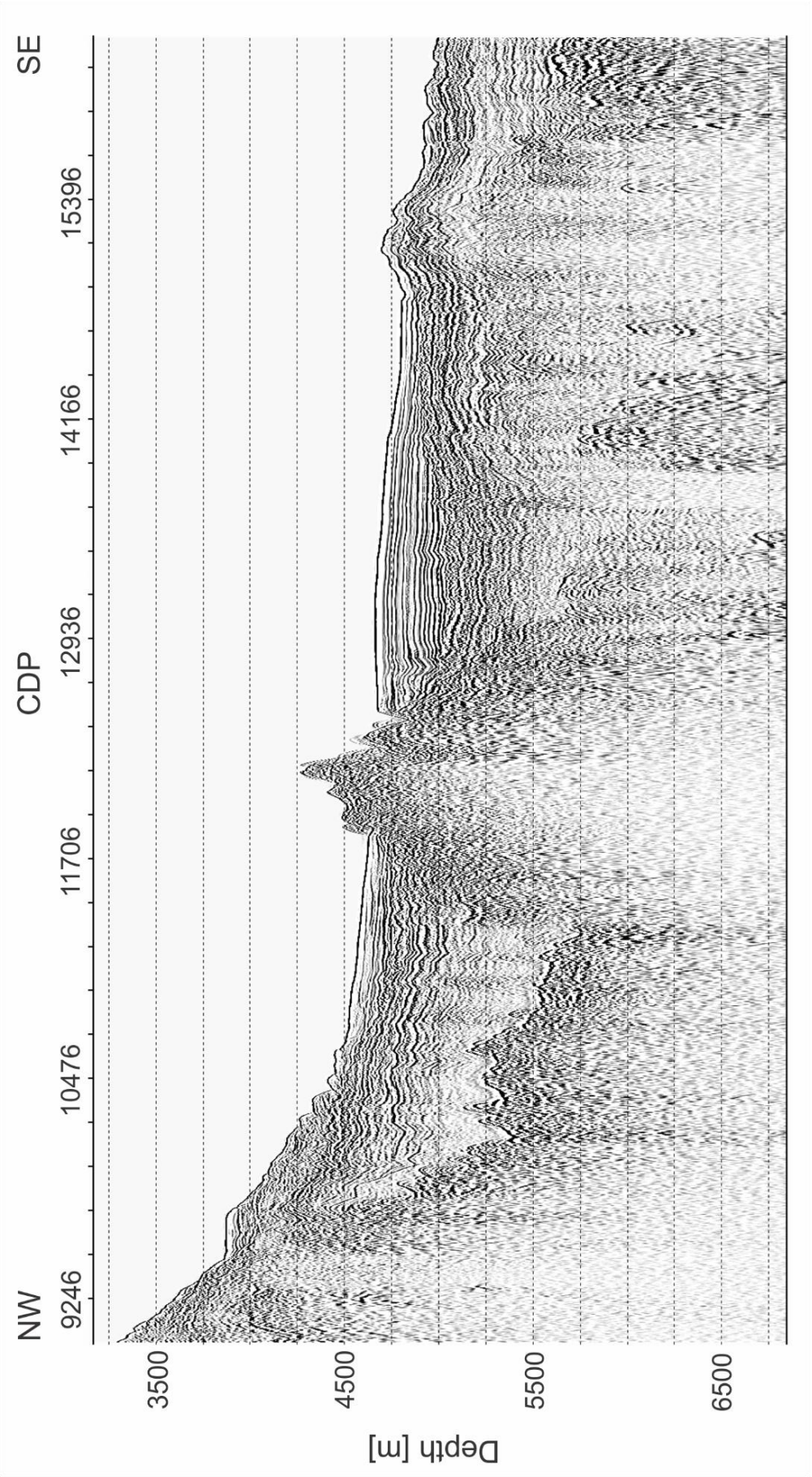

Fig. A.8: Processed seismic reflection profile AWI-20160003 converted to depth

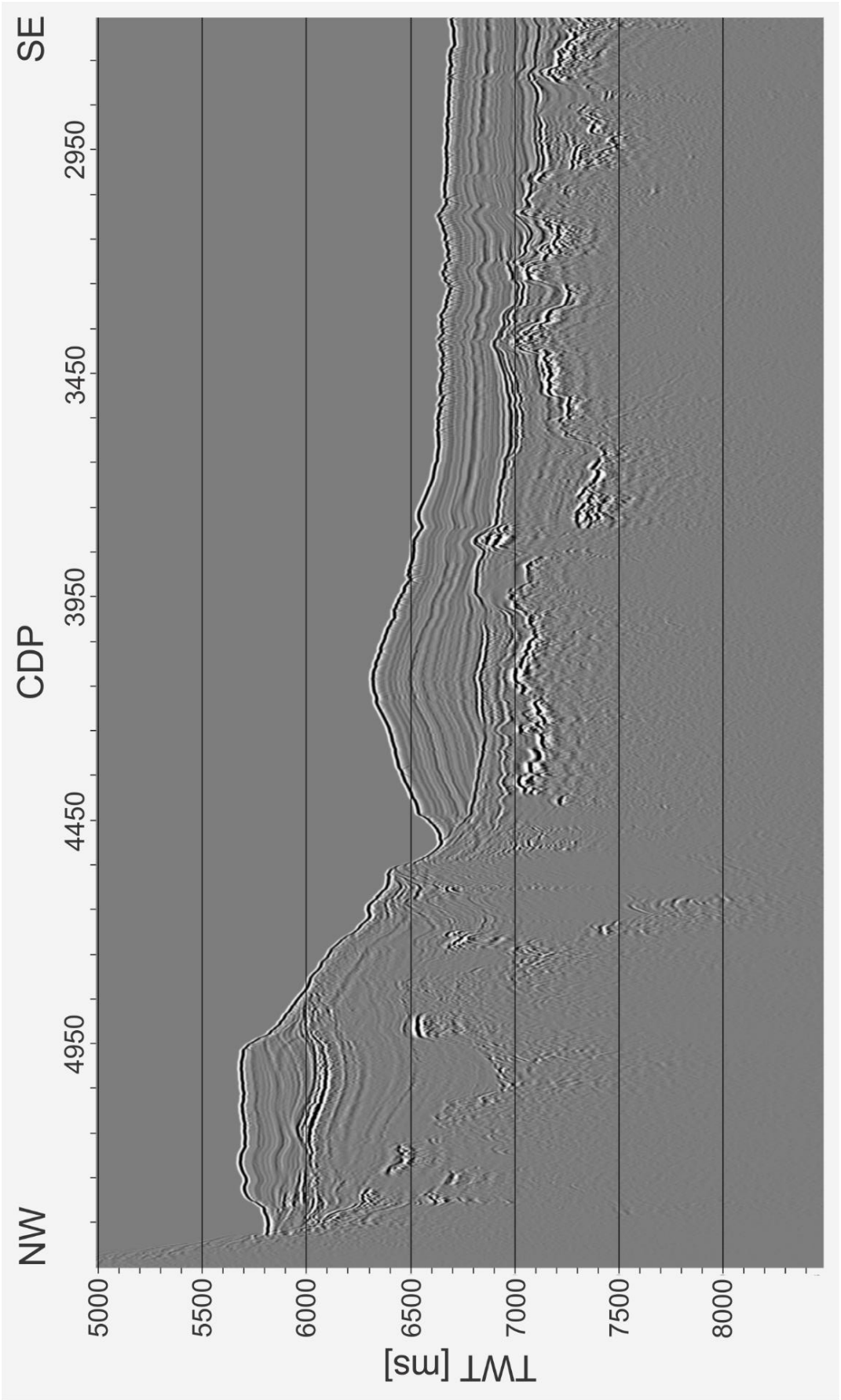

Fig. A.9: Processed seismic reflection profile AWI-20160301

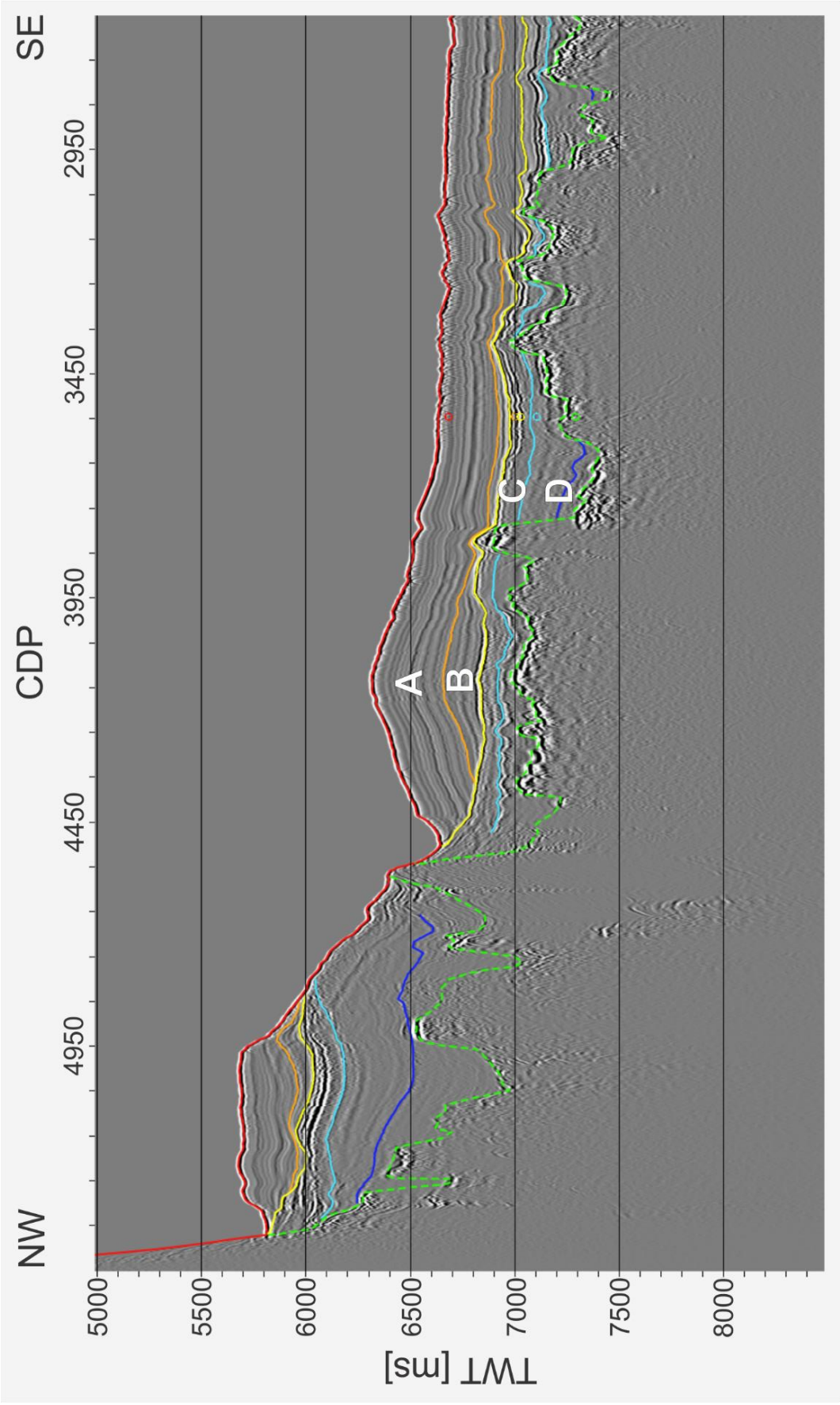

Fig. A.10: Processed seismic reflection profile AWI-20160301 with seismic interpretation. Little, colored circles mark the intersection points with horizons from profile tan0207-cr5a

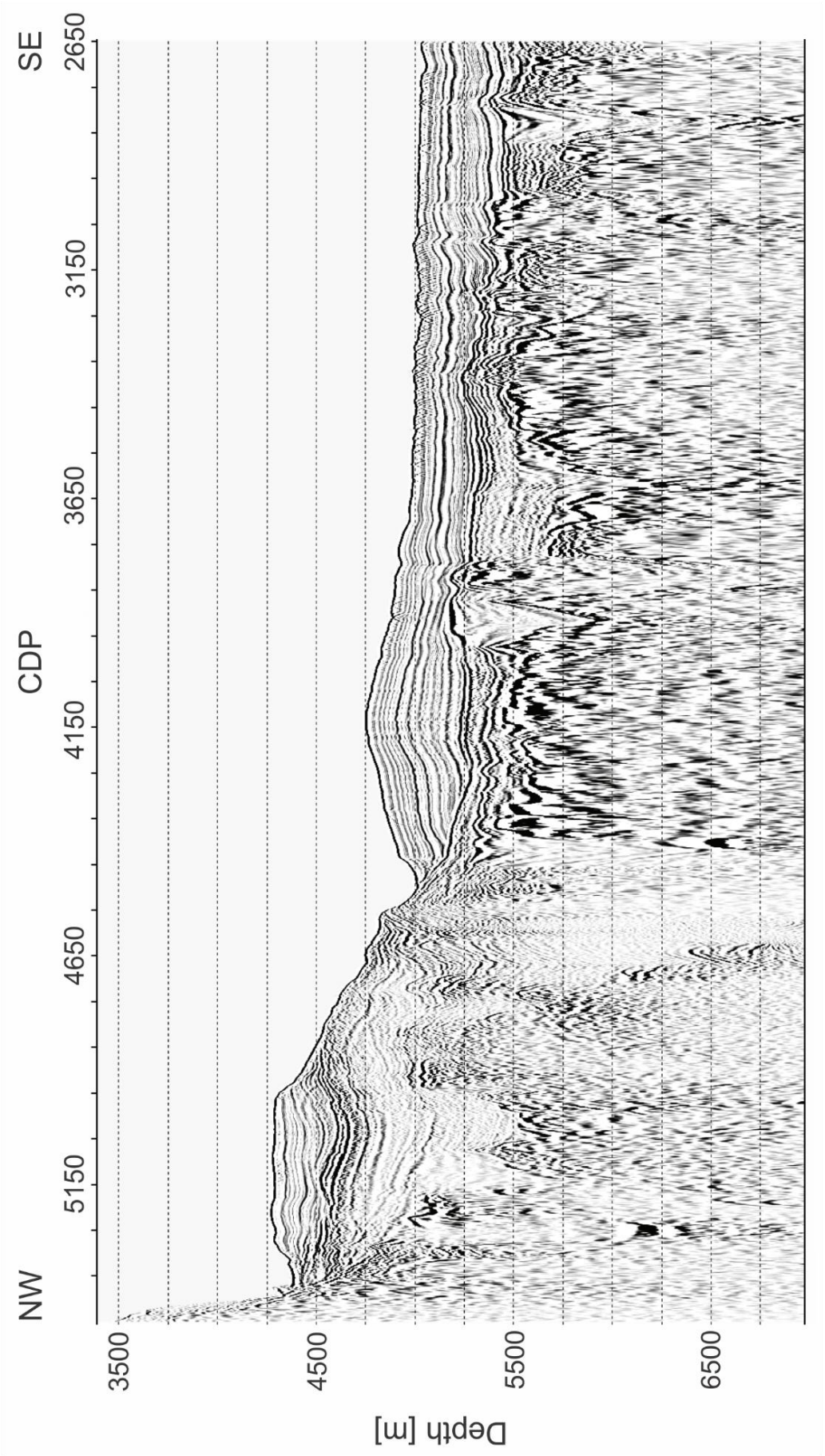

Fig. A.11: Processed seismic reflection profile AWI-20160301 converted to depth

B. Seismic reflection profiles from New Zealand

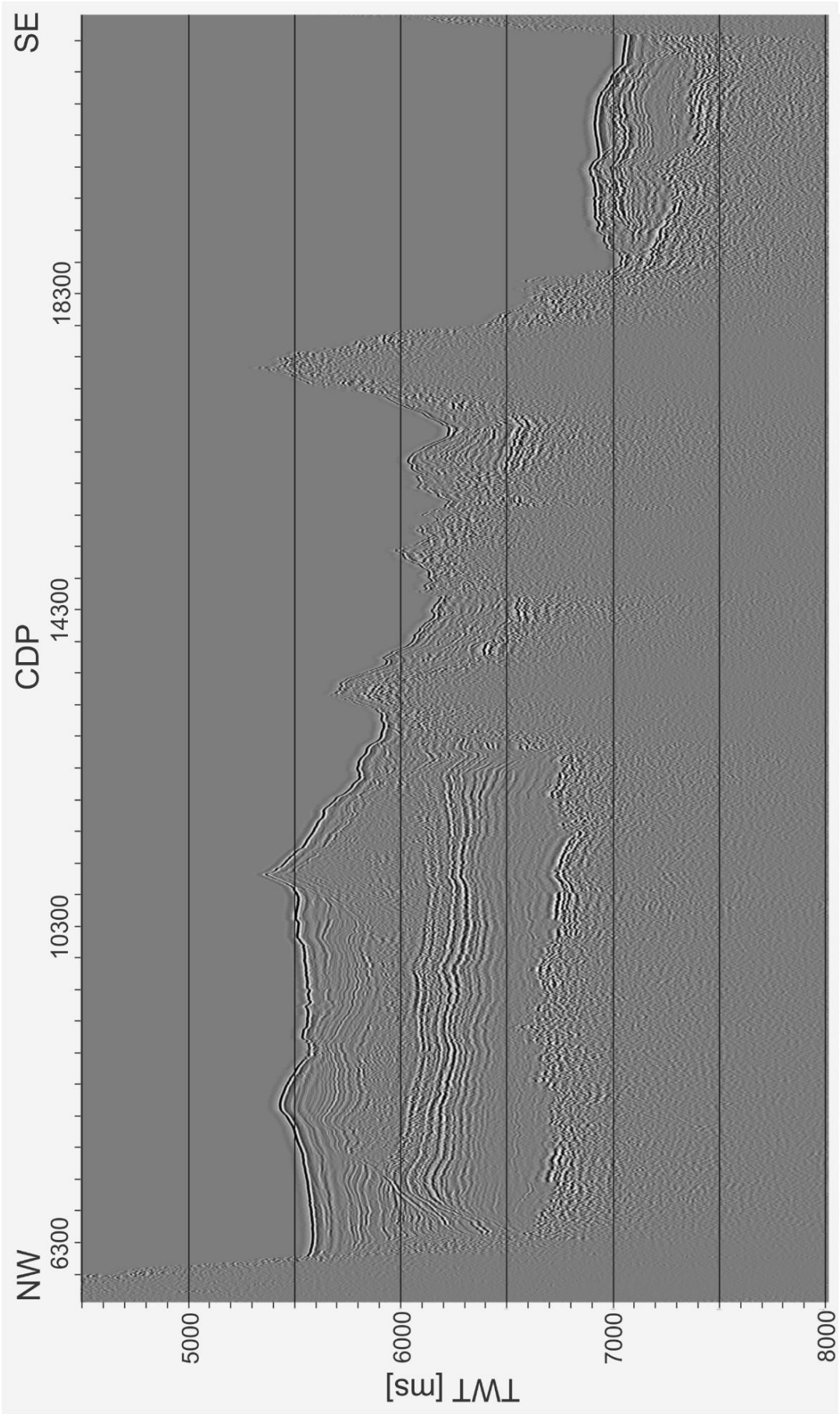

Fig. B.1: Seismic reflection profile tan0207-bt2

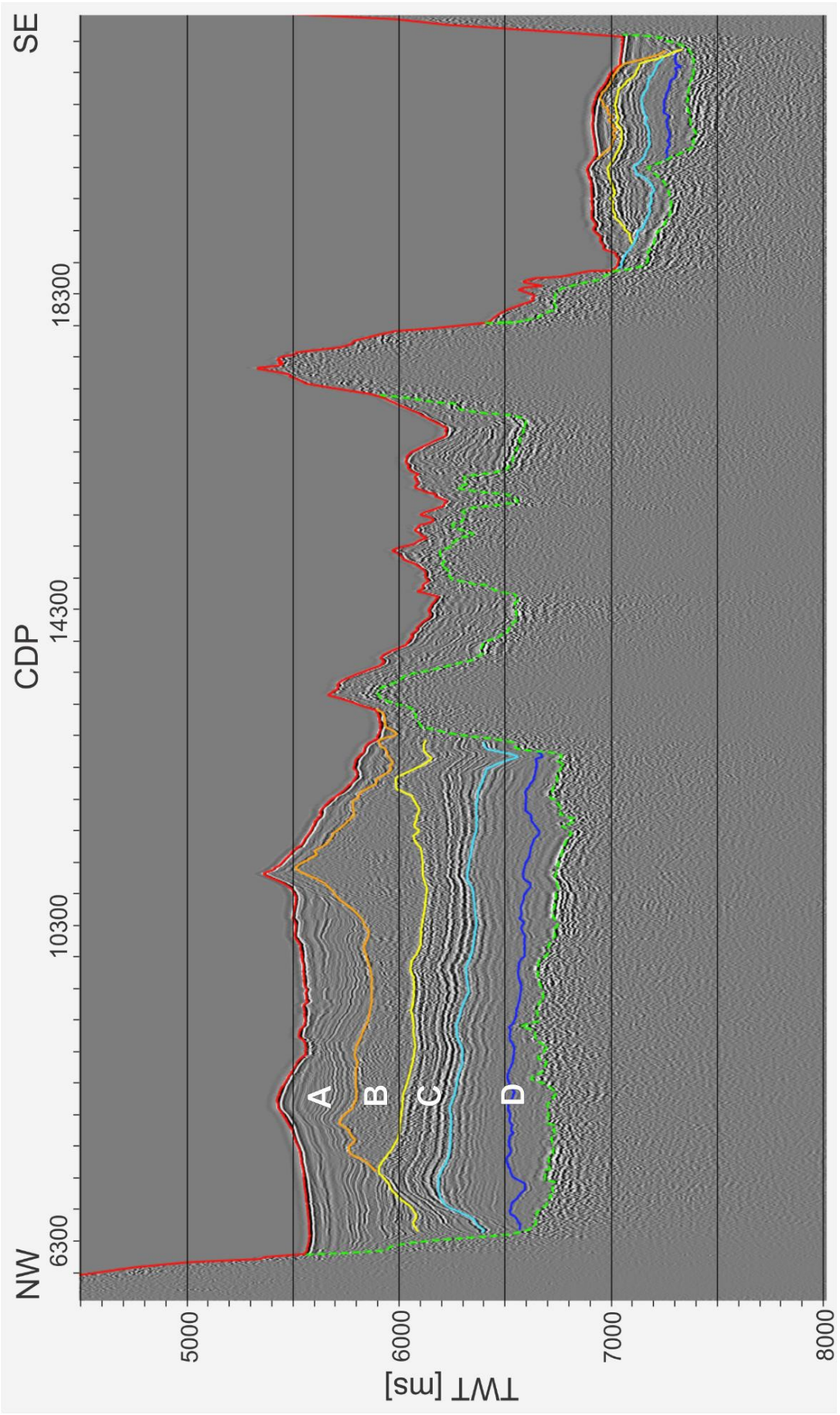

Fig. B.2: Seismic reflection profile tan0207-bt2 with seismic interpretation

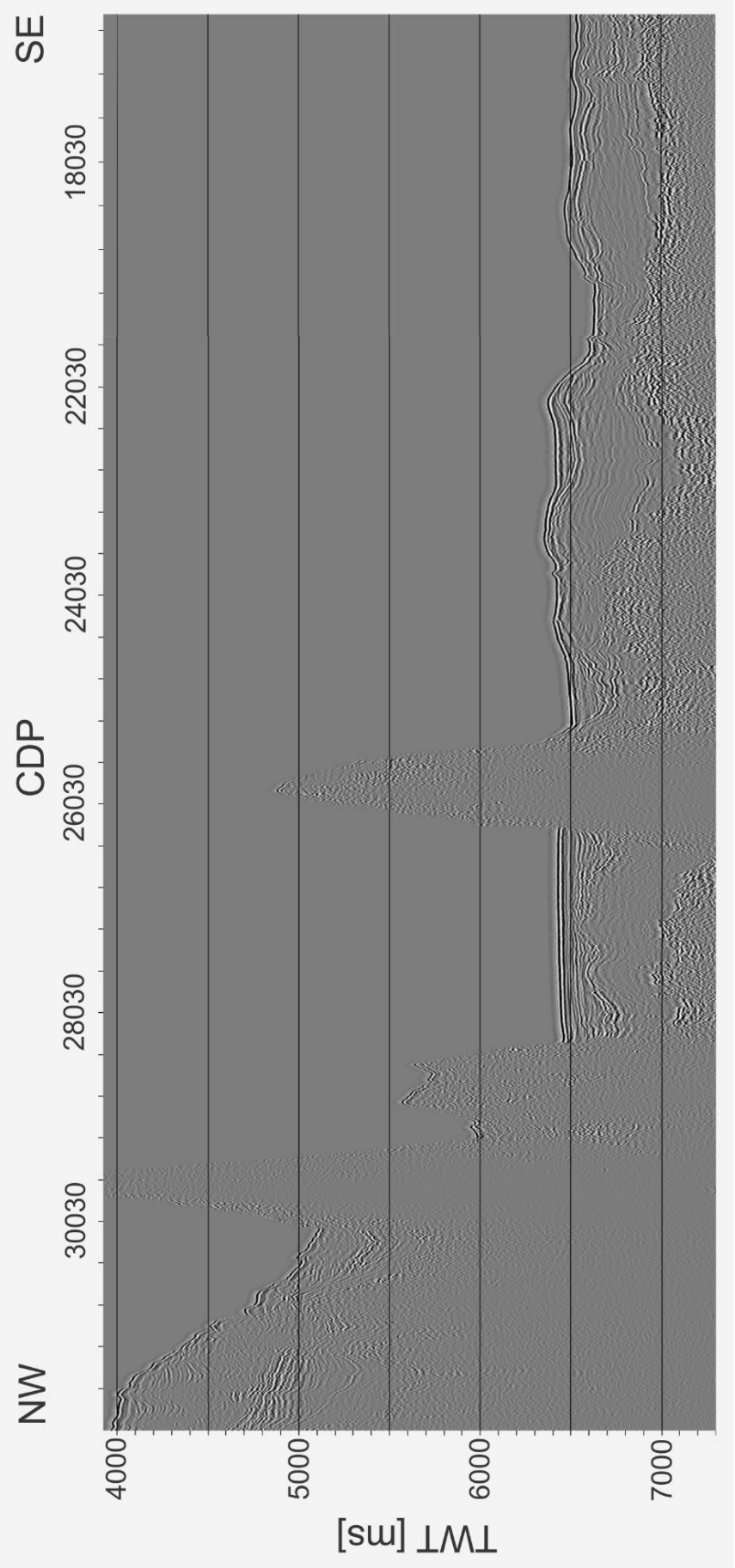

Fig. B.3: Seismic reflection profile tan0207-cr1

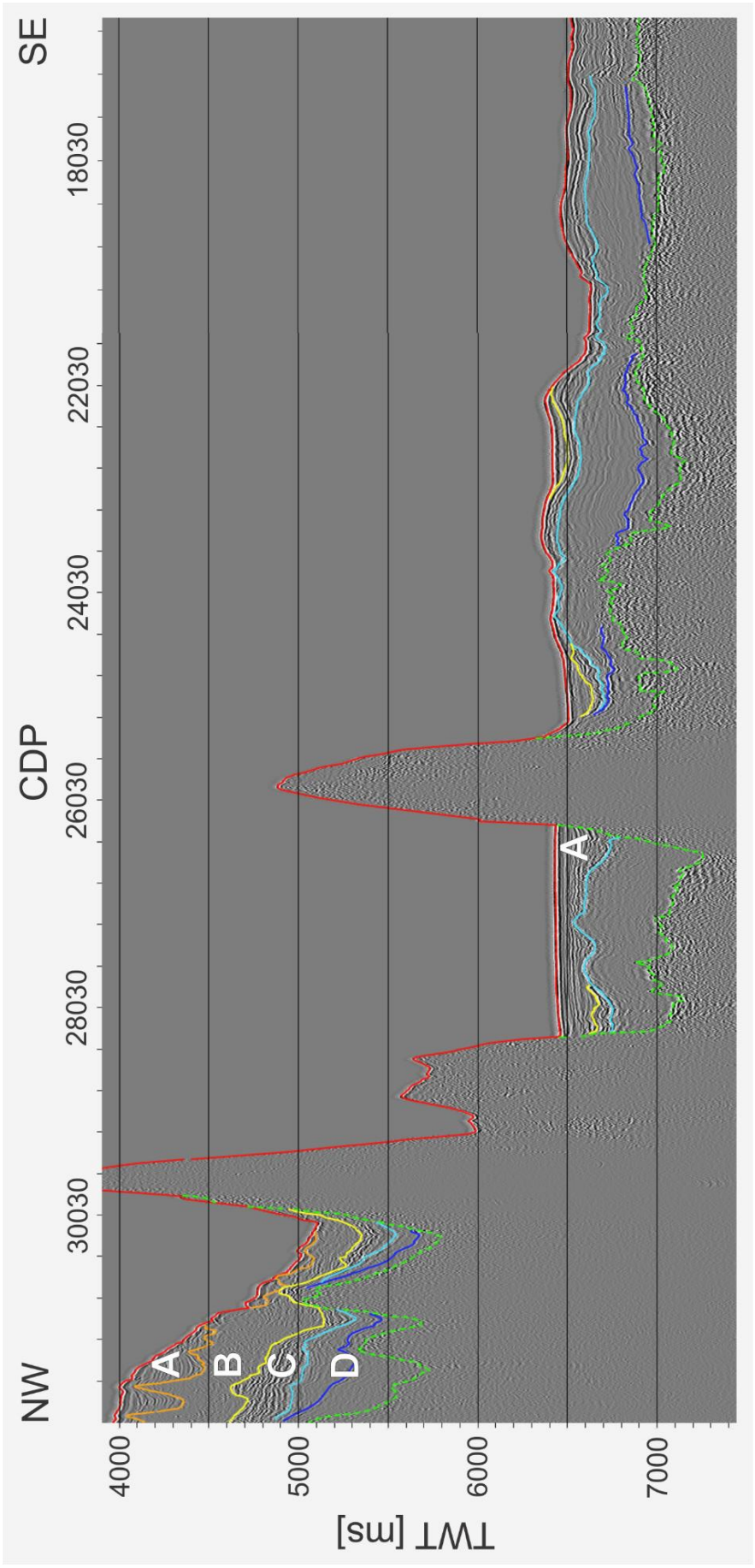

Fig. B.4: Seismic reflection profile tan0207-cr1 with seismic interpretation

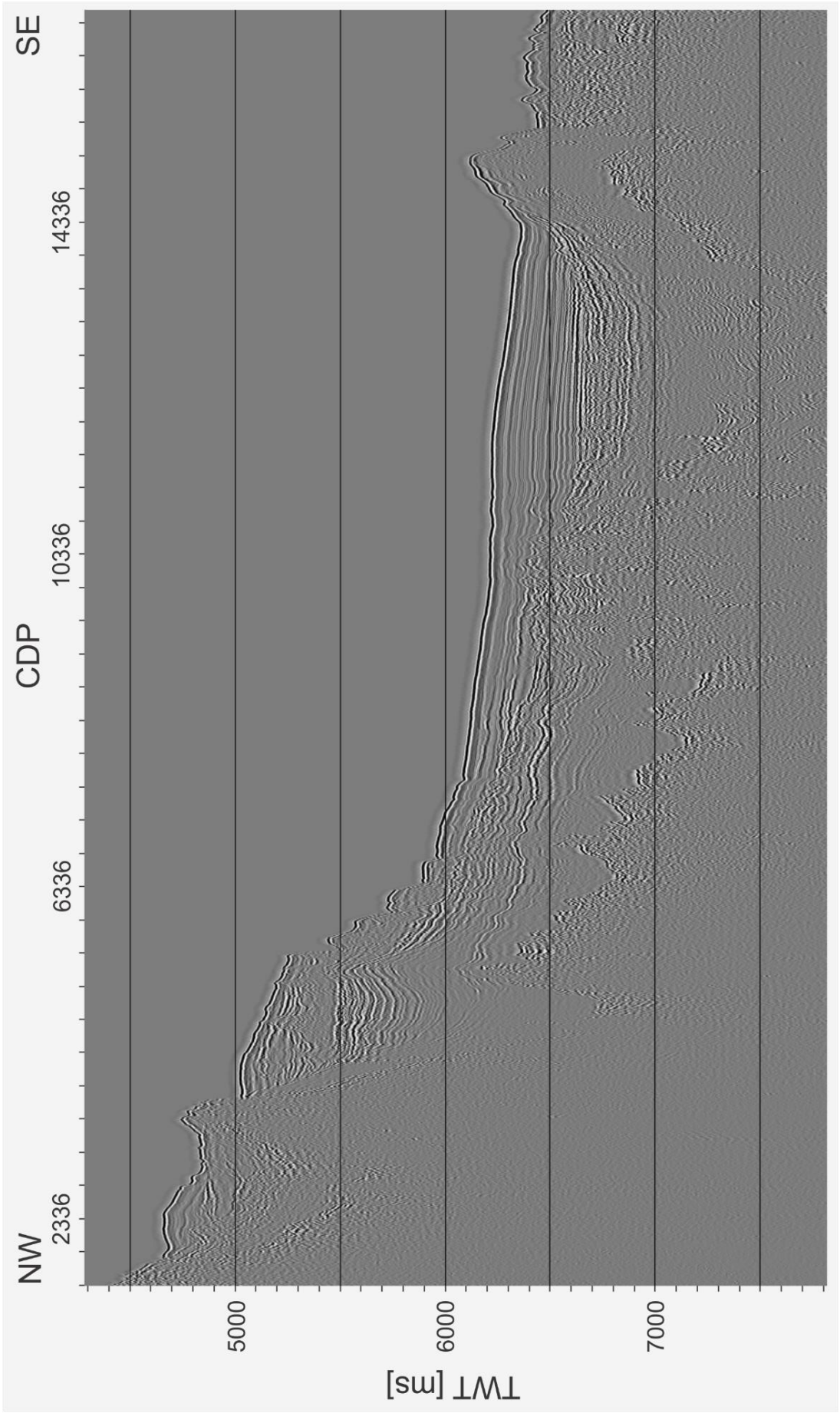

Fig. B.5: Seismic reflection profile tan0207-cr2

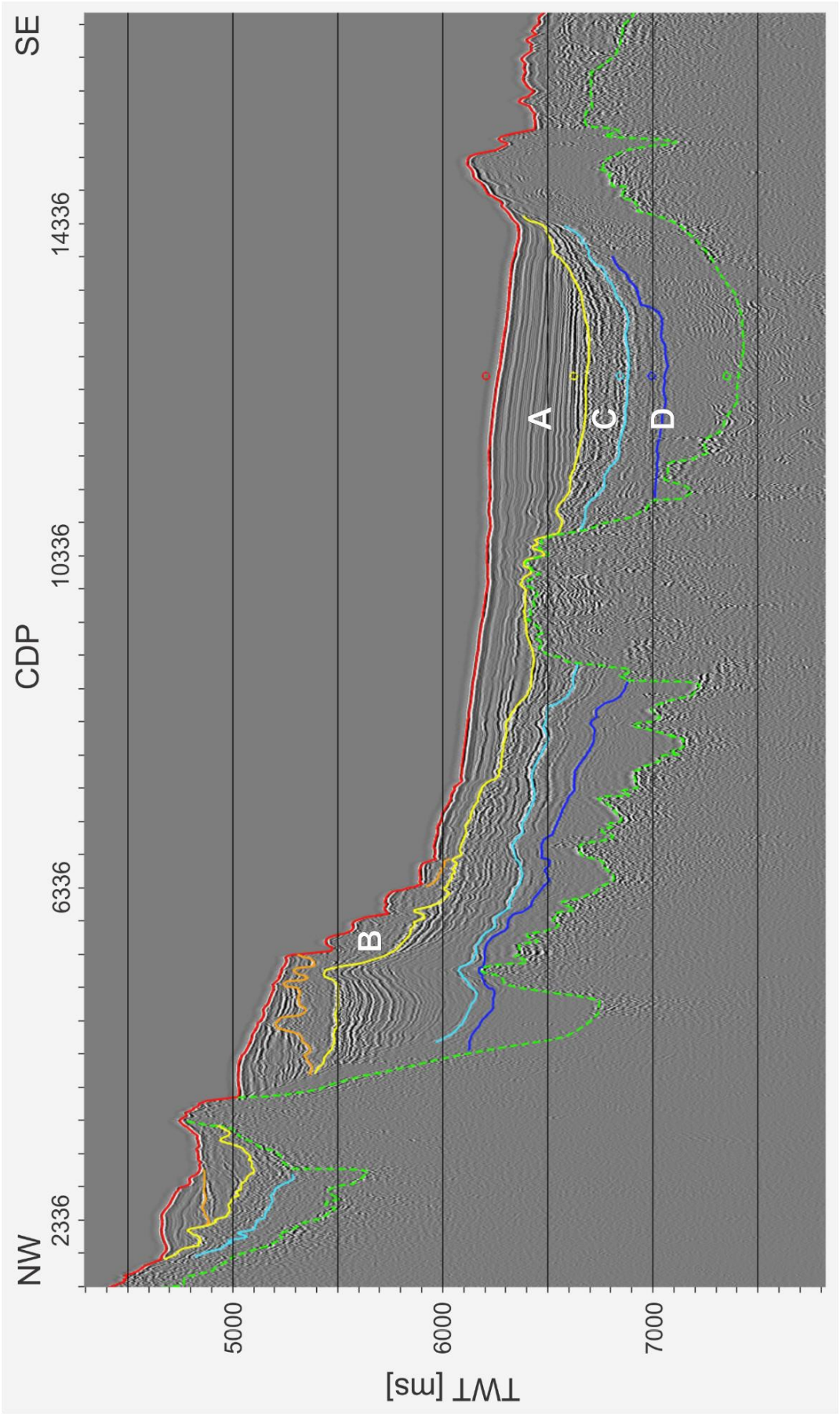

Fig. B.6: Seismic reflection profile tan0207-cr2 with seismic interpretation. Little, colored circles mark the intersection points with horizons from profile AWI-20160003

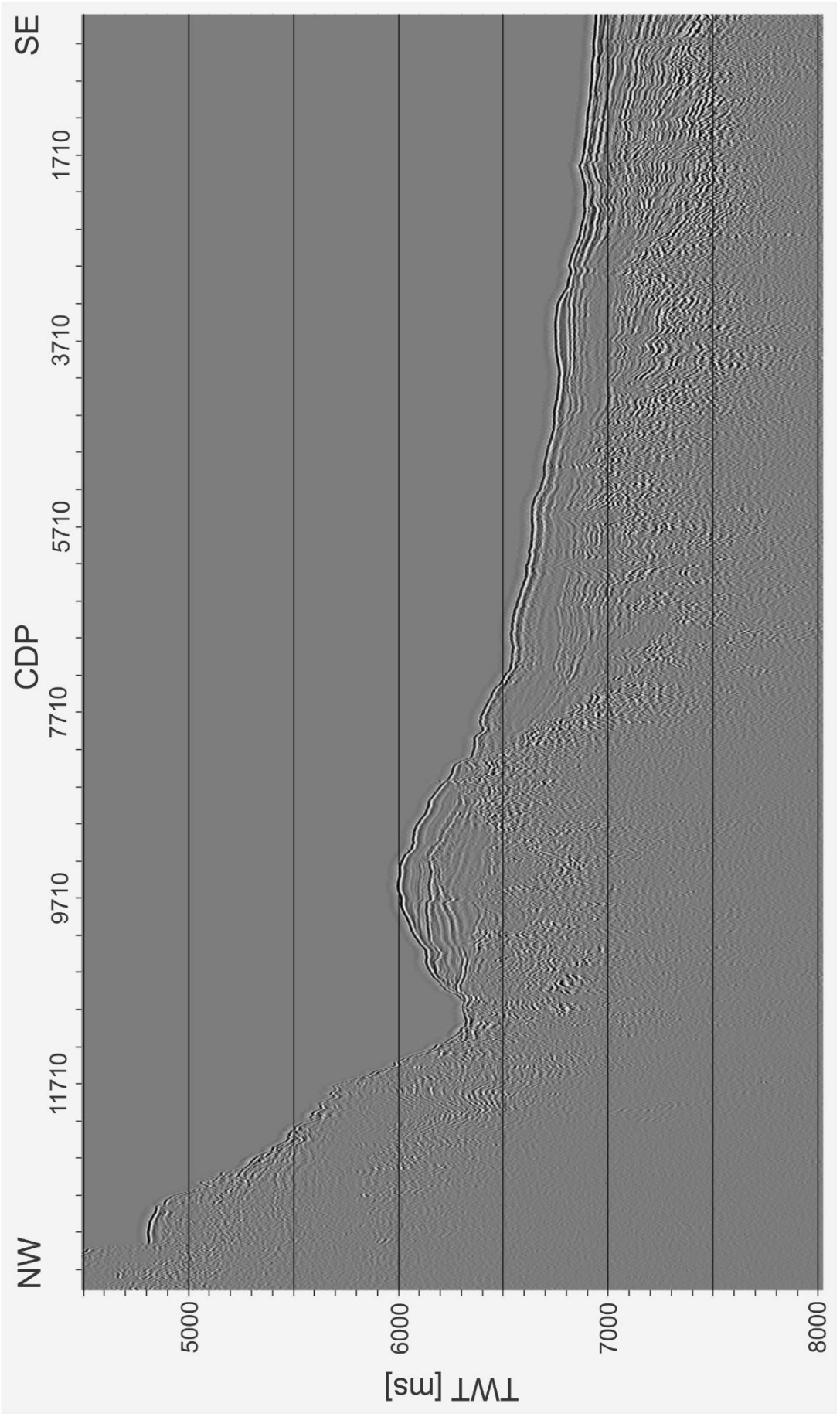

Fig. B.7: Seismic reflection profile tan0207-cr3

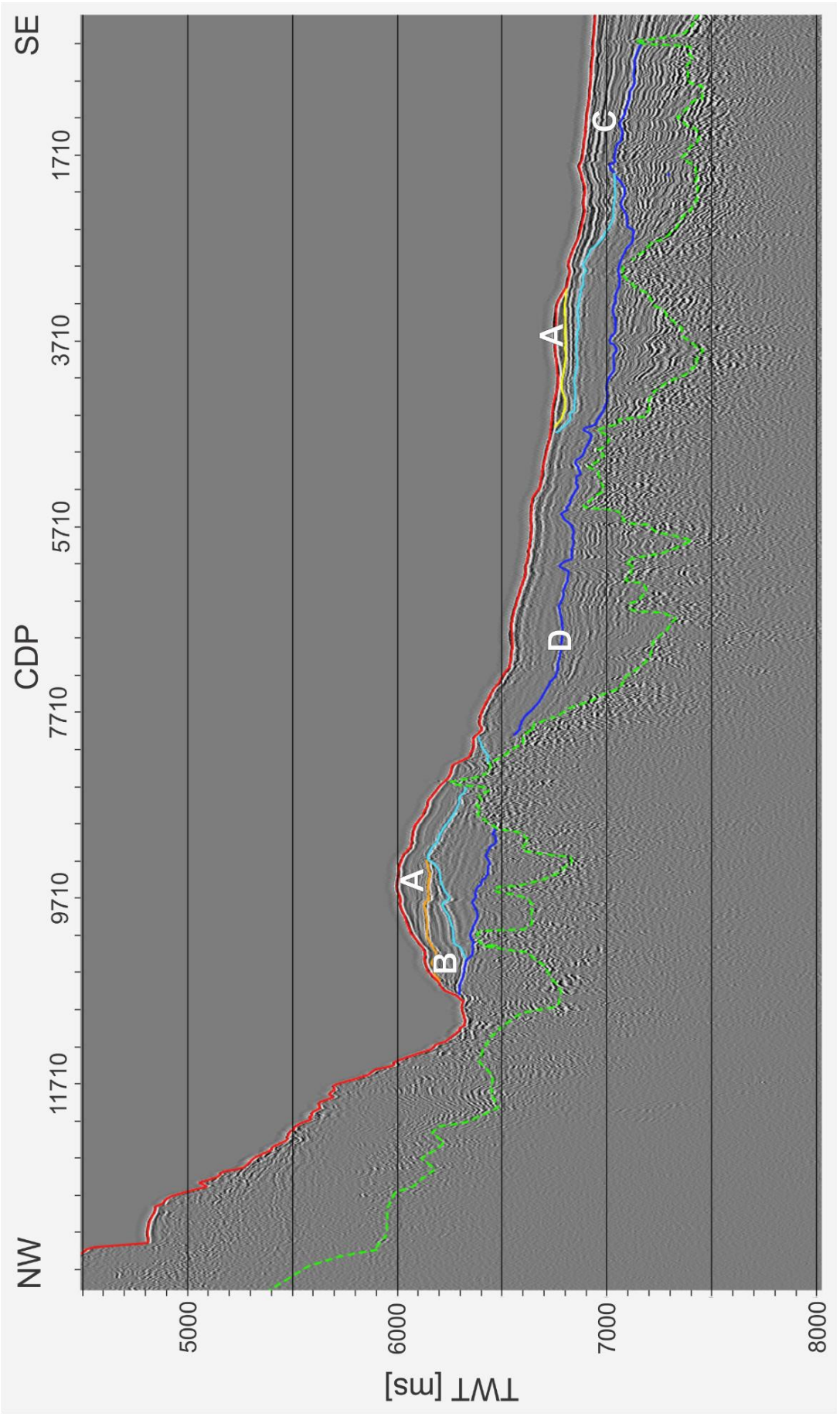

Fig. B.8: Seismic reflection profile tan0207-cr3 with seismic interpretation

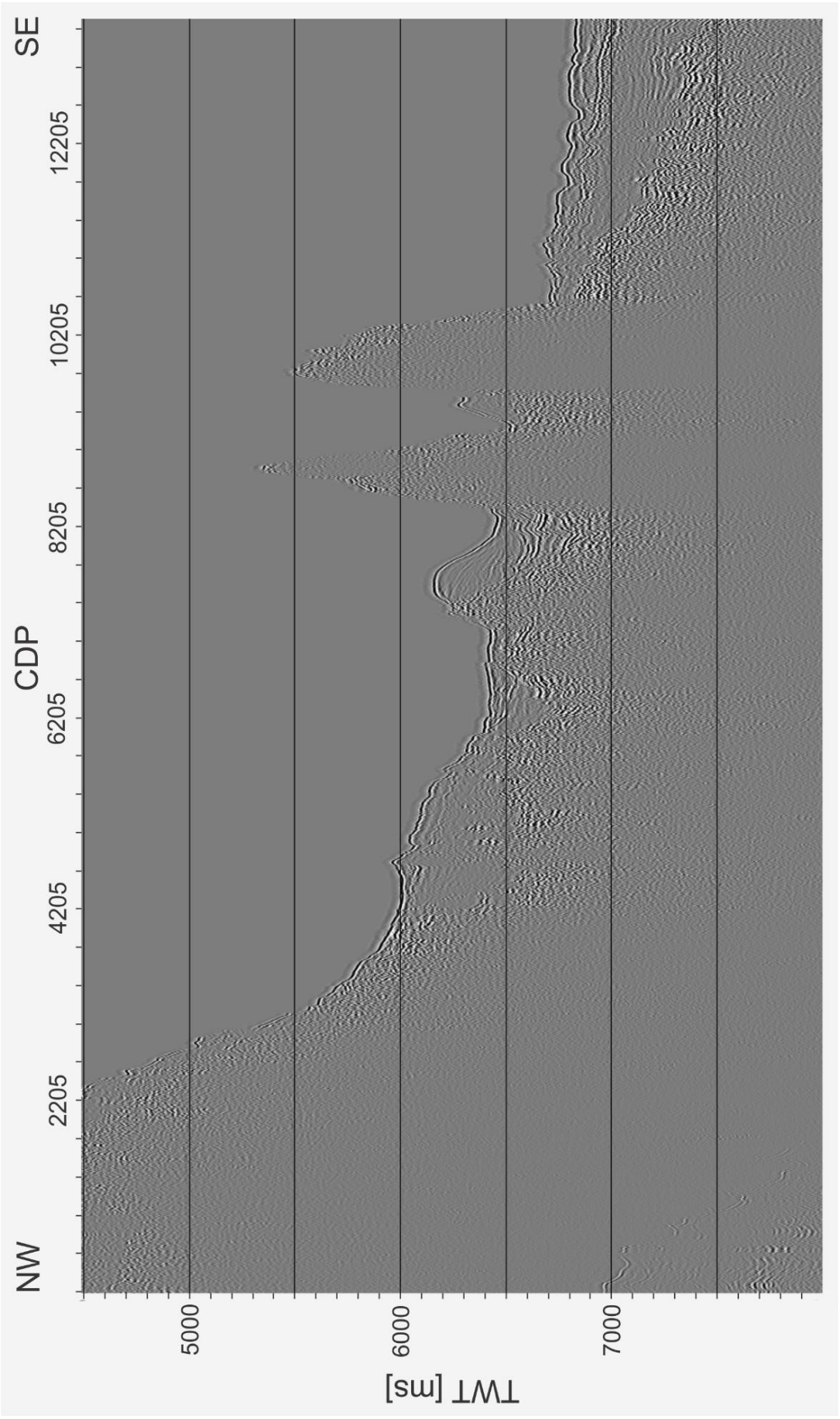

Fig. B.9: Seismic reflection profile tan0207-cr4

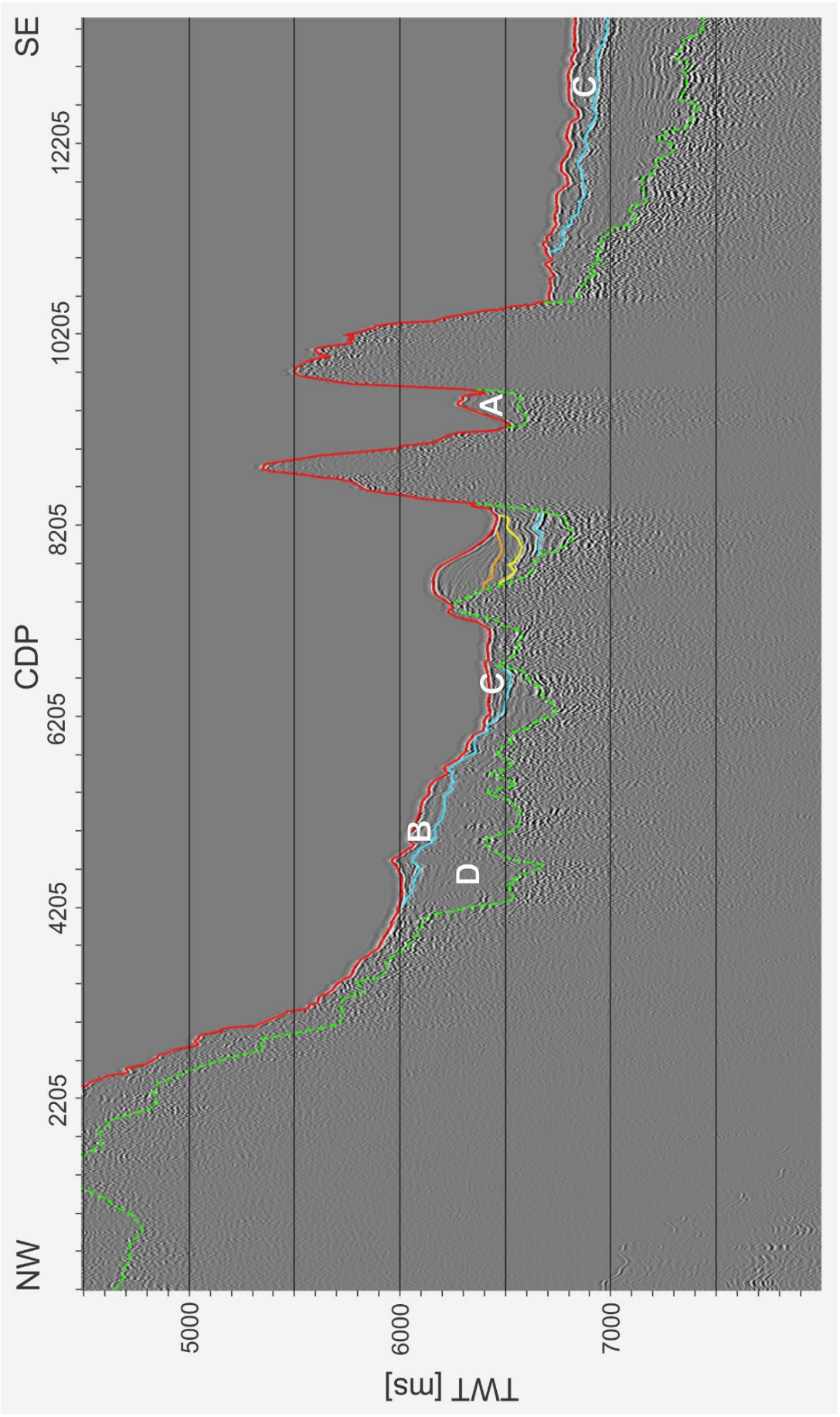

Fig. B.10: Seismic reflection profile tan0207-cr4 with seismic interpretation

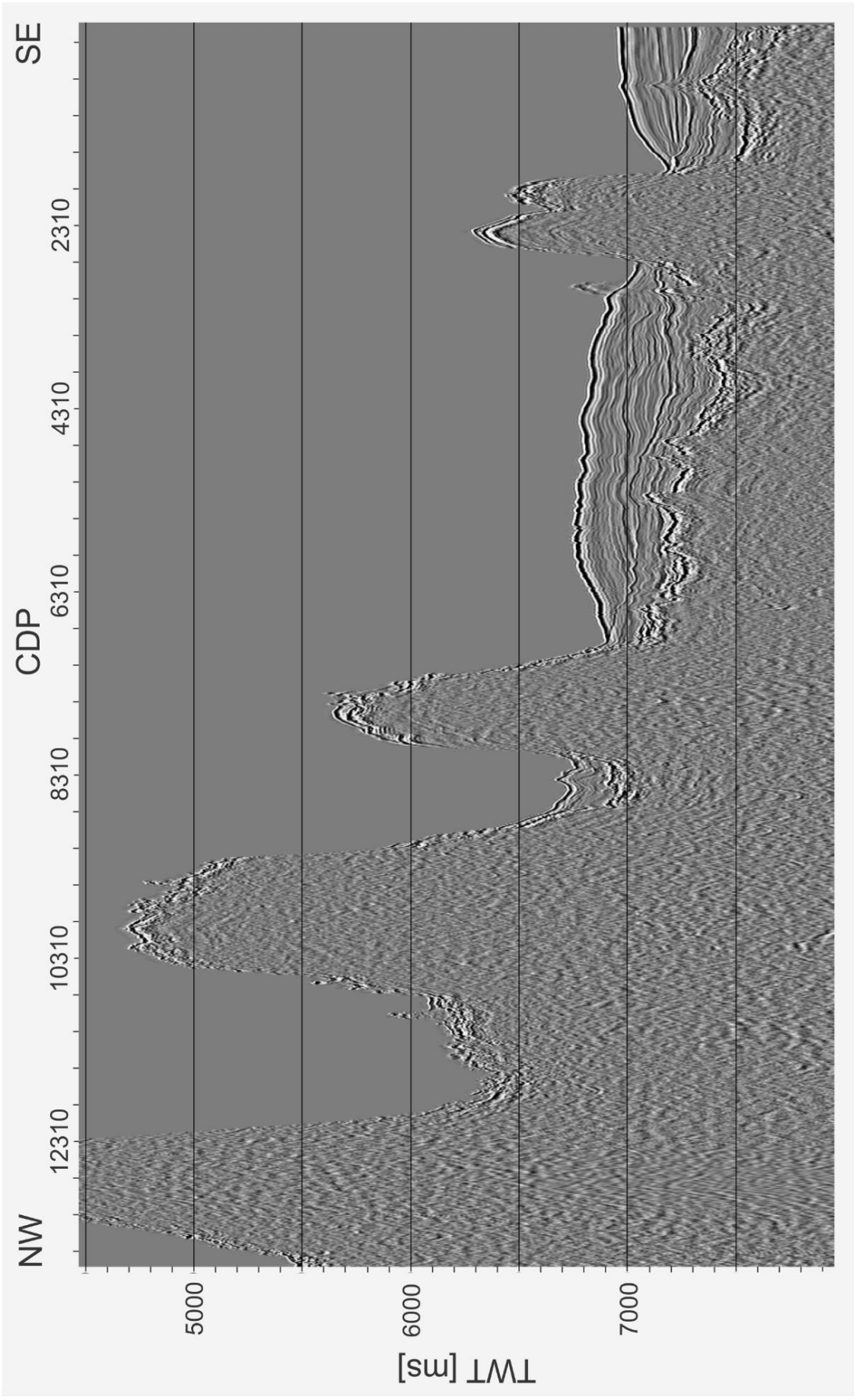

Fig. B.11: Seismic reflection profile cr5

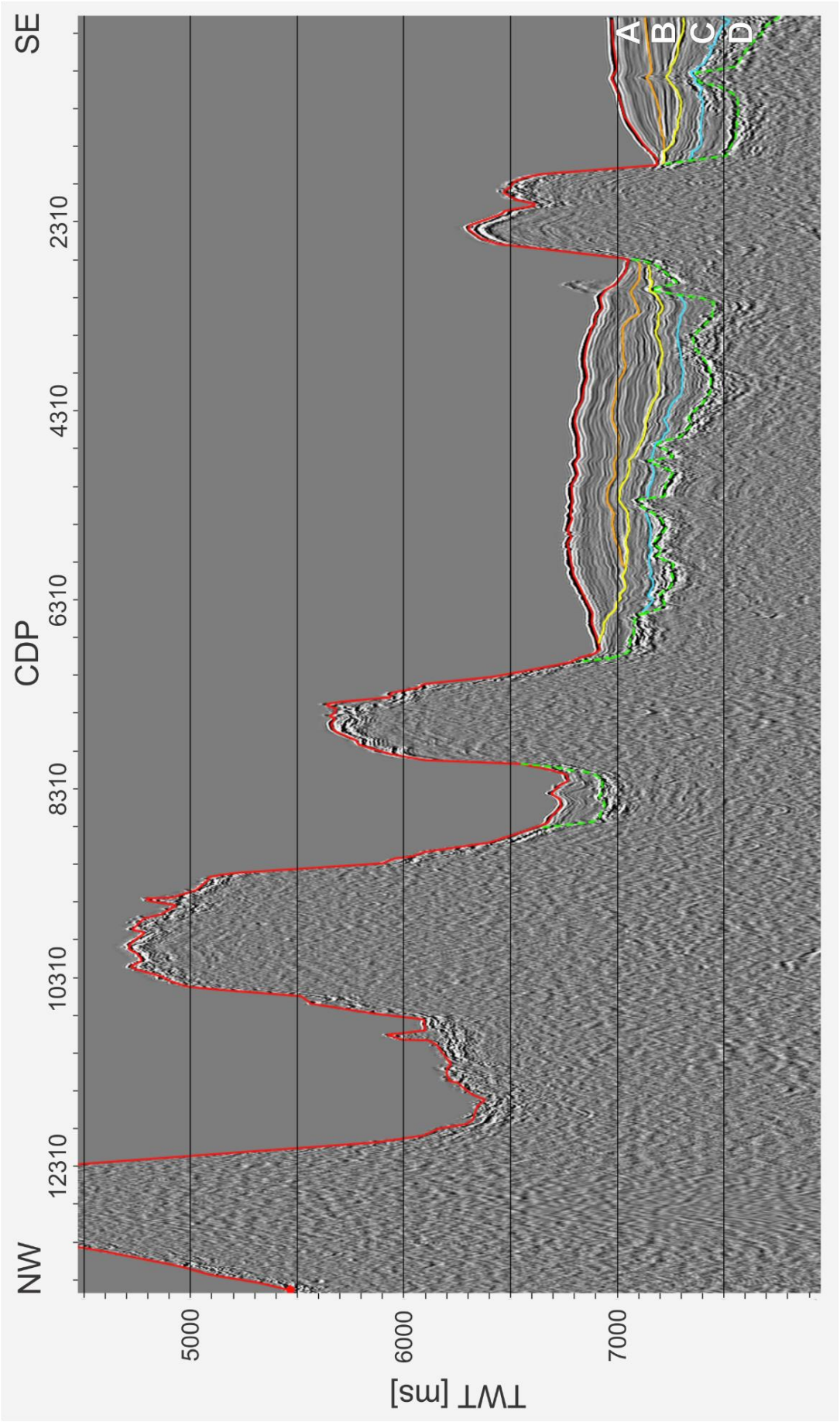

Fig. B.12: Seismic reflection profile cr5 with seismic interpretation

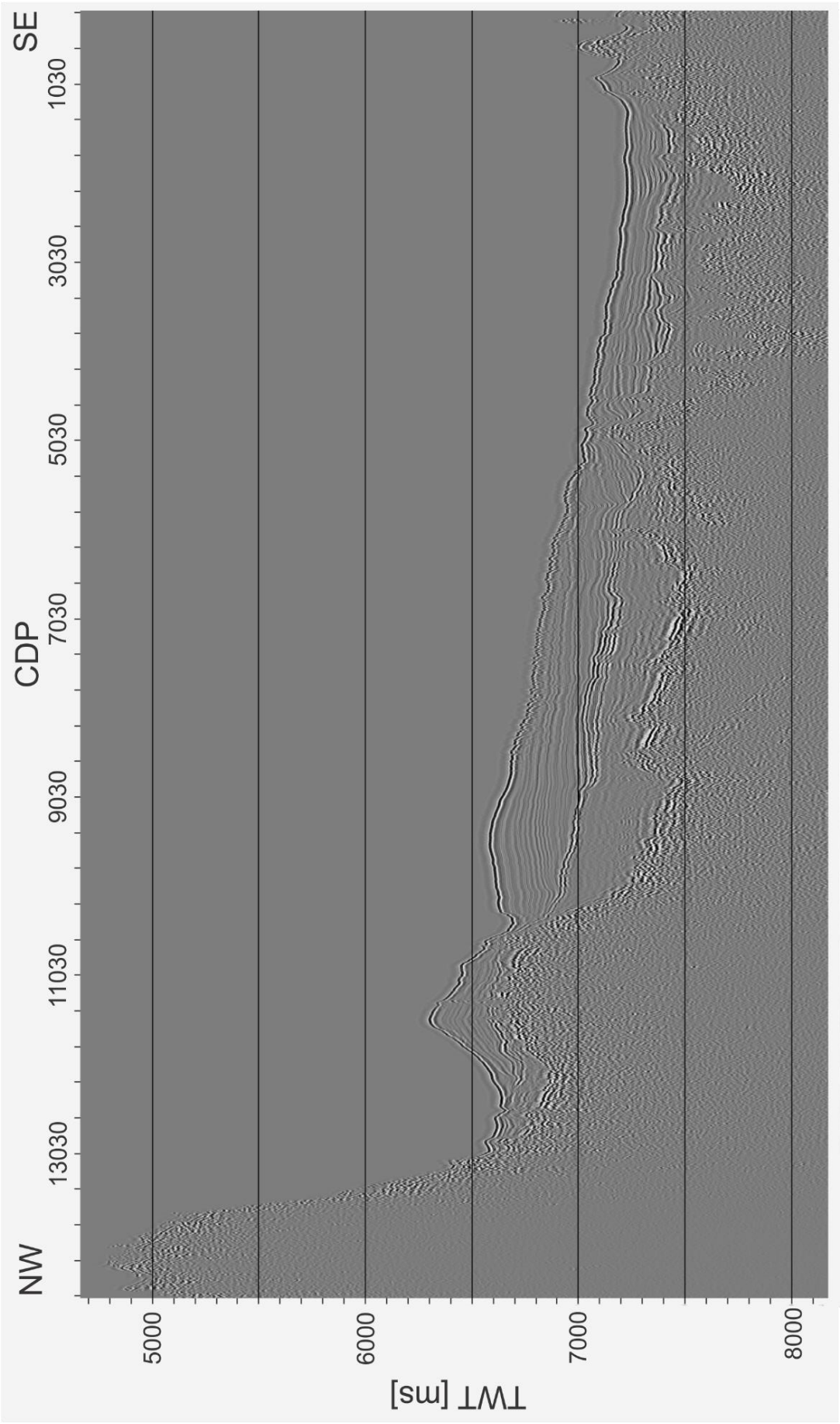

Fig. B.13: Seismic reflection profile tan0207-cr5a

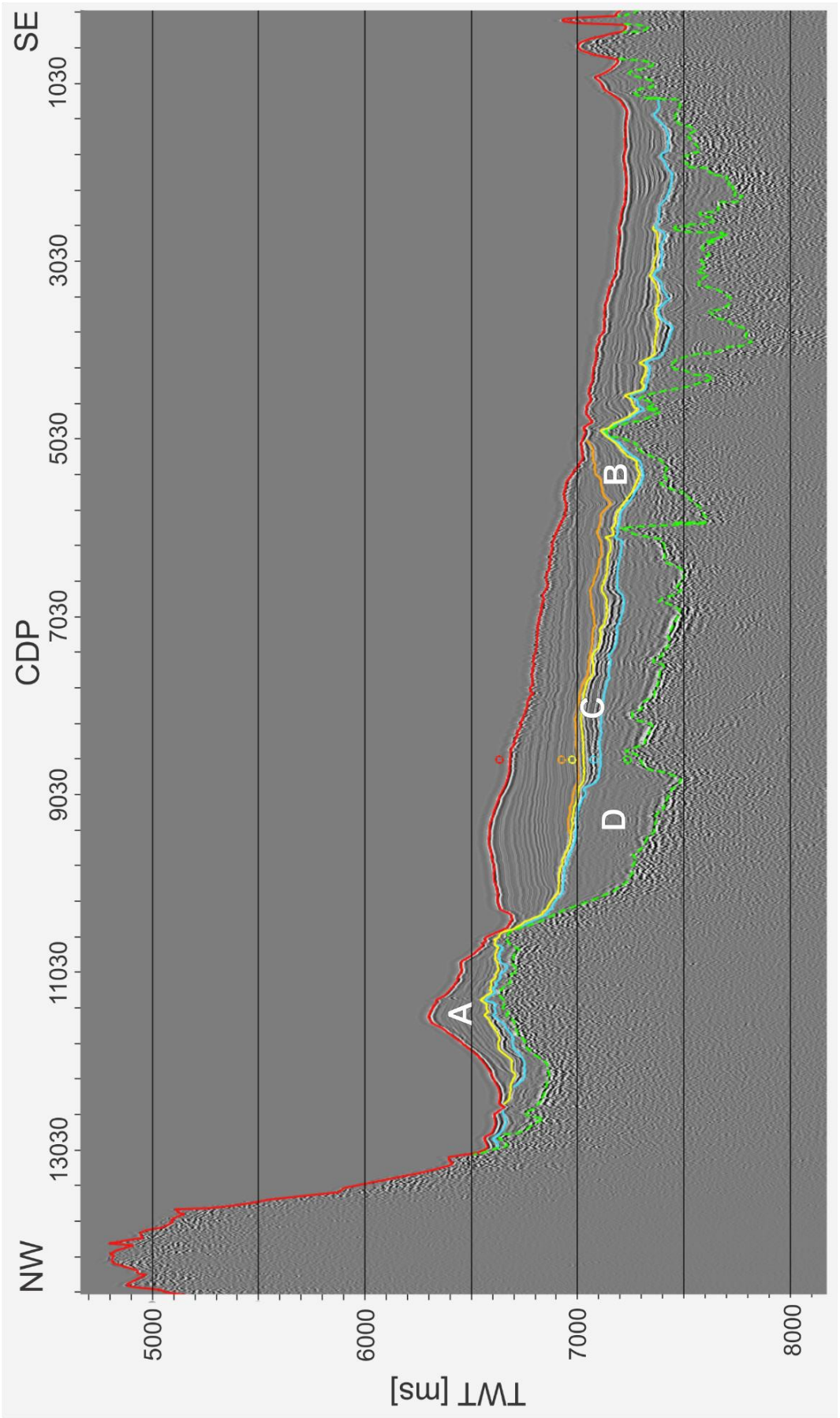

Fig. B.14: Seismic reflection profile tan0207-cr5a with seismic interpretation. Little, colored circles mark the intersection points with horizons from profile AWI-20160301

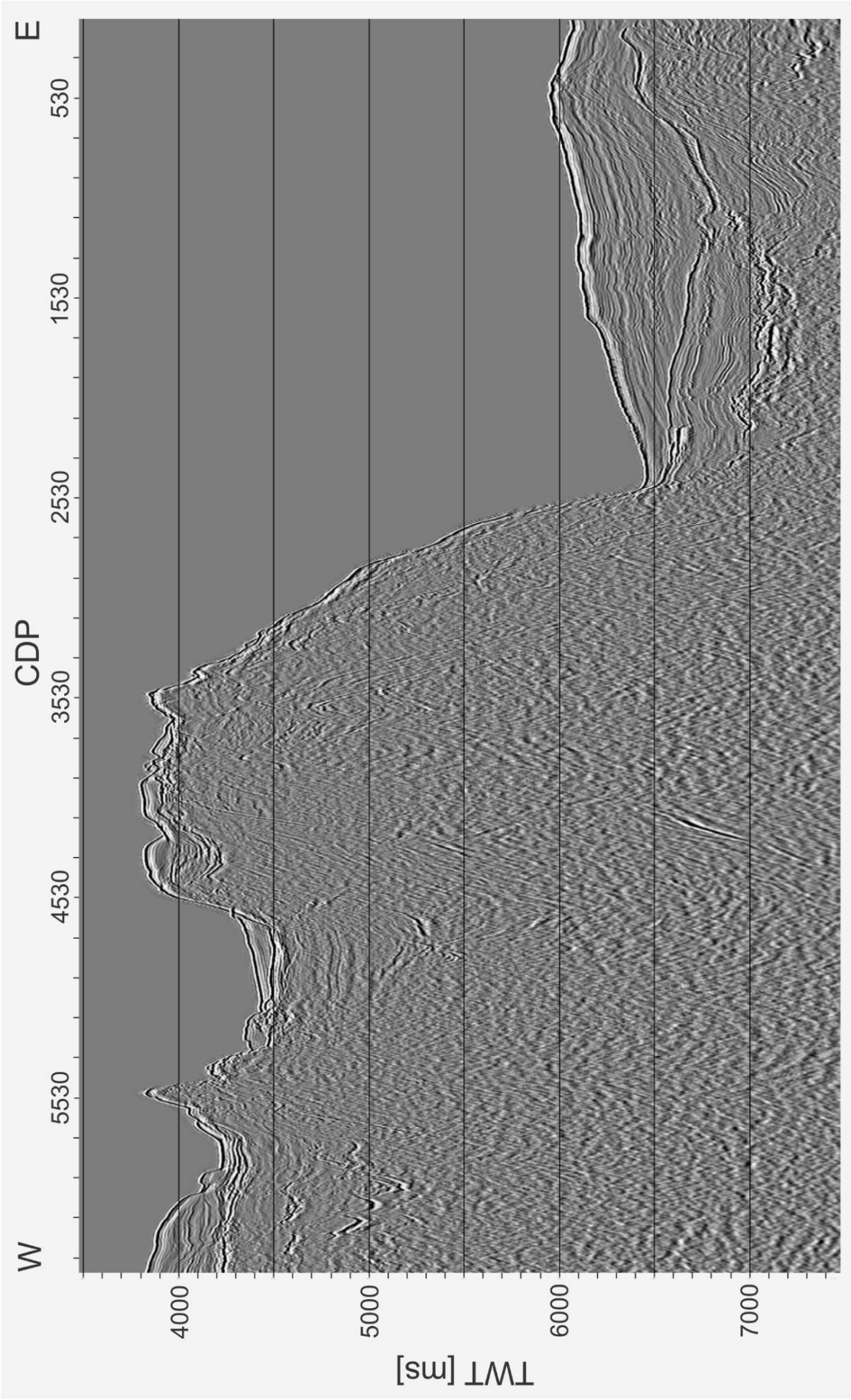

Fig. B.15: Seismic reflection profile cr6

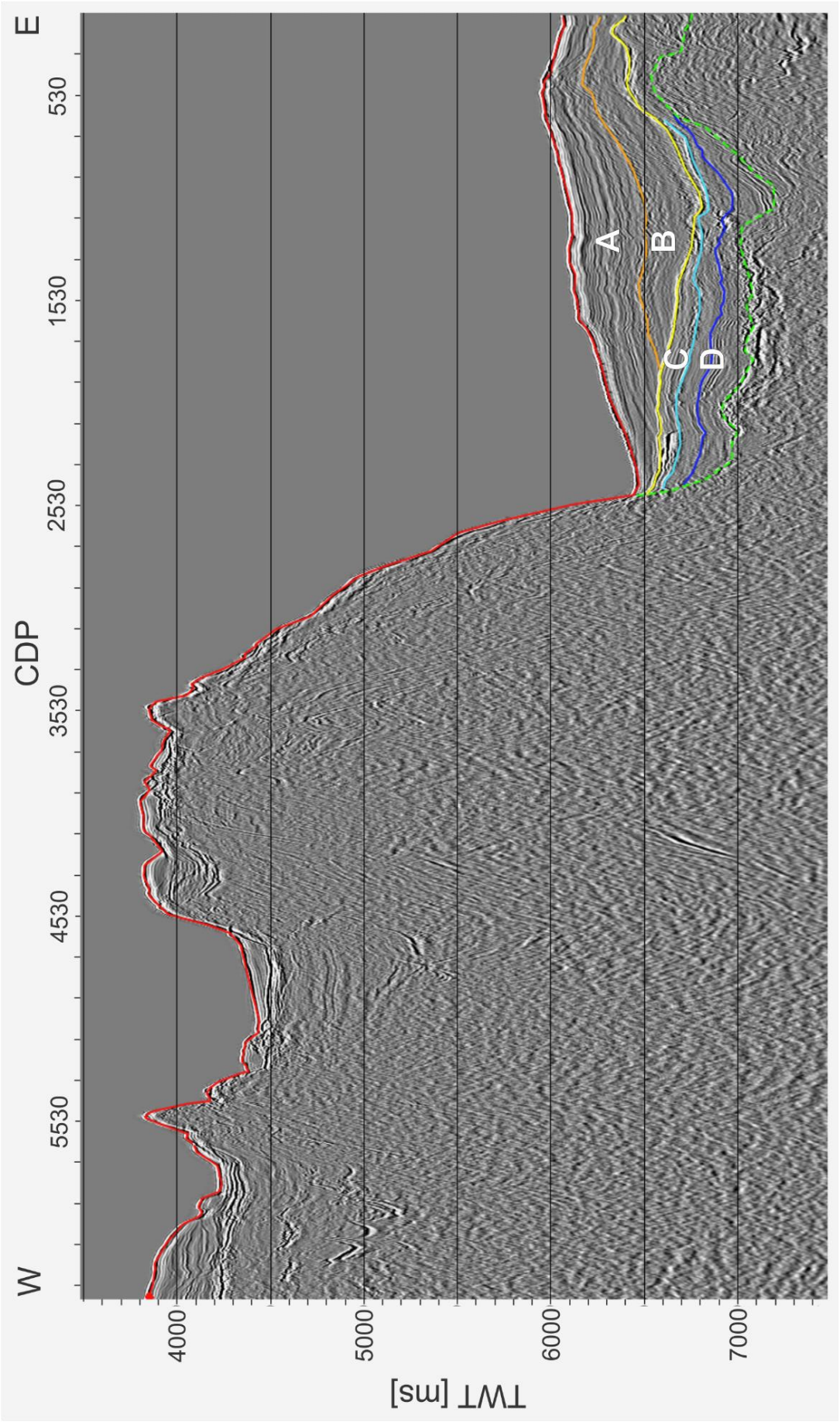

Fig. B.16: Seismic reflection profile cr6 with seismic interpretation

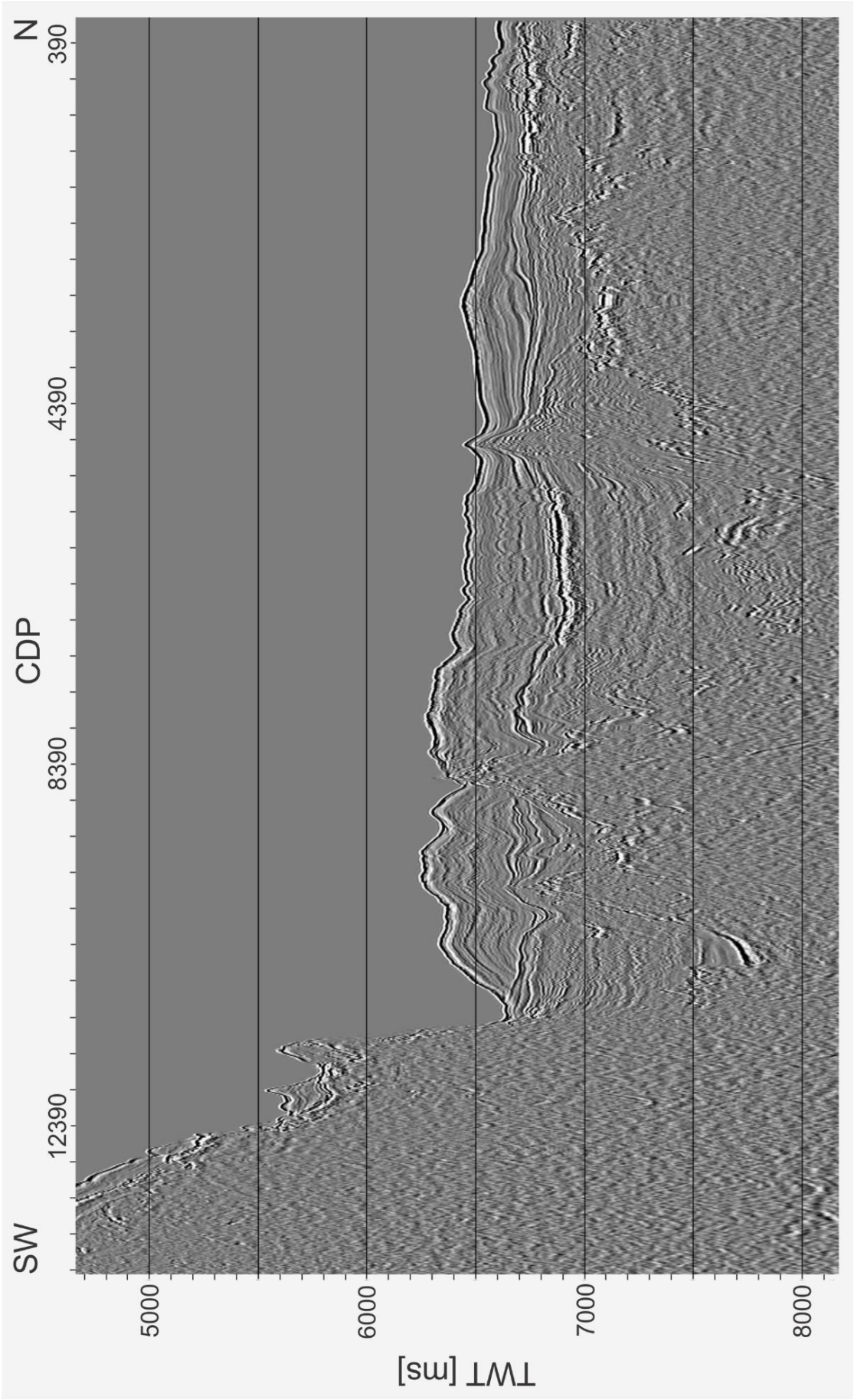

Fig. B.17: Seismic reflection profile hkdc12

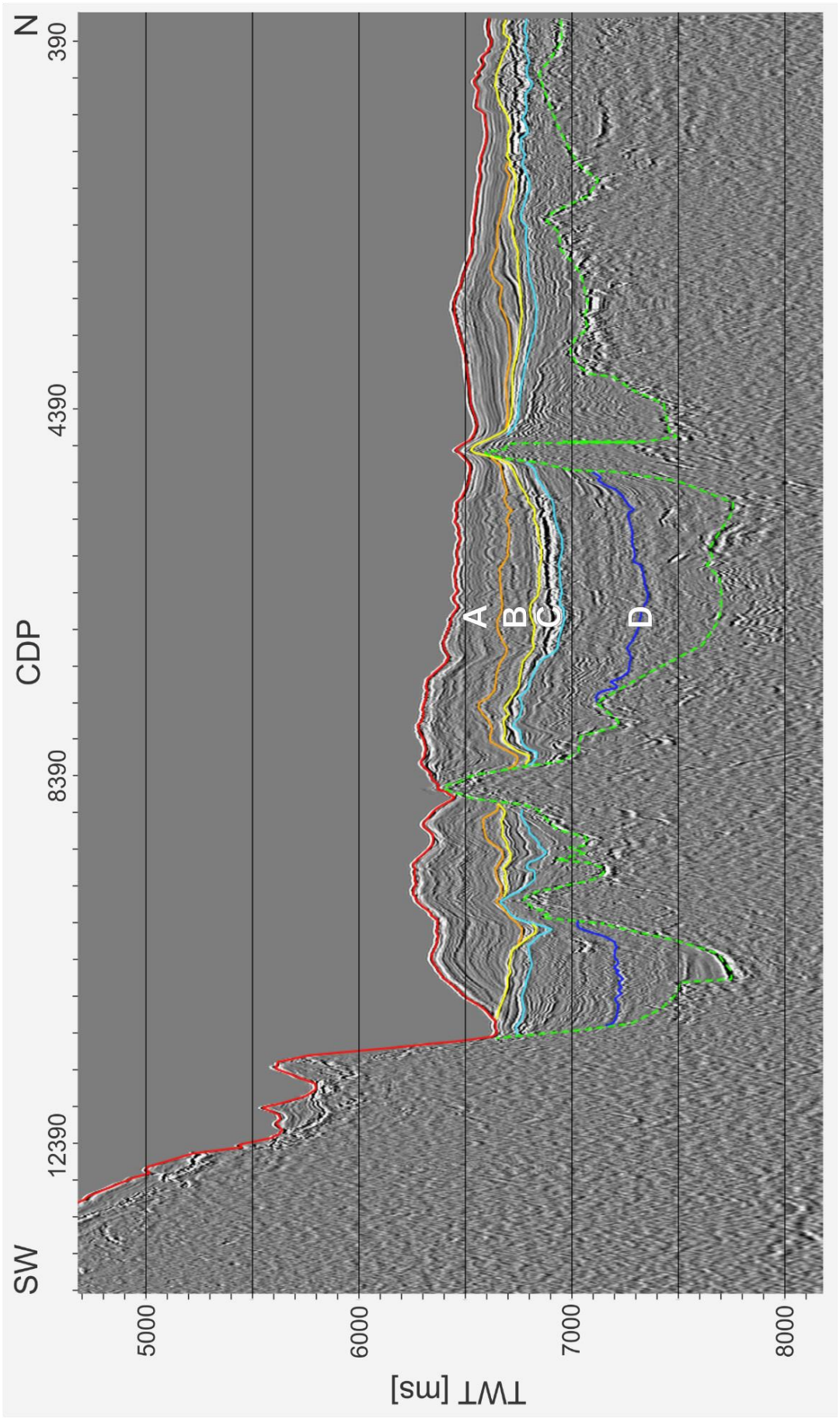

Fig. B.18: Seismic reflection profile hkdc12 with seismic interpretation

C. Parasound profiles from SO246

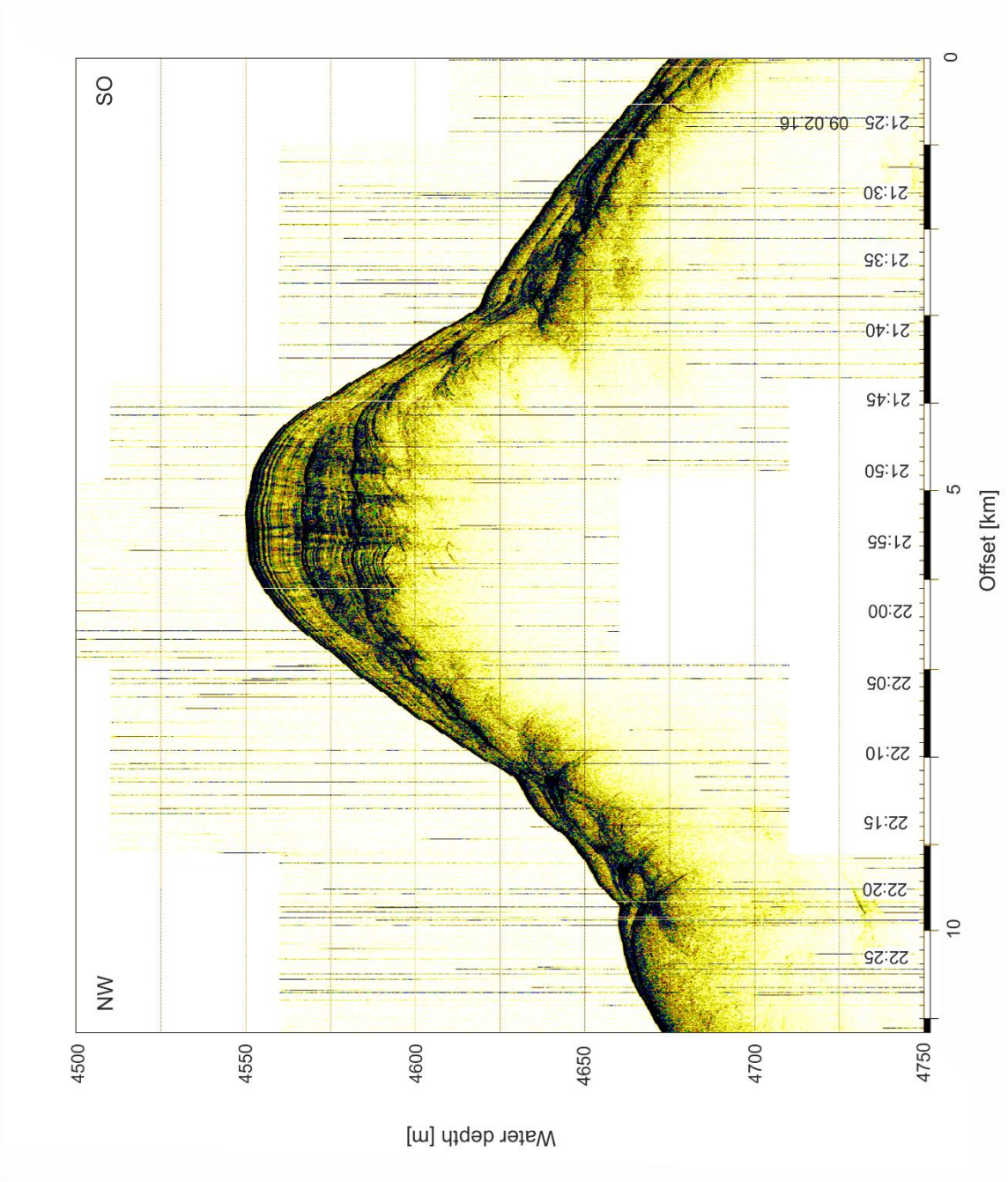

Fig. C.1: Parasound profile 1-a from AWI-20160001

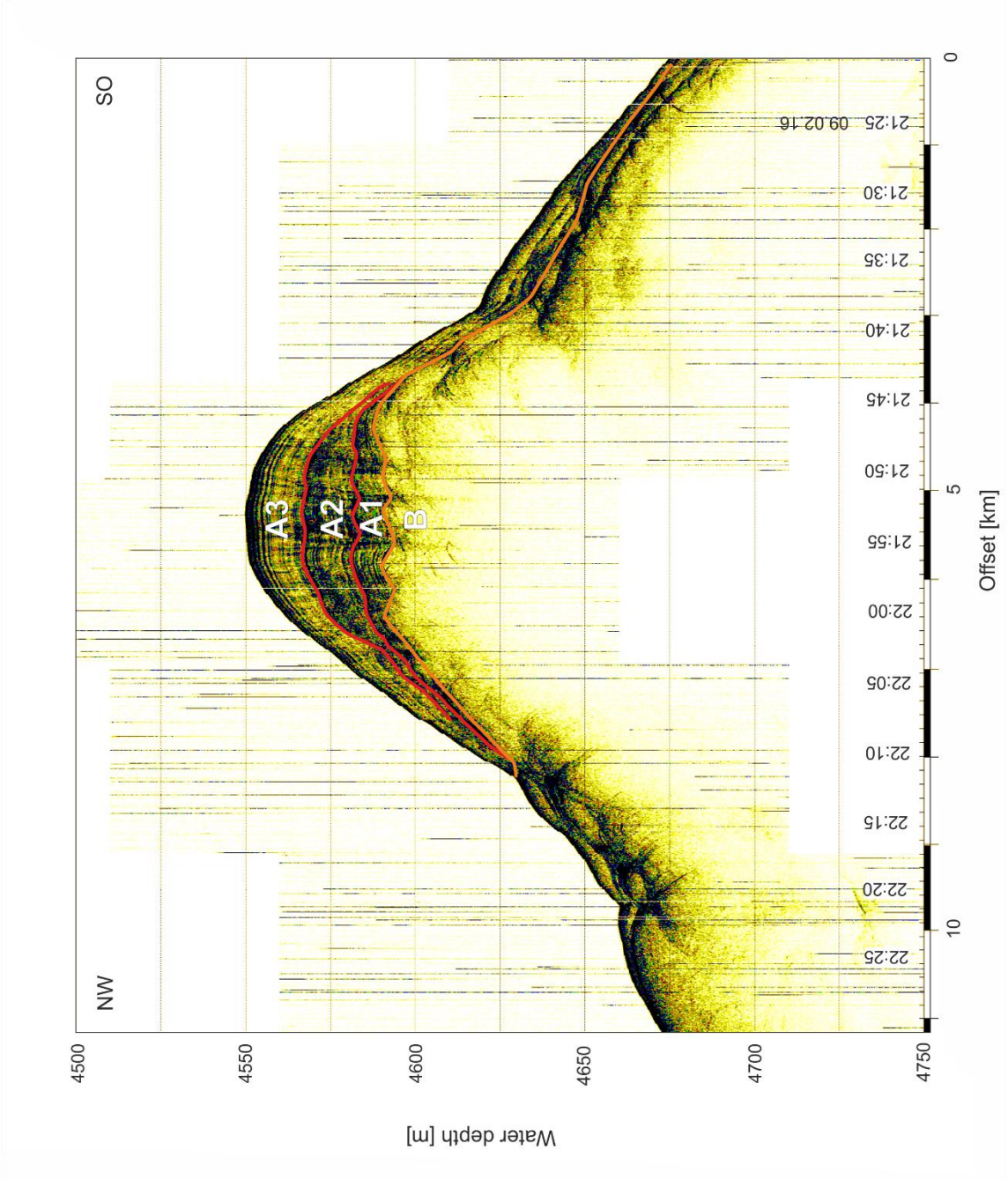

Fig. C.2: Parasound profile 1-a from AWI-20160001 with interpretation

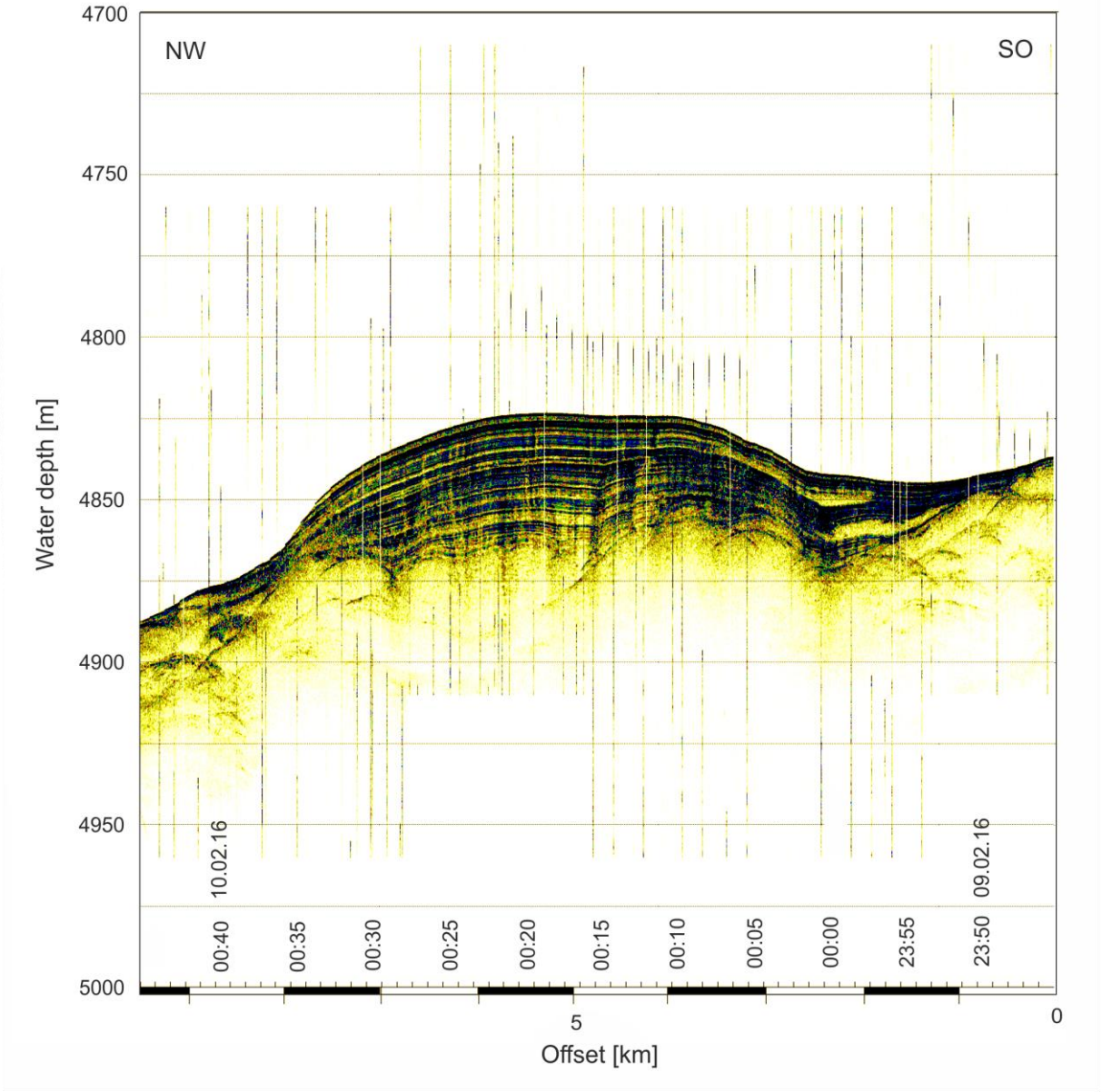

Fig. C.3: Parasound profile 1-b from AWI-20160001

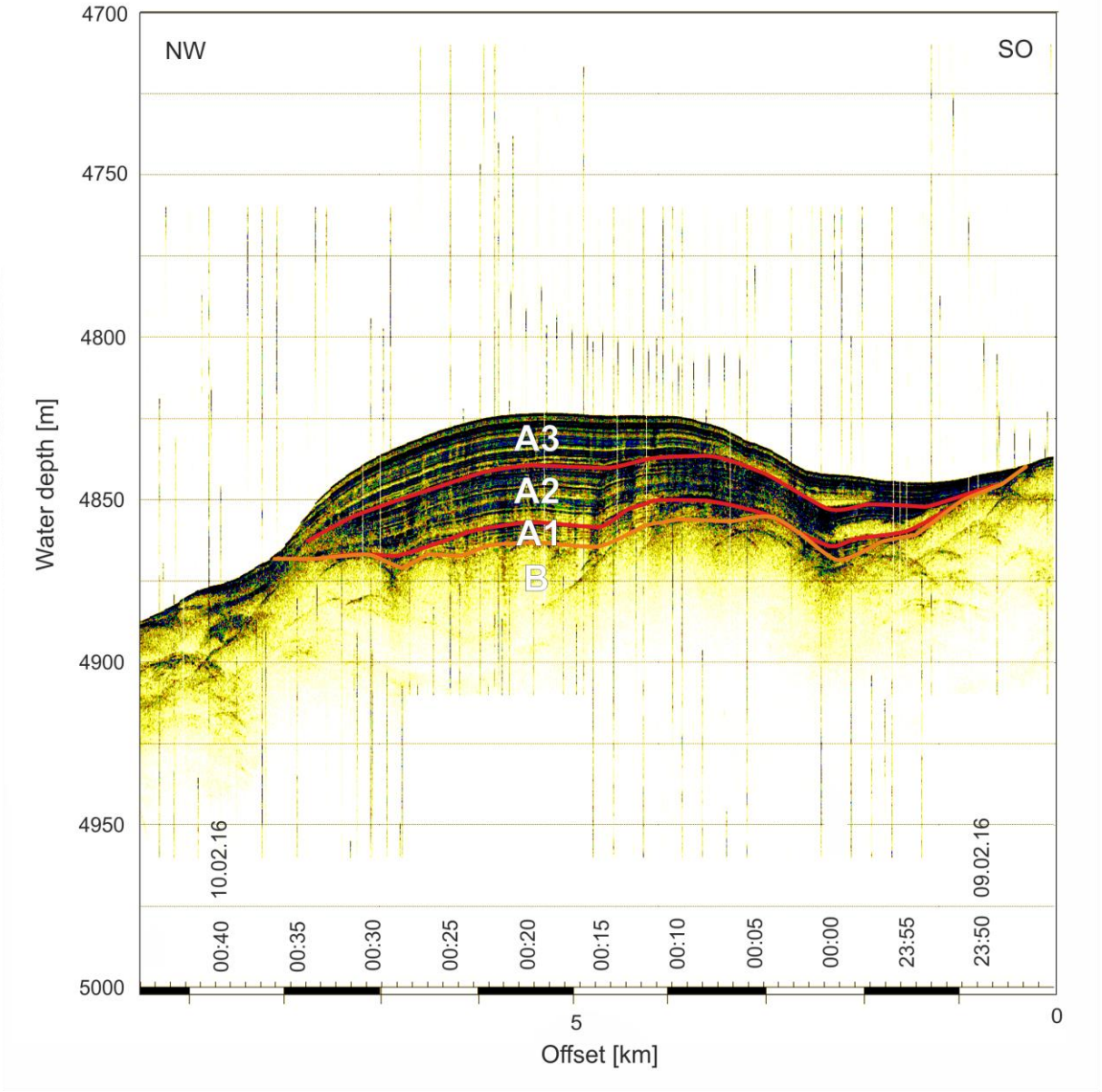

Fig. C.4: Parasound profile 1-b from AWI-20160001 with interpretation

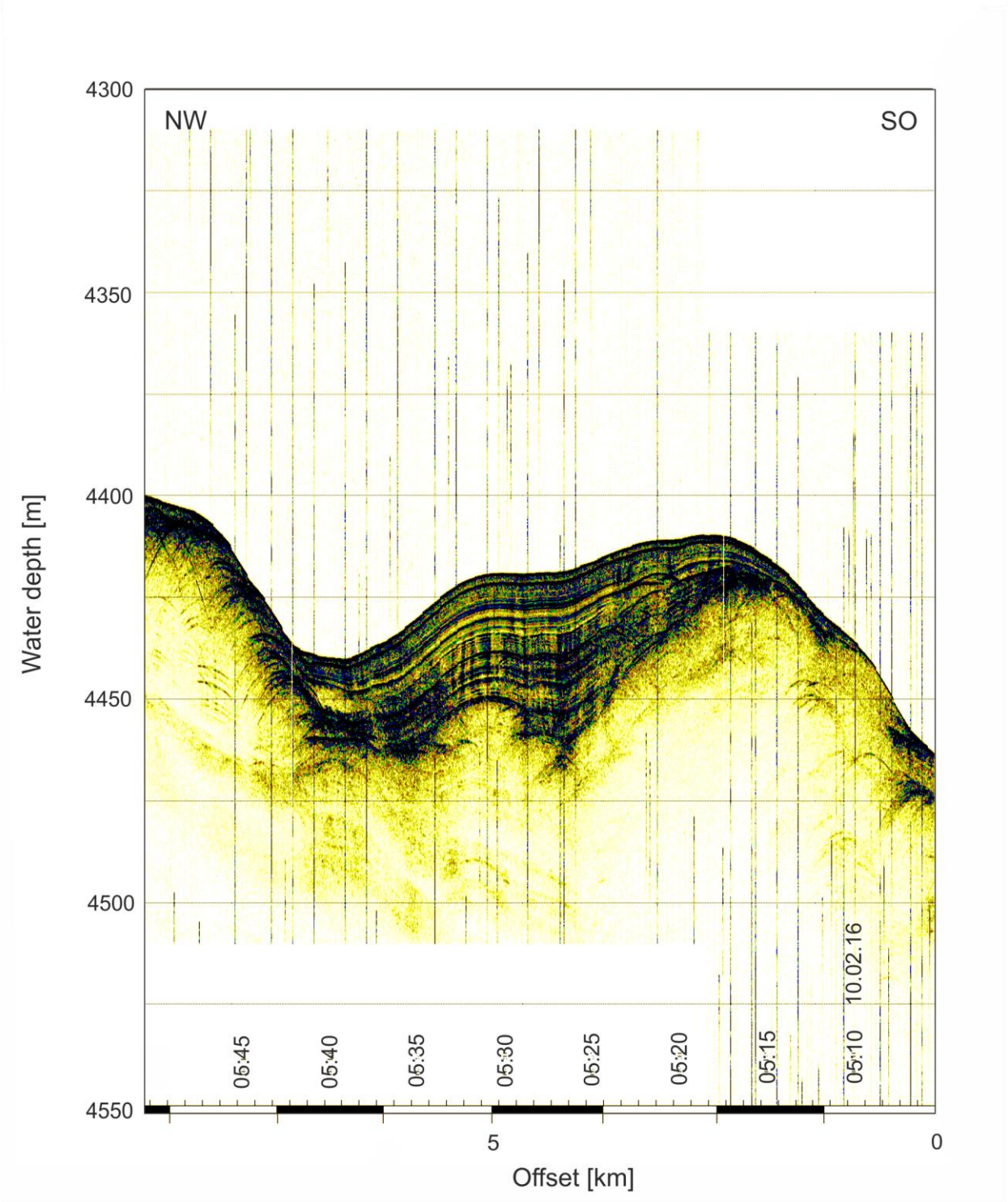

Fig. C.5: Parasound profile 1-c from AWI-20160001

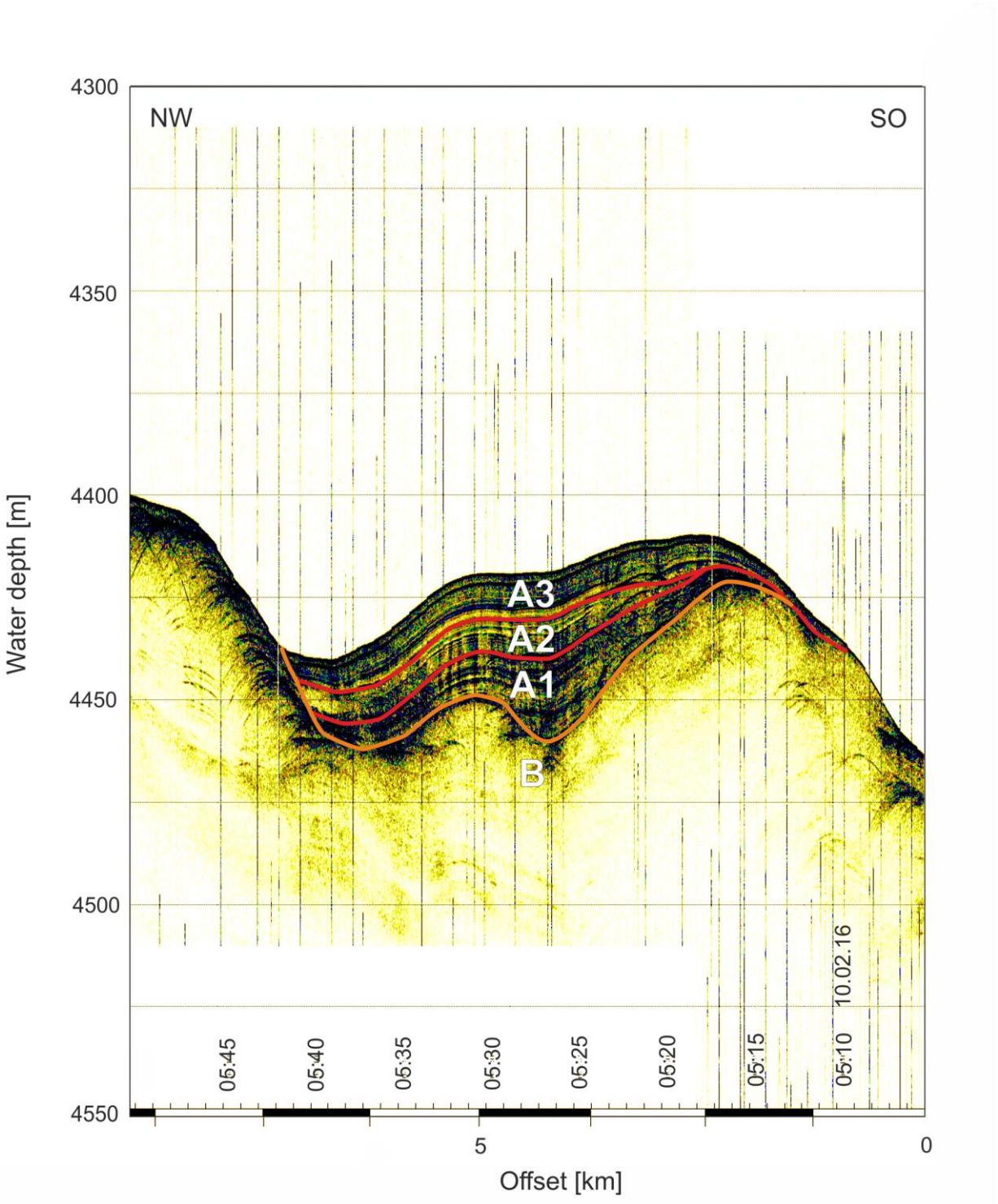

Fig. C.6: Parasound profile 1-c from AWI-20160001 with interpretation

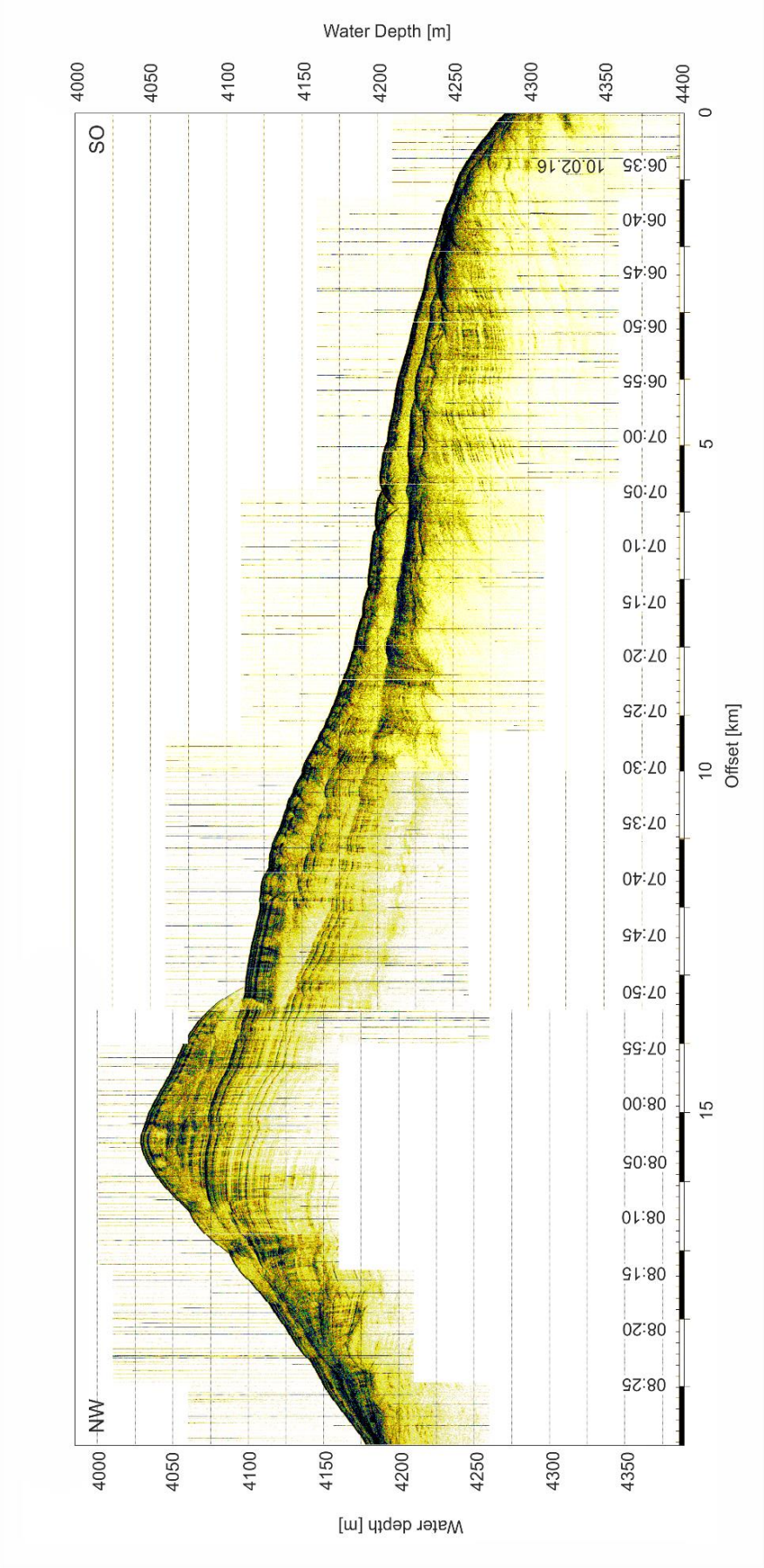

Fig. C.7: Parasound profile 1-d from AWI-20160001

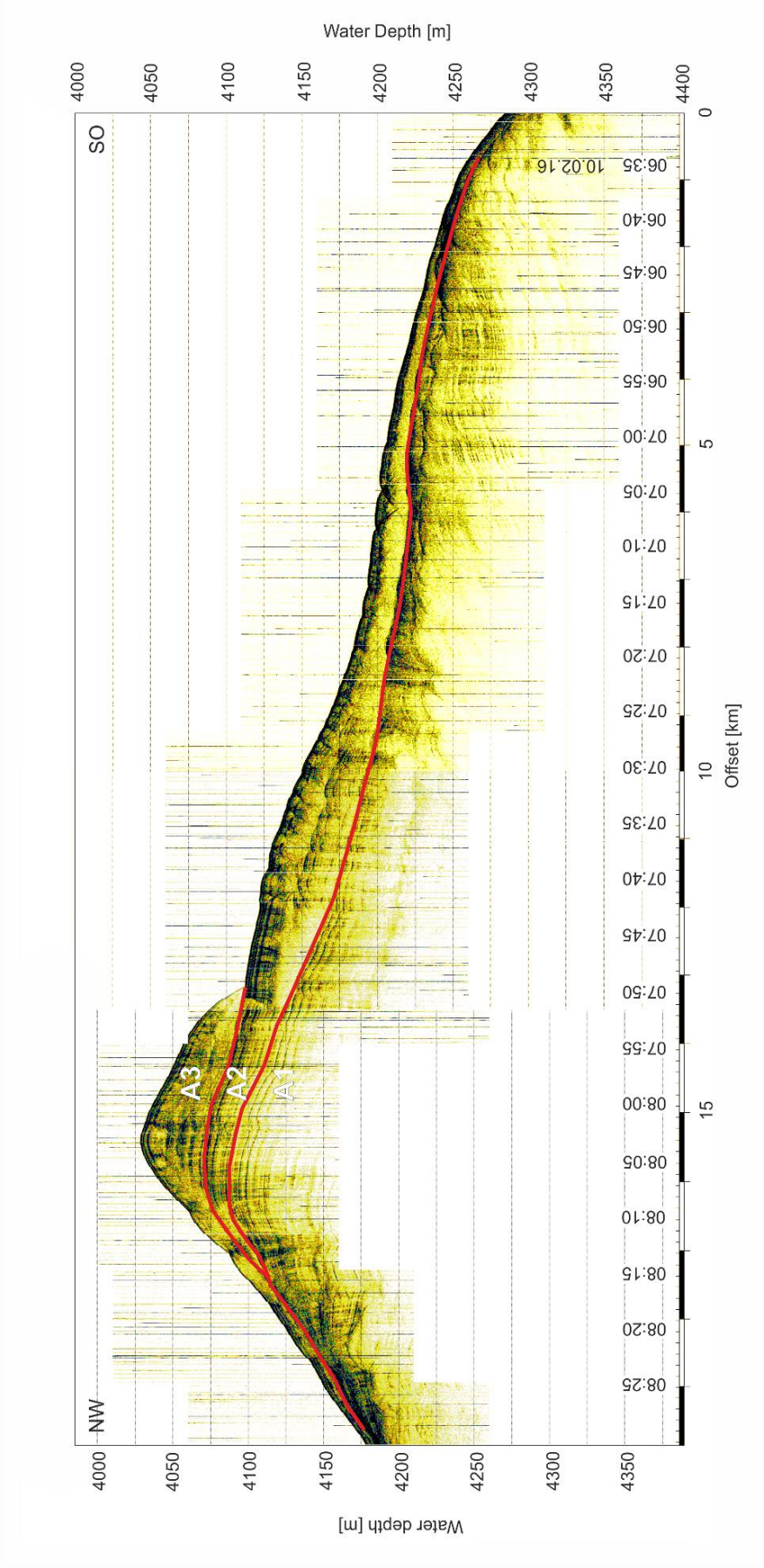

Fig. C.8: Parasound profile 1-d from AWI-20160001 with interpretation

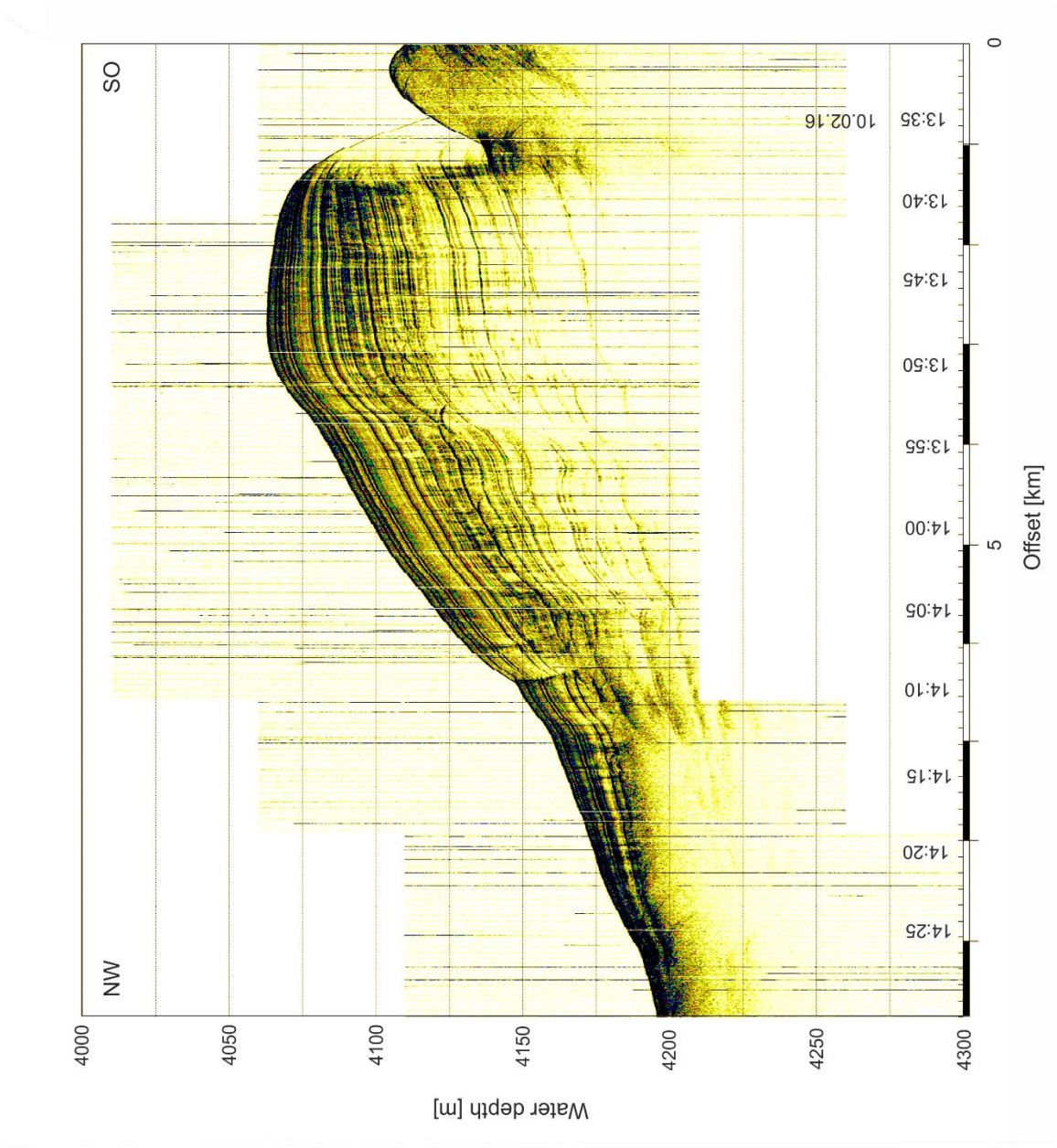

Fig. C.9: Parasound profile 1-e from AWI-20160001

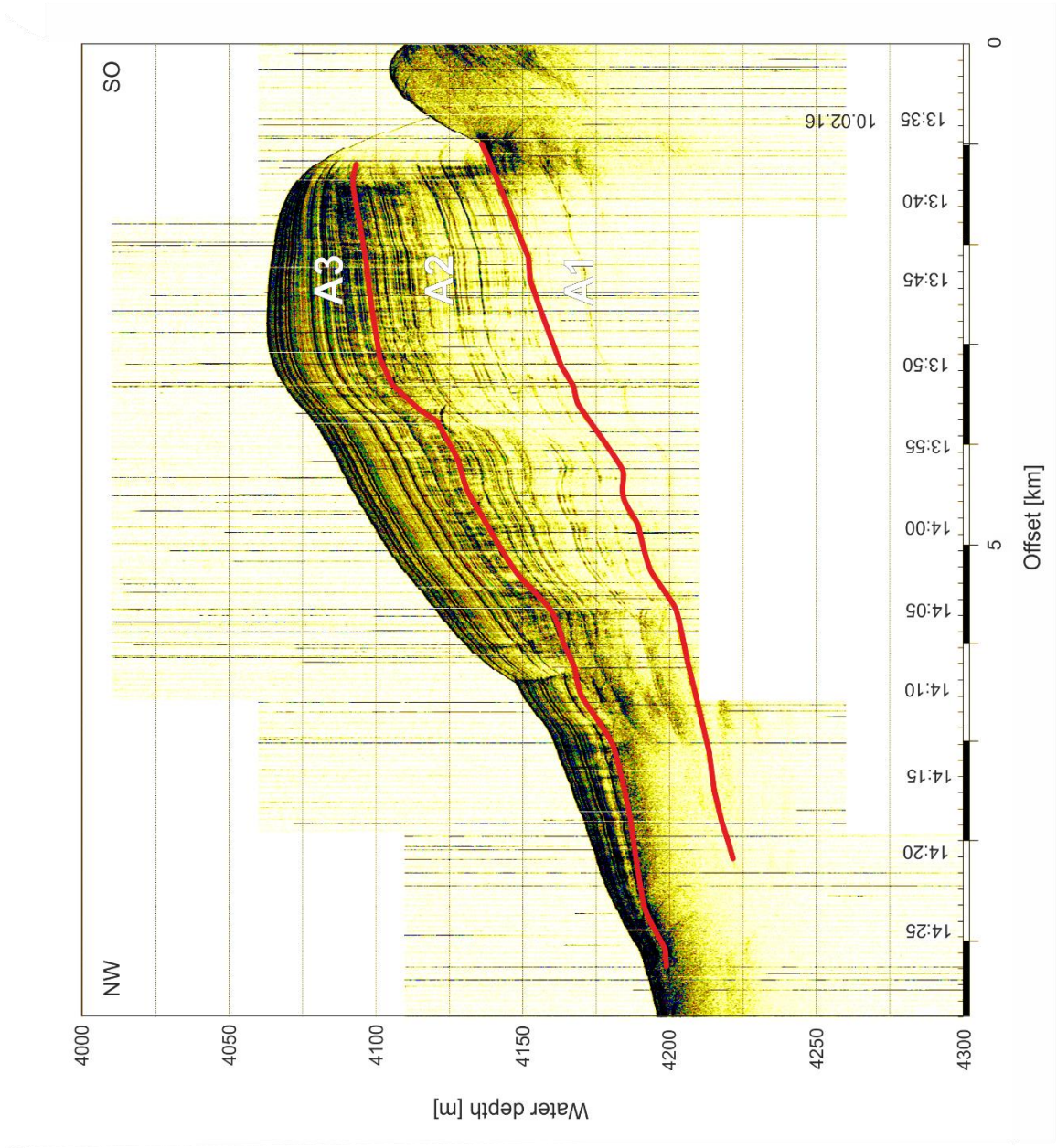

Fig. C.10: Parasound profile 1-e from AWI-20160001 with interpretation

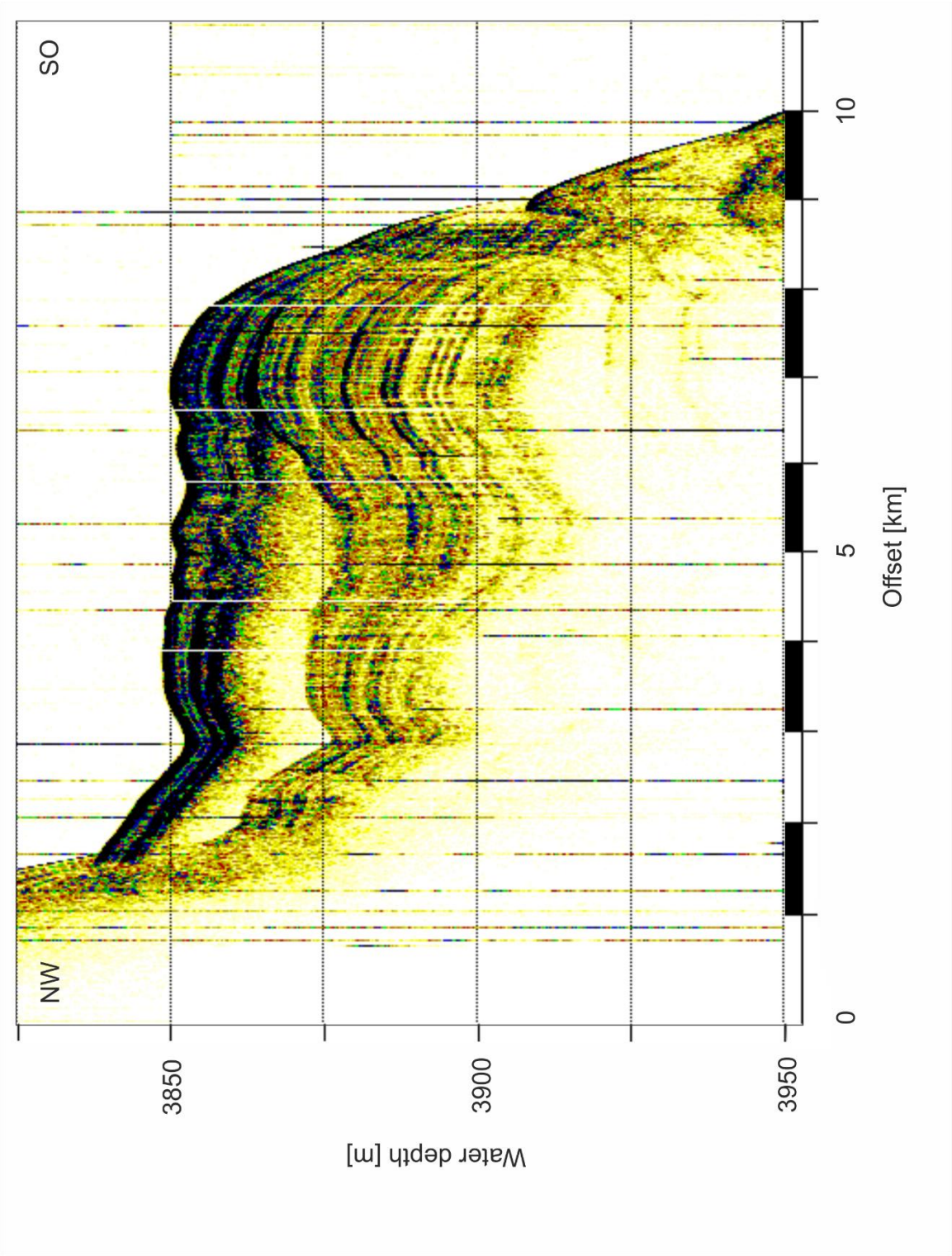

Fig. C.11: Parasound profile 3-a from AWI-20160003

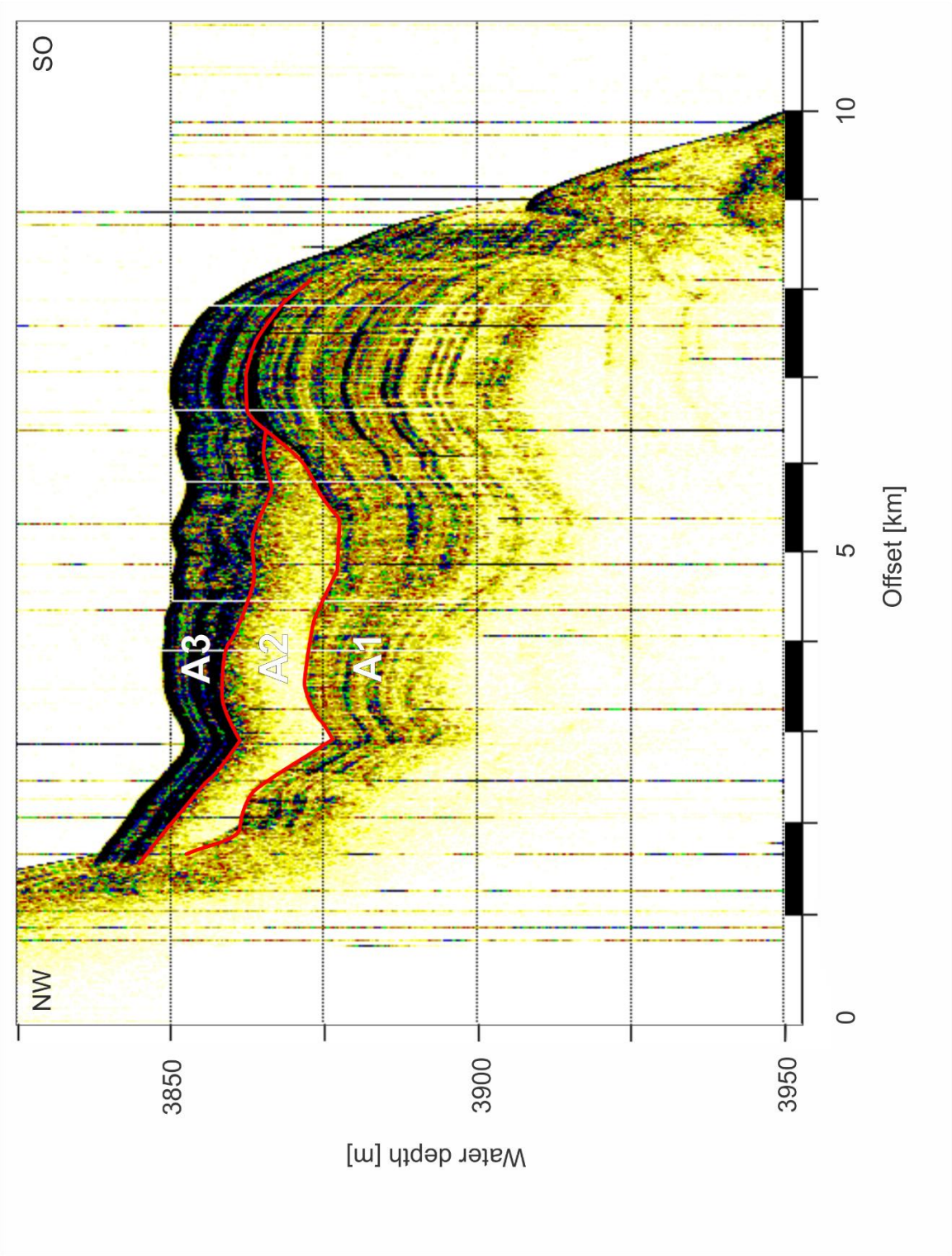

Fig. C.12: Parasound profile 3-a from AWI-20160003 with interpretation

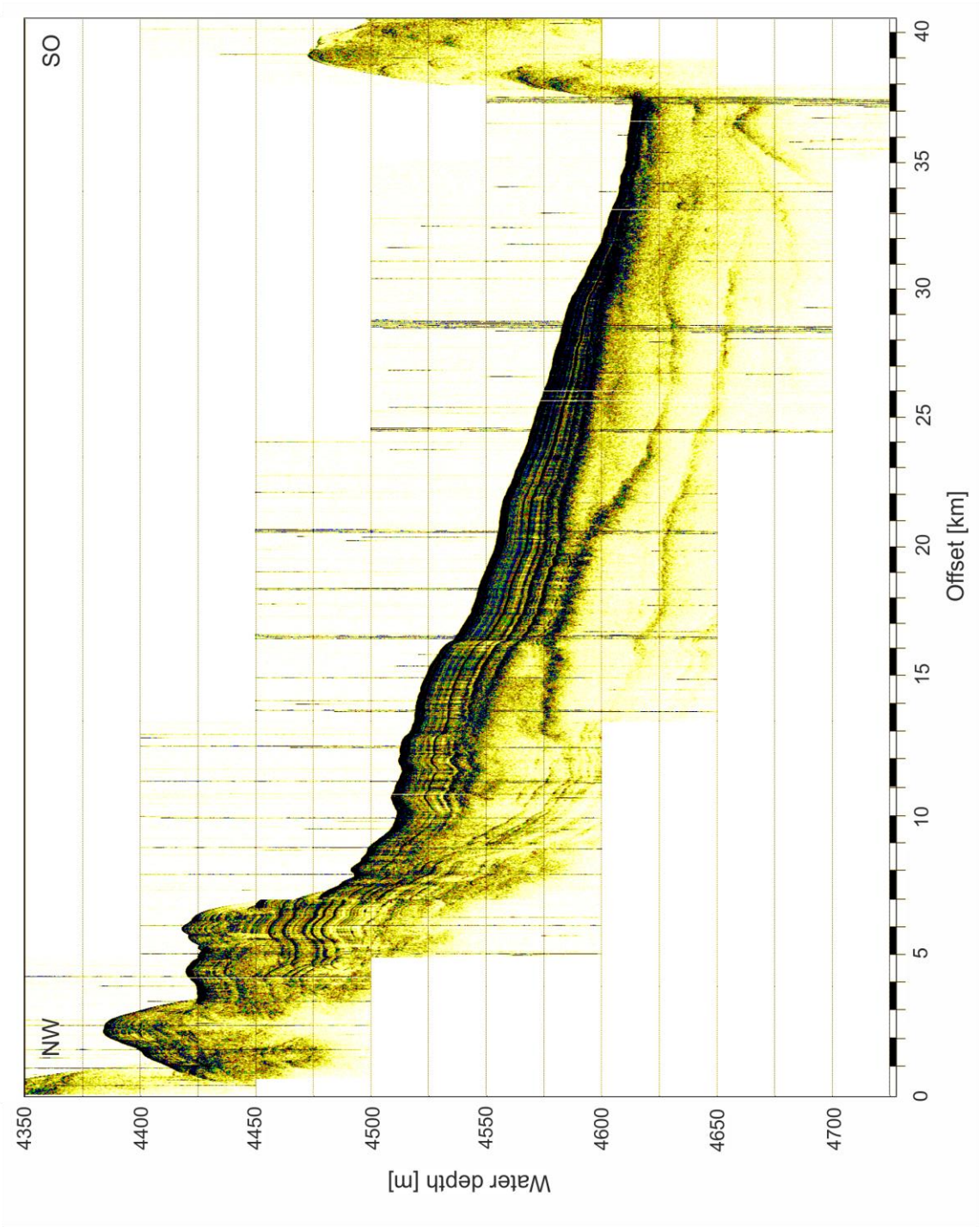

Fig. C.13: Parasound profile 3-b from AWI-20160003

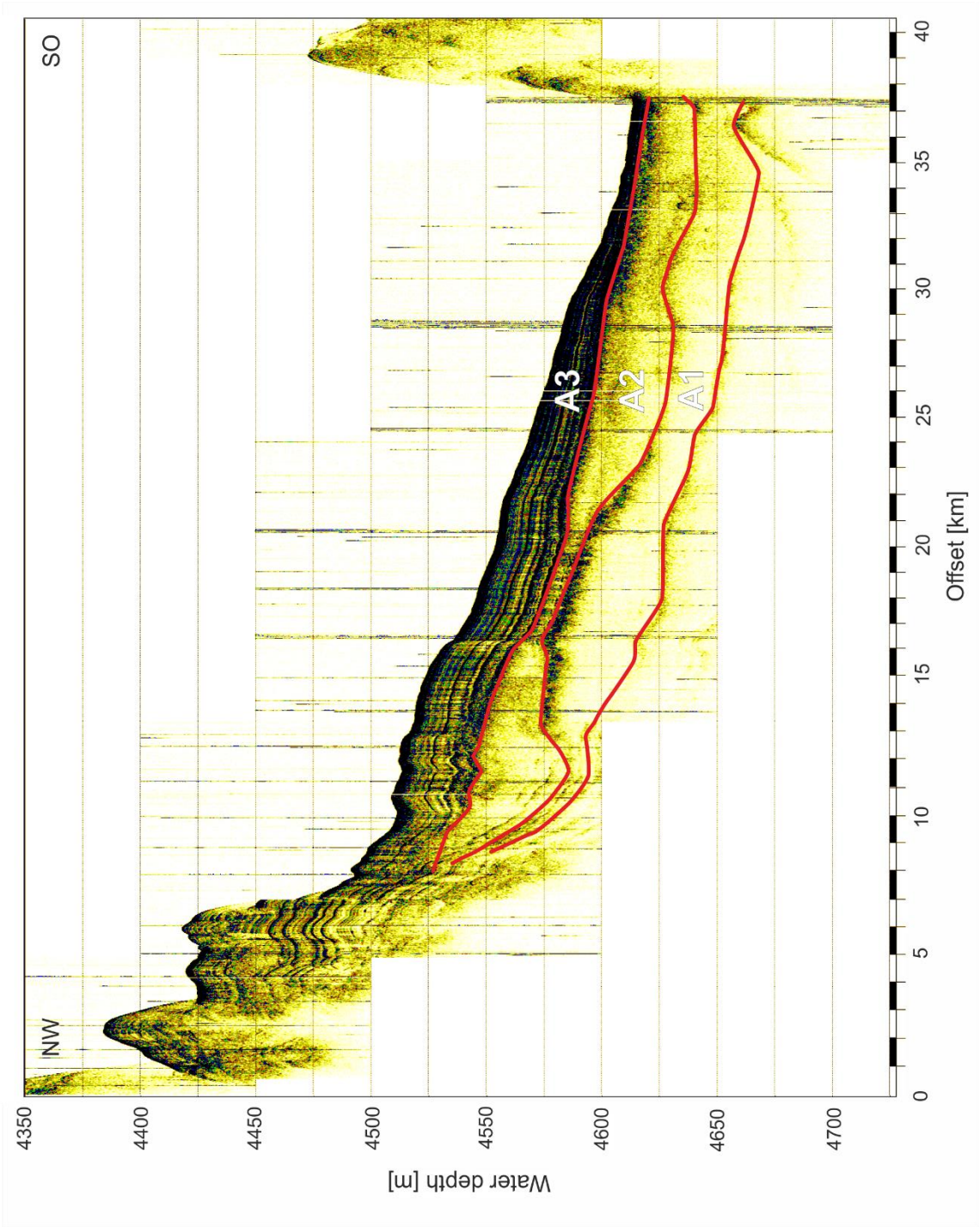

Fig. C.14: Parasound profile 3-b from AWI-20160003 with interpretation

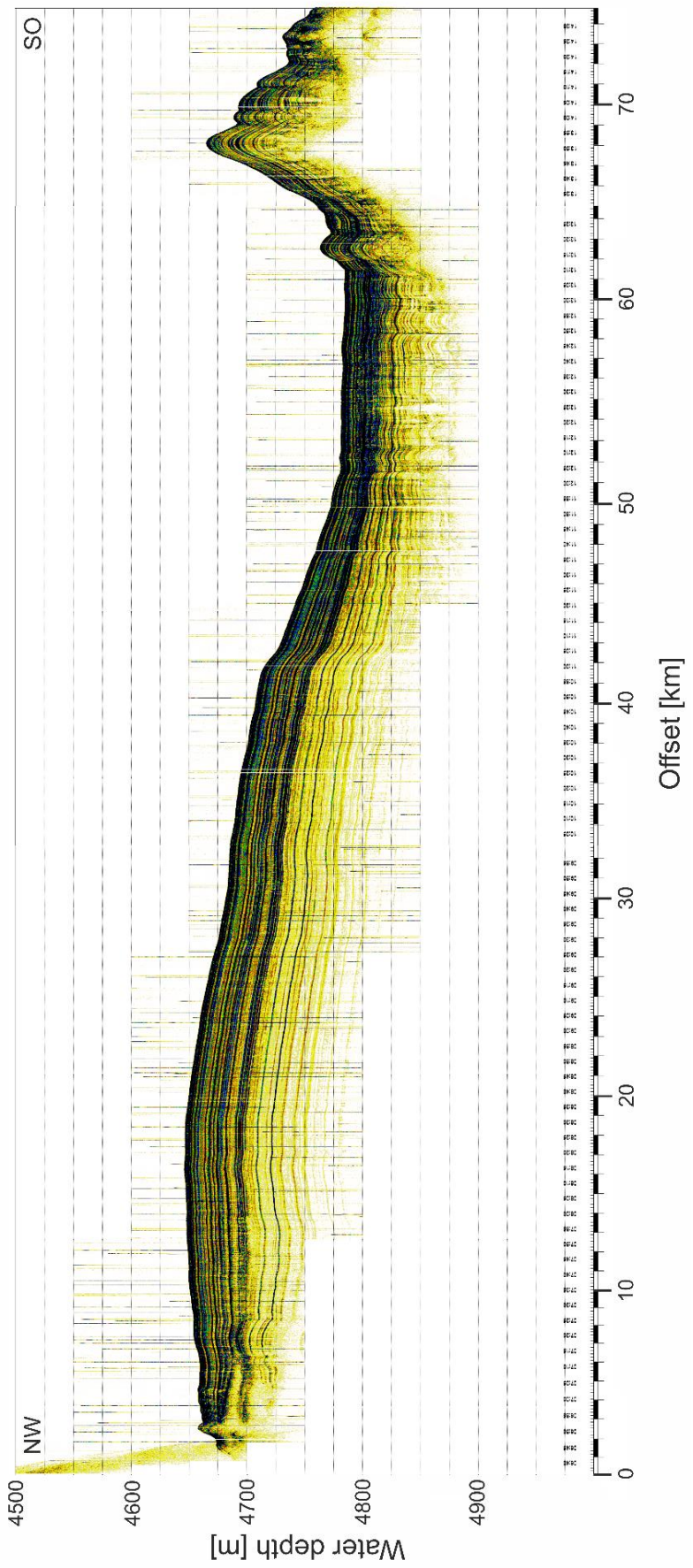

Fig. C.15: Parasound profile 3-c from AWI-20160003

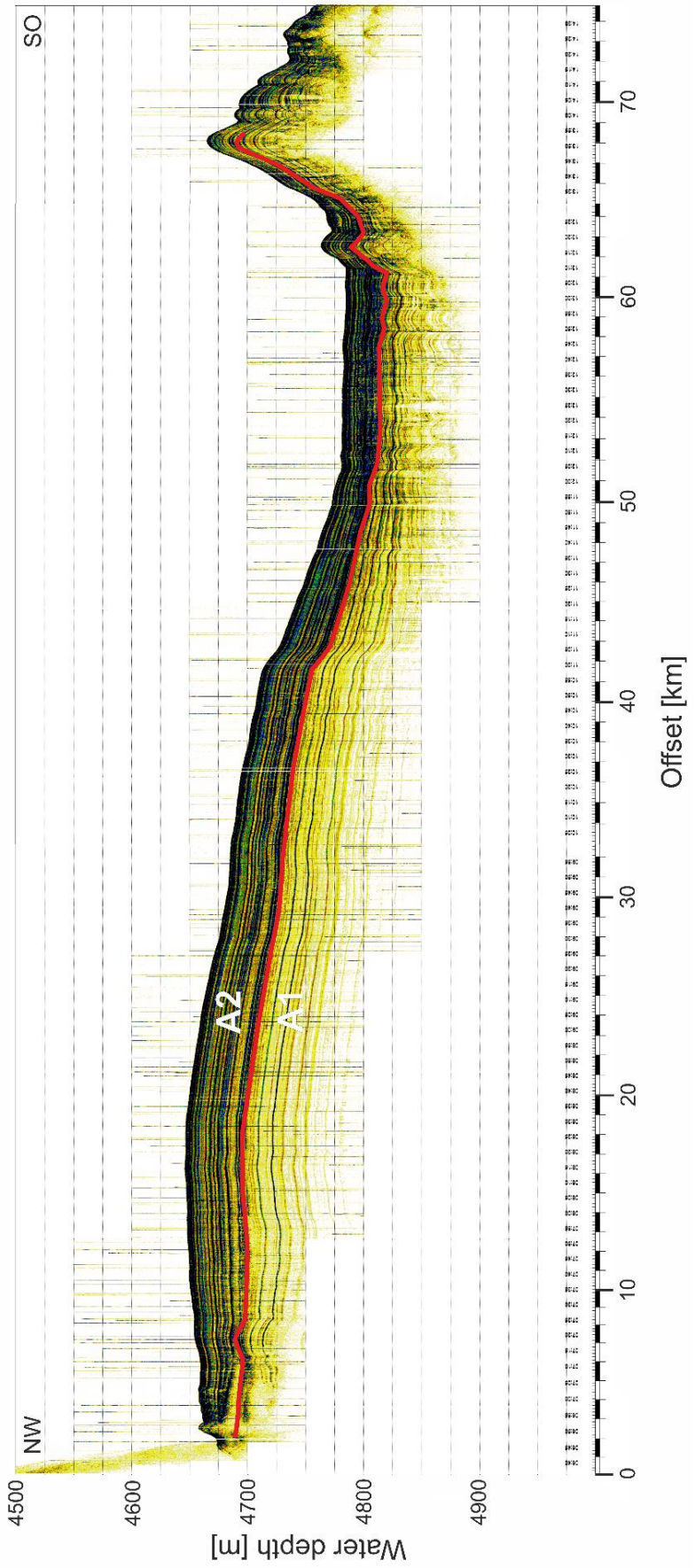

Fig. C.16: Parasound profile 3-c from AWI-20160003 with interpretation

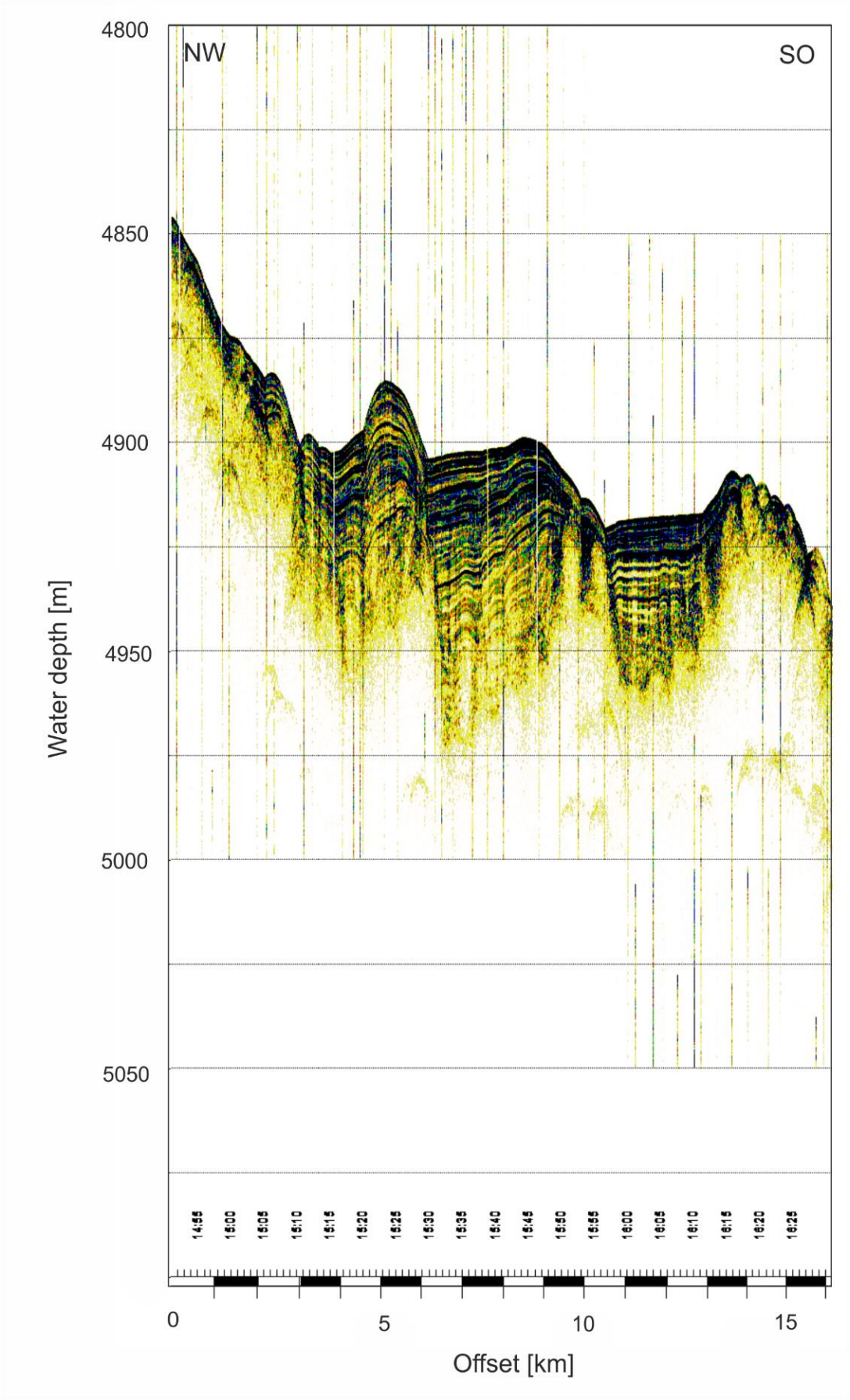

Fig. C.17: Parasound profile 3-d from AWI-20160003

D. Bathymetric data

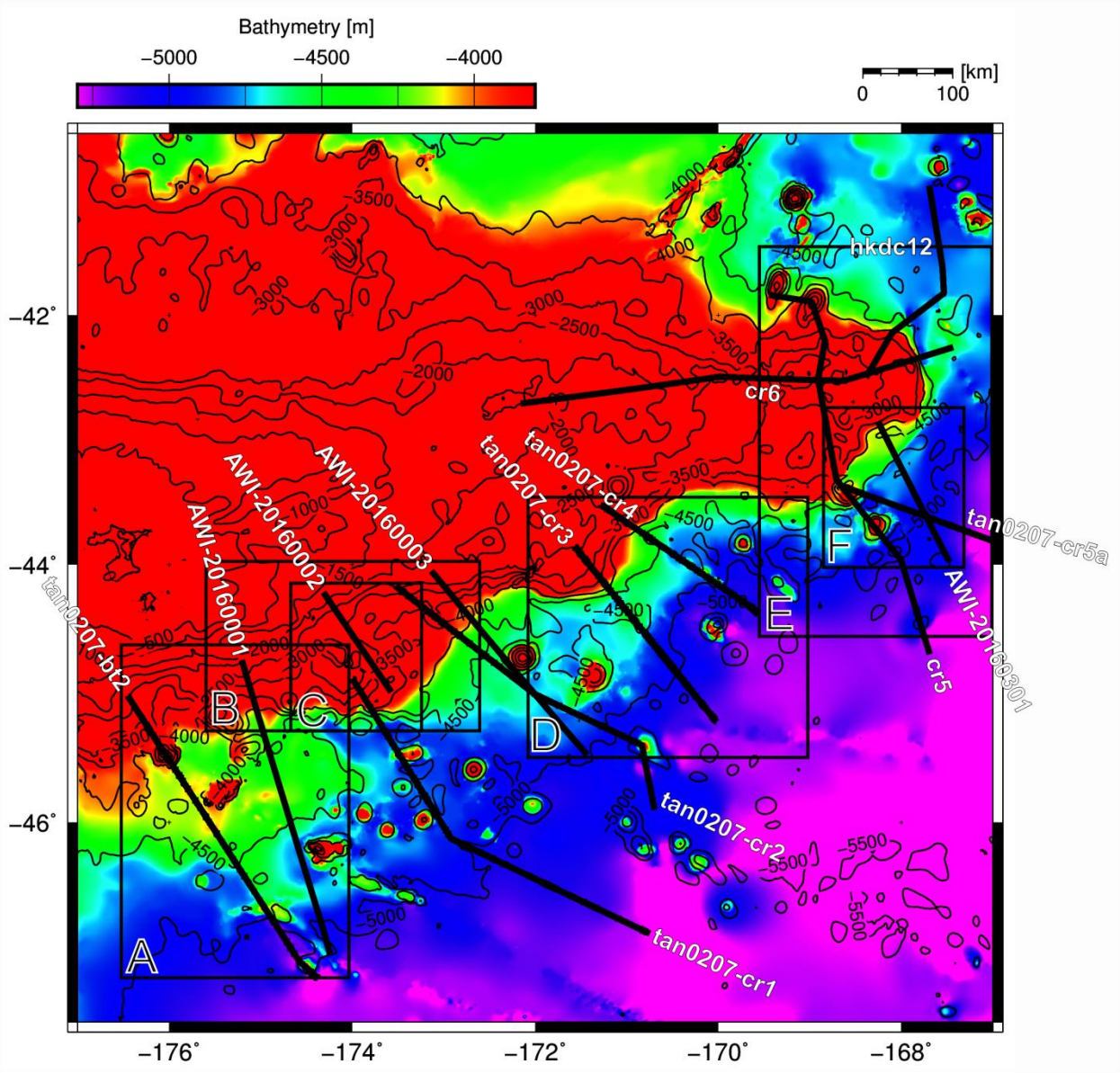

Fig. D.1: Bathymetric map of the work area; black boxes show locations of bathymetric detail maps. Seismic profiles are shown in black.

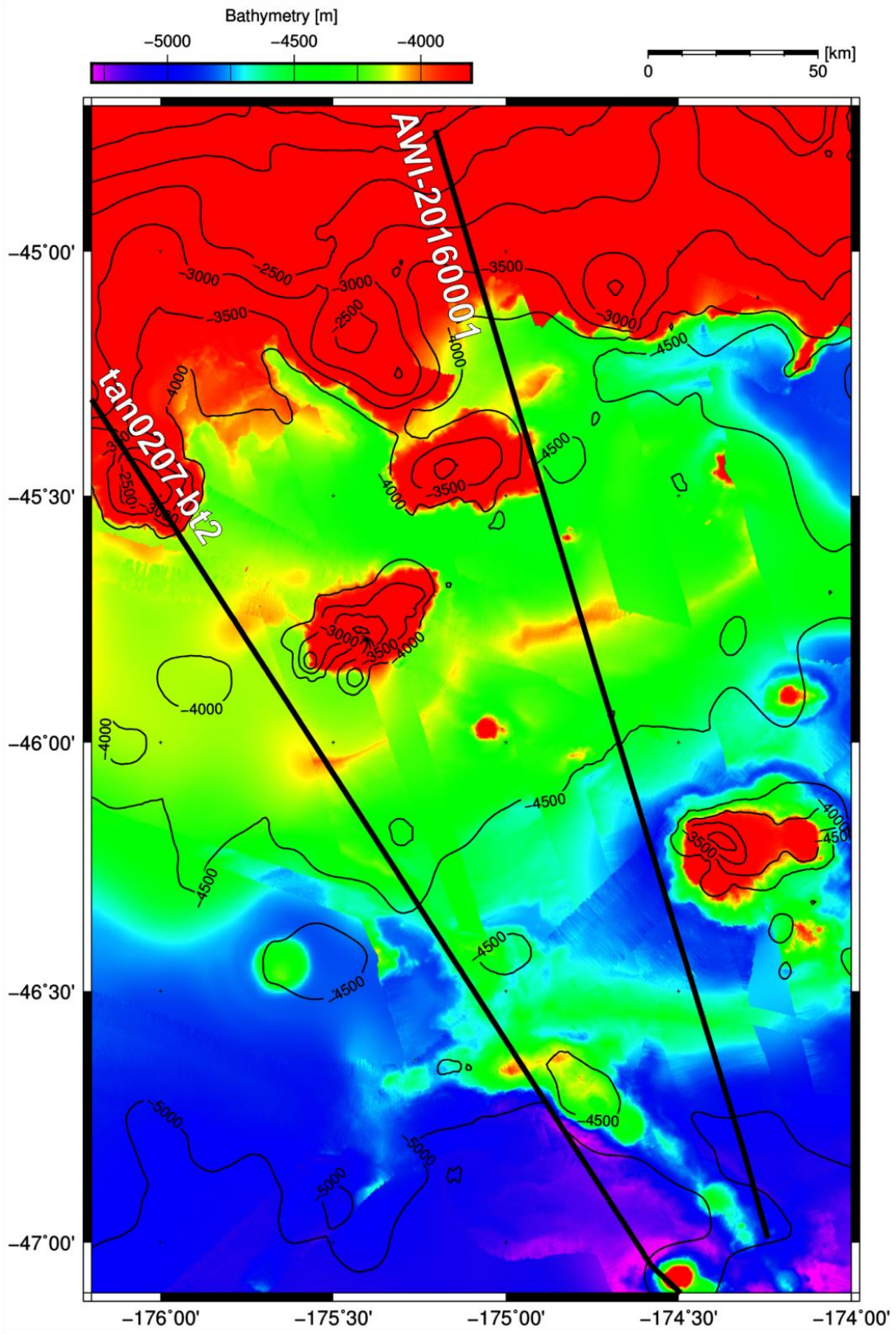

Fig. D.2: Bathymetric detail map A. Seismic profiles are shown in black.

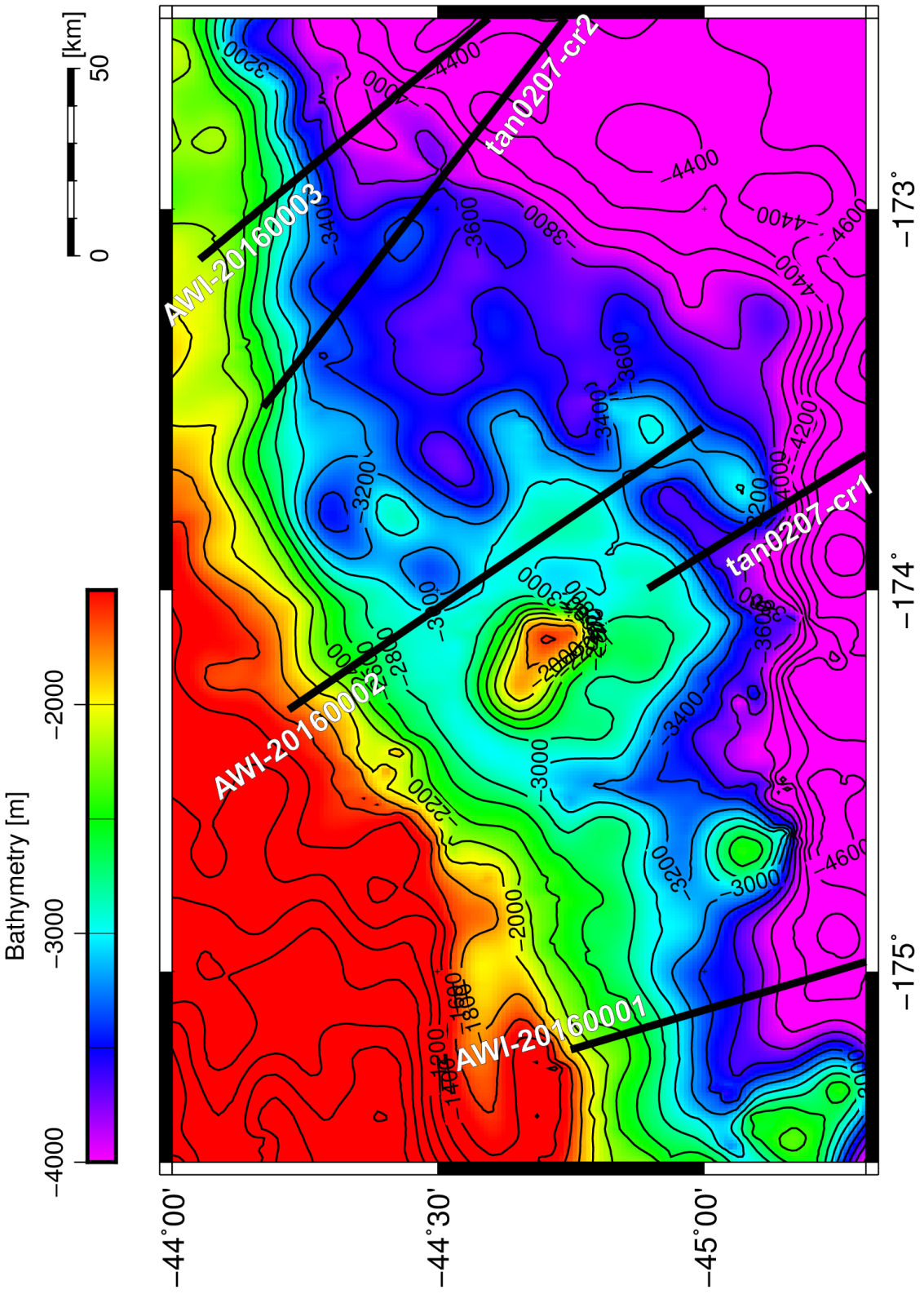

Fig. D.3: Bathymetric detail map B. Seismic profiles are shown in black.

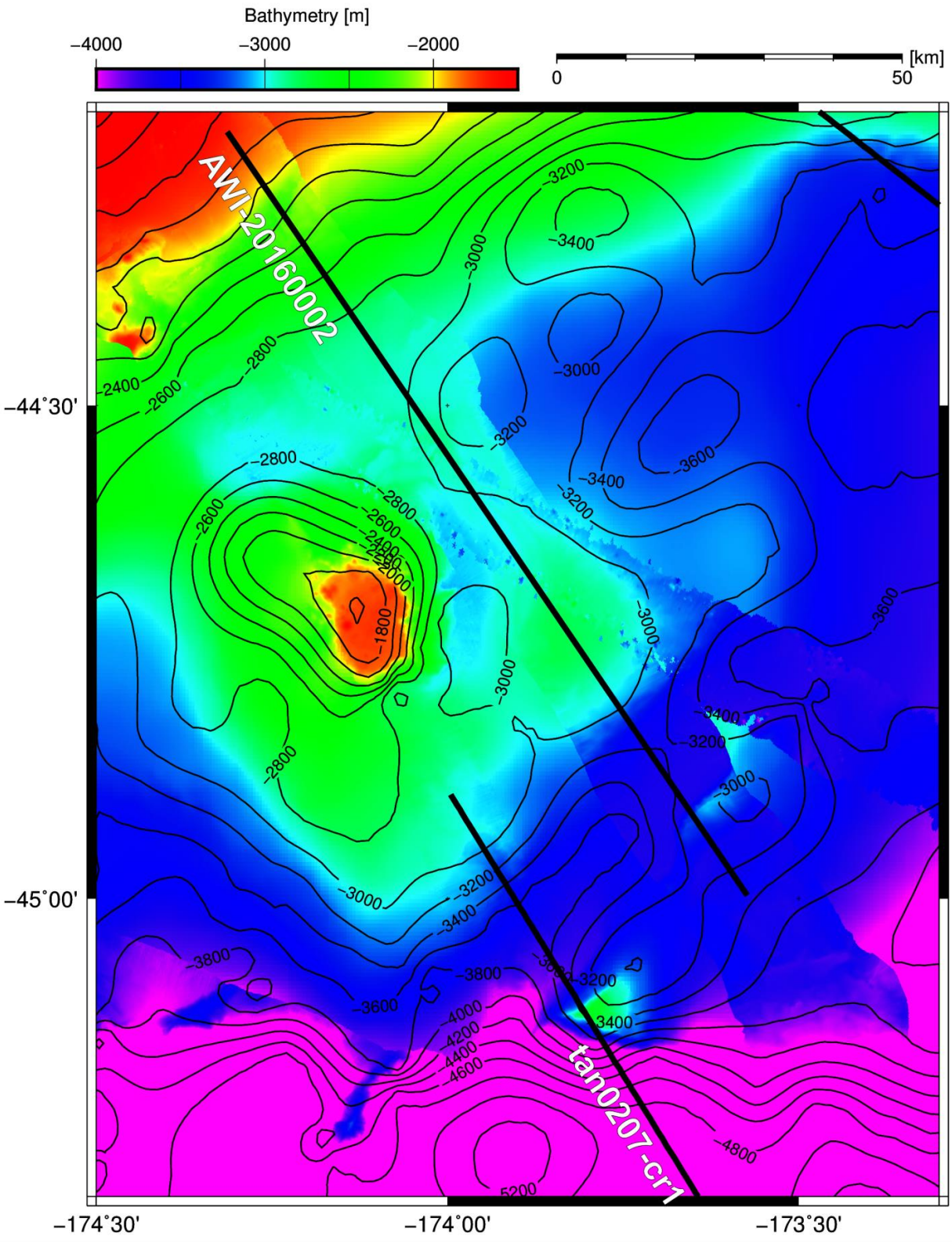

Fig. D.4: Bathymetric detail map C. Seismic profiles are shown in black.

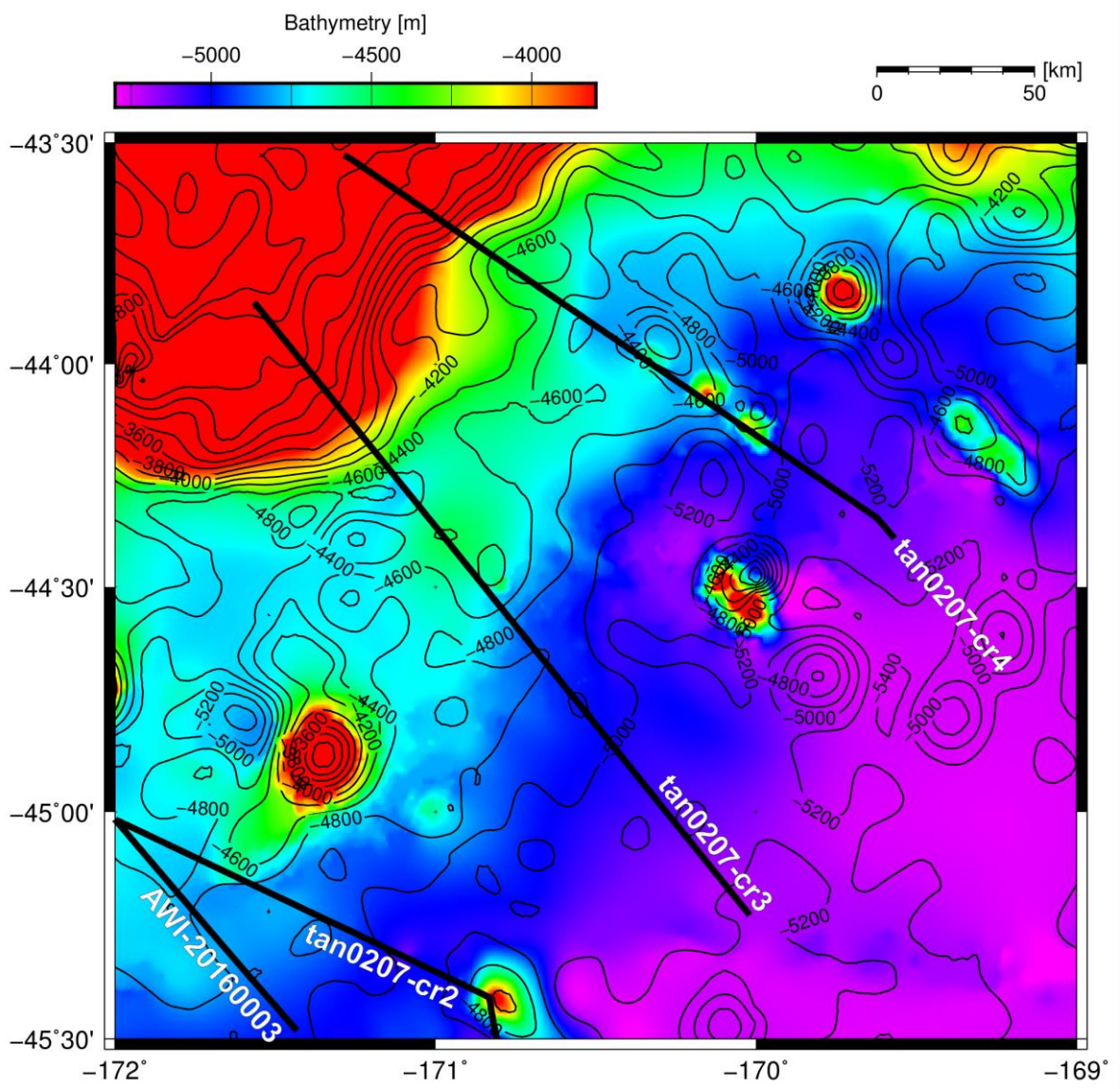

Fig. D.5: Bathymetric detail map D. Seismic profiles are shown in black.

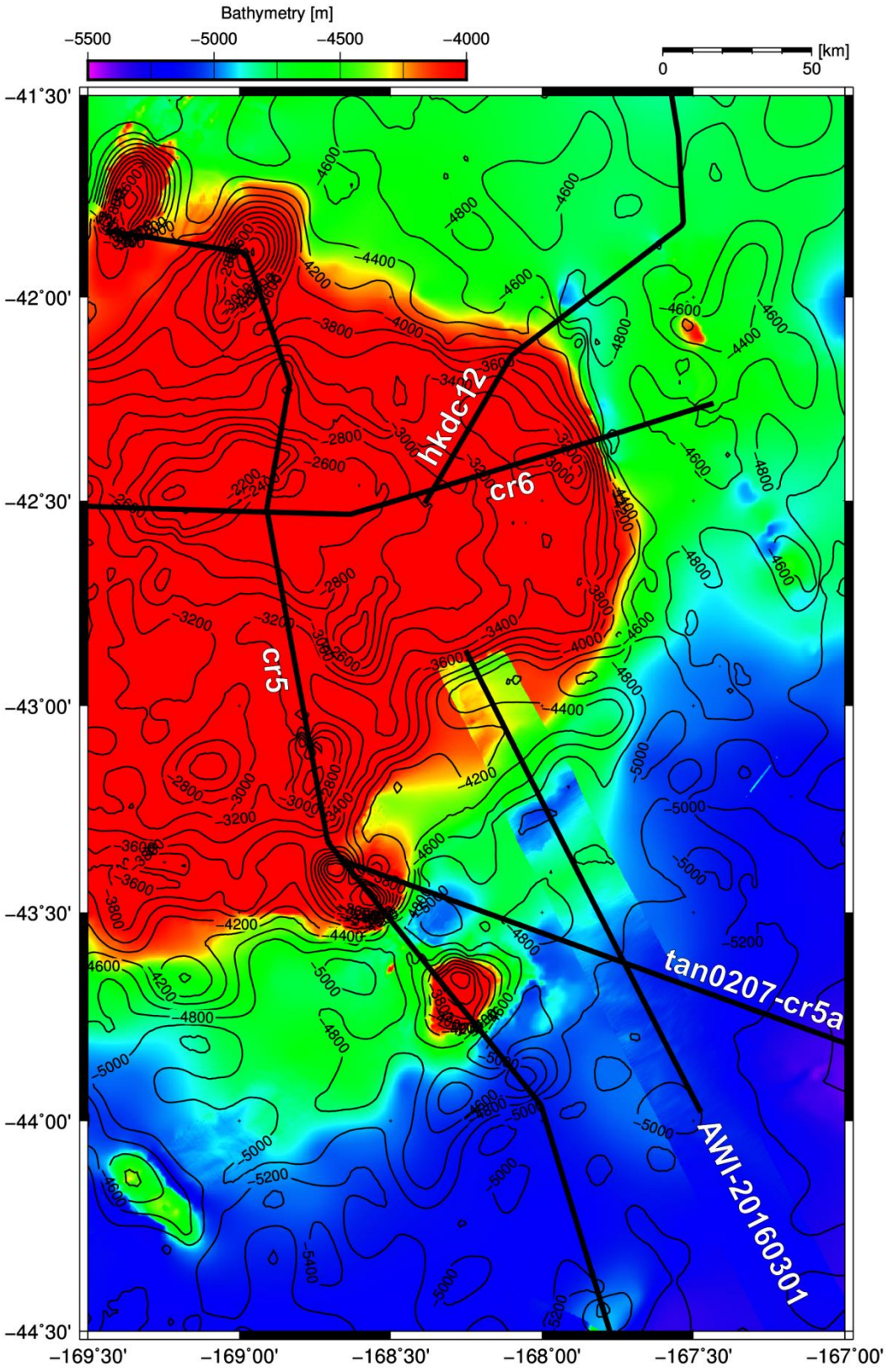

Fig. D.6: Bathymetric detail map E. Seismic profiles are shown in black.

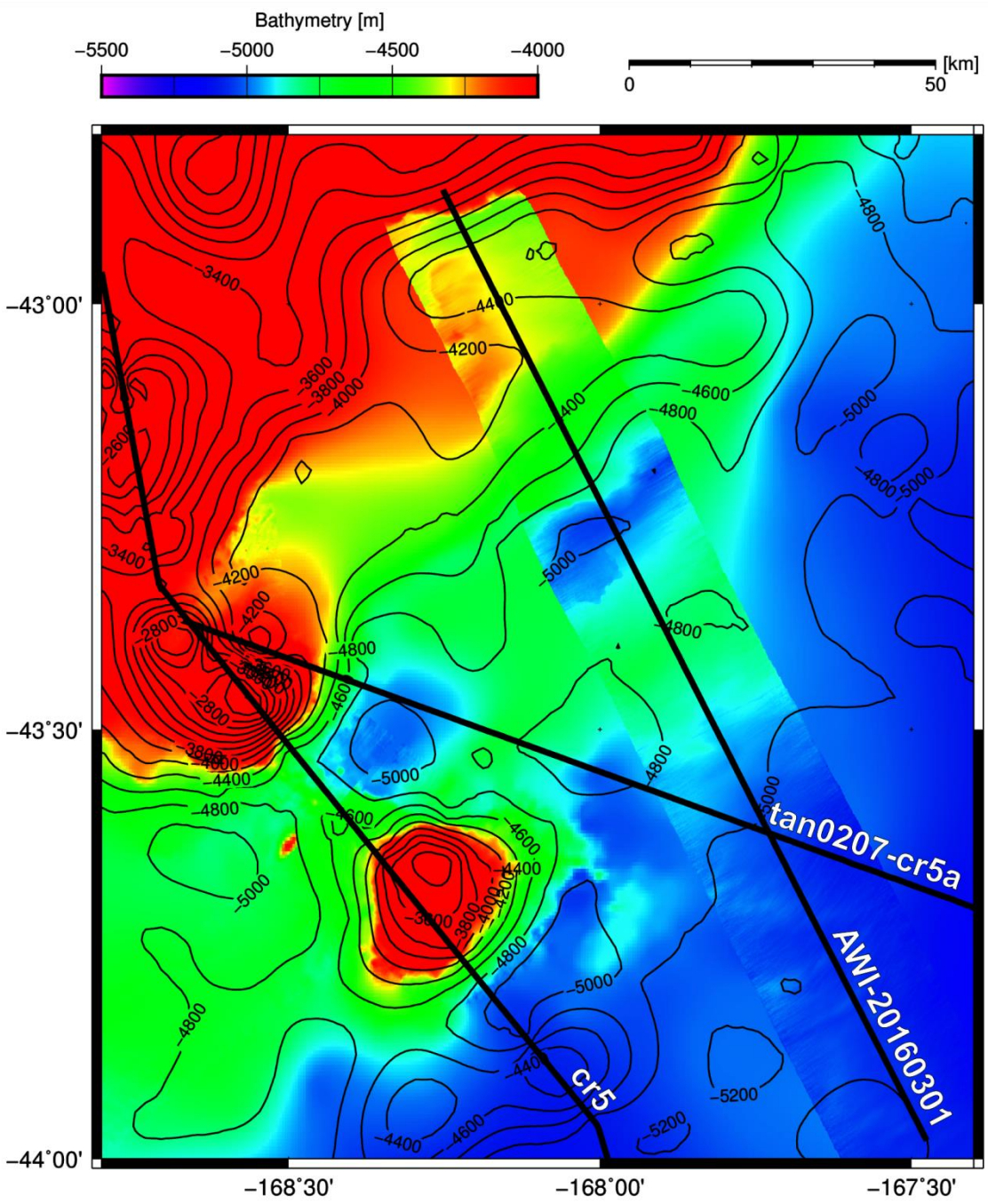

Fig. D.7: Bathymetric detail map F. Seismic profiles are shown in black.

E. Additional maps

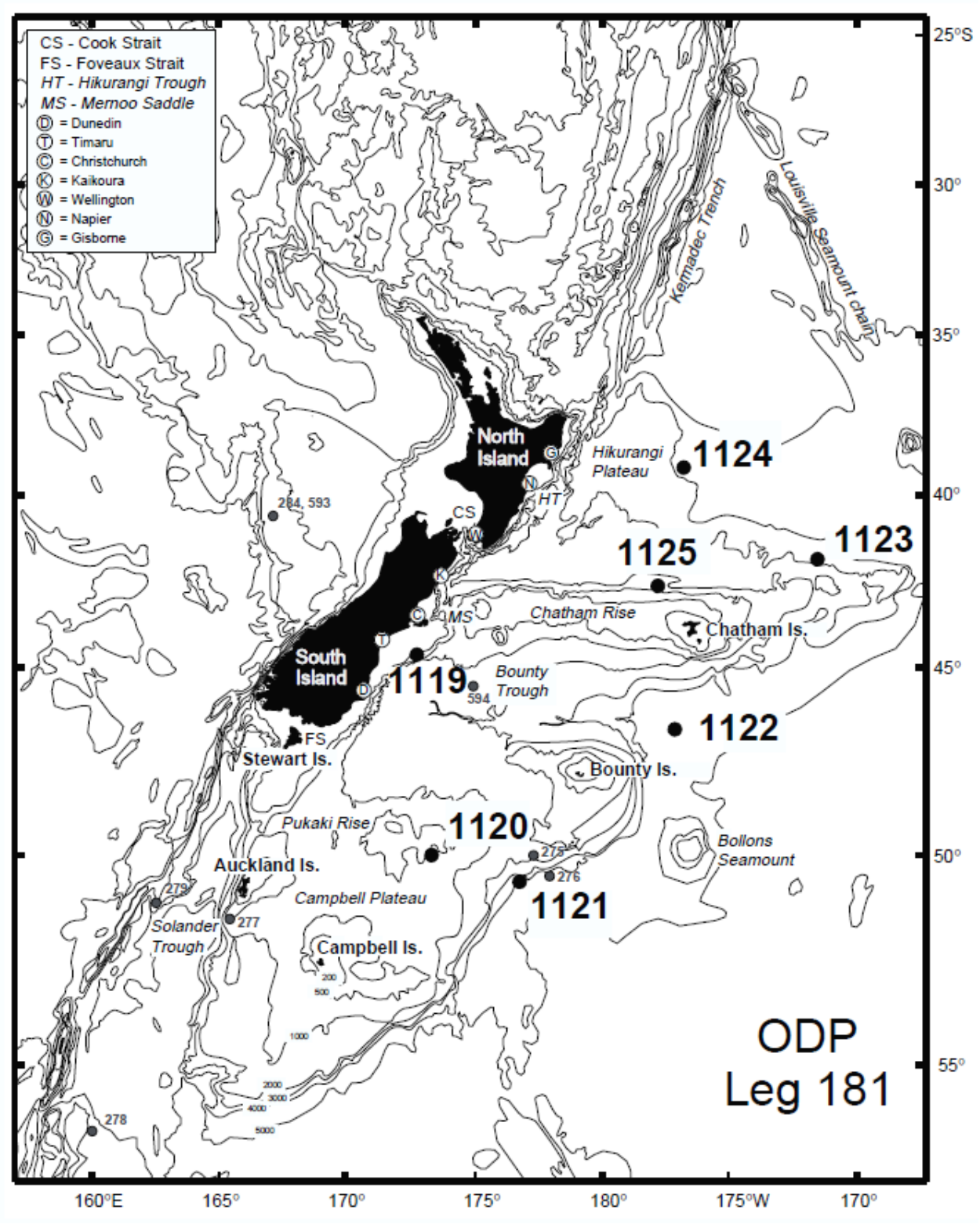

Fig. E.1: Map of drill site locations from Leg 181 (from Carter et al., 1999b)